Exploring the interactions between Vinculin and vinculin-binding site containing proteins

Masters by Research

2020

Tom Paige

Acknowledgements

I would like to thank for all their great help and guidance Dr Ben Goult, Dr Rejina Khan, Dr Lorena Varela-Alvarez, Jack Doolan, Dr Karen Baker the Mulvihill and Geeves labs as well as technical services.

Abstract

Focal adhesion complexes are mechanosensitive adhesion complexes that regulate key cellular processes such as cell migration and cell survival. These complexes connect the extracellular matrix (ECM) to the Actin network through a matrix-Integrin-Talin-Vinculin-Actin complex. Vinculin is a linker protein that through its N-terminal head domain (VD1) binds to cryptic vinculin binding sites (VBS) in talin, while its tail domain binds to actin linking the actin network to the ECM. This study investigates key interactions between vinculin and VBS containing proteins. Proteins such as the chlamydial virulence factor TarP which hijacks vinculin to aid in bacterial internalisation, the Talin helix 50 VBS which seems unique in its ability to accommodate VD1 mutations that disrupt binding and lastly α-Catulin a vinculin homologue which could share interactions with any known vinculin binding proteins.

We identified that the *C.caviae* Tarp VBS3 showed increased affinity for VD1 compared to the VBS1 and Pulldown assays showed that TarP may bind VD1 in a 1:3 ratio. We propose that TarP binding VD1 in a 1:3 ratio alongside the differences in affinity between its VBS indicate the possibility of infection stage specificity between VBSs.

Talin H50 appears to accommodate VD1 mutants due to of lack polar/ionic bonds, alongside smaller side chained amino acids in the interface when compared to other VBS.

Lastly, α-catulin shows conserved secondary structure with vinculin, as well as a potential interaction between α-catulin and the adhesion protein Paxillin. Indicating that α-catulin like vinculin may bind paxillin and be recruited to focal adhesion complexes.

Contents

Figure and Table List

Abbreviations

FACs, Focal adhesion complexes

DAPC, Dystrophin associated protein complex

TarP, Translocating Actin recruiting phosphoprotein.

EB, Elementary Body

RB, Reticulate Body

T3SS, Type three secretion system

WH2, Wiskott-Aldrich homology 2

LD, Leucine/Aspartic acid motif

ABS, Actin binding site

VBS, Vinculin binding site

ECM, Extracellular Matrix

VT, Vinculin tail

VD1,**2**,**3**,**4**, Vinculin head domains 1,2,3,4

DD, Dimerization domain

ARP2/3, Actin recruiting protein 2 and 3

NMR, Nuclear magnetic resonance

PAGE , Polyacrylamide gel electrophoresis

RIAM, Rap1-GTP-interacting adapter molecule

SDS, Sodium dodecyl sulphate

FPLC, Fast protein liquid chromatography

IPTG, Isopropyl ß-D-1-thiogalactopyranoside

RSB, Reducing sample Buffer

LB, Lysogeny Broth

TROSY, Transverse relaxation optimized spectroscopy

UV, Ultraviolet

CD, Circular Dichroism

OD, Optical density

TM, Melting temperature

ACH, α-Catulin head

ACT, α-Catulin tail

NAs, Nascent adhesions

IMC, Inner membrane clasp

OMC, Outer membrane clasp

PIP2, Phosphatidylinositol 4,5-bisphosphate

HSPG, Heparan sulfate proteoglycan

PDI, Protein disulfide isomerase

PI3K, Phosphoinositide 3-kinase

SNARE, Soluble N-ethylmaleimide–sensitive factor attachment protein

cFLIP, Cellular Flice-inhibitory protein

NMJ, Neuromuscular junction

DMD, Duchenne muscular dystrophy

Grb2, Growth factor receptor-bound protein 2

nNOS, Neuronal Nitric oxide synthase

POMT1, Protein O-mannosyltransferase 1

ISLO-1, SLO-1 interacting protein

P-Mlc2, Phosphorylated Myosin Light Chain 2

PBS, Phosphate buffered saline

$\boldsymbol{K_d}$, Dissociation constant

MST, Microscale Thermophoresis

GST, Glutathione *S*-transferase

Hz, Hertz

MSA, Multiple sequence alignment

1 Introduction

1.1 Cell-matrix Focal adhesion complexes

The diversity in extracellular matrix (ECM) components in terms of type, topographical arrangement, ligand binding sites as well as physical differences when under varying degrees of forces are something that are acutely critical in cell development. This is seen when ablation of integrin subunits is embryonically lethal (Fässler et al., 1996). The way the cell communicates with the ECM is through bi-directional adhesion complexes, which utilise large cytoskeletal protein complexes to link ECM components to the interior of the cell. ECM components for example the fibrous protein Fibronectin are bound the extracellular portion of Integrins. Integrin proteins create the transmembrane link between the ECM and cytoskeletal proteins in the cell interior, in particular the mechanosensitive proteins Talin, Vinculin and the structural protein Actin which forms large fibrous networks involved in cell motility, cell-cell contact, cell cycle regulation and cell death (figure 1). This linkage of ECM-integrin-talin-vinculin-actin is the basic core of a focal complex, but as many as 232 proteins are found in be involved in the ‘adhesome’ (Winograd-Katz et al., 2014). As a cell migrates the cell membrane at the ‘front’ of the cell extends flat protrusions called Lamellipodium, which are highly enriched with branched actin networks (Jacquemet et al., 2015). Upon contacting the ECM, the cell forms nascent adhesions (NAs) which contain only a few hundred adhesion proteins, and which are only ~100 nm. NAs are transient (Changede et al., 2015) and tend to form first and in the faster actin retrograde flow zones found in lamellipodium.

Larger more stable complexes can form when motor proteins such as Myosin IIa alongside actin binding proteins such as α-actinin bind to actin filaments to generate tension on these complexes (Choi et al., 2008). This generation of tension by myosin IIa as well as the ECM itself allows internal cytoskeletal proteins such as talin and vinculin (Ciobanasu et al., 2014; Pasapera et al., 2010) to act alongside numerous other cytoskeletal and signalling proteins to adjust cellular processes such as actin network growth and the eventual growth of NAs into a mature focal adhesion complexes (FACs).

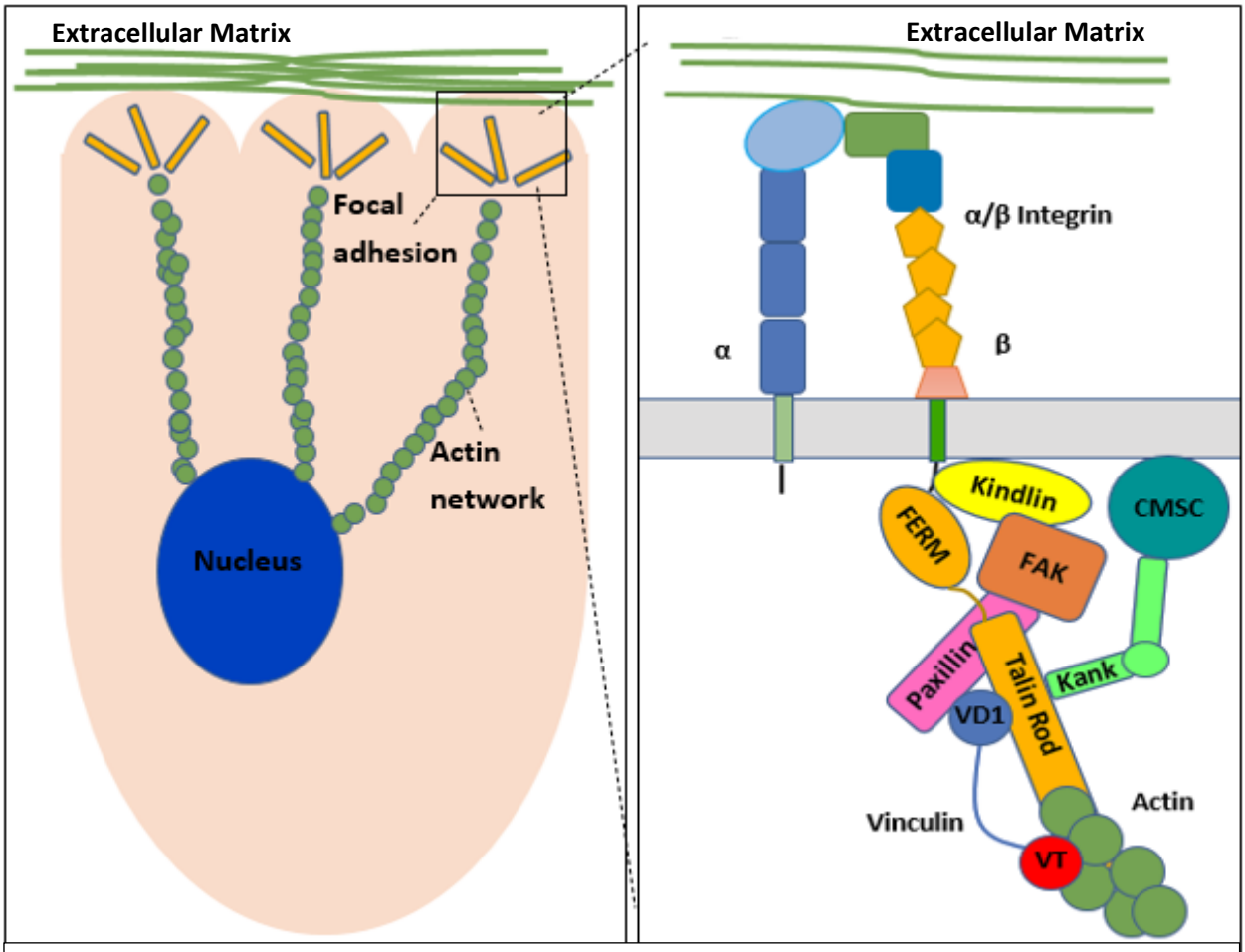

Figure 1-(left) Cellular interaction with the extracellular matrix through actin rich lamellipodia and filopodia extensions forms NA sites which eventually mature as forces increase and adhesion proteins into are recruited forming focal adhesions. This allows cell migration and cellular sensing regulation. (Right) Close up of a mature focal adhesion showing the connection between the ECM, the α/β Integrin and focal adhesion proteins, Talin (FERM and Rod), Kindlin, focal adhesion kinase (FAK), Paxillin, Vinculin (VD1 vinculin head, VT vinculin tail), Kank proteins, cortical microtubule stabilising complex (CMSC) and actin. Redrawn from Jacquemet et al.,2015.

FACs can sense the ECM environment by specificity of ligand bound to the integrin receptor and by the mechanical forces applied through that connection. This Bi-directional outside-in and inside-out signalling allows dynamic regulation of signals applied to either side of the FACs. Outside in signalling where the integrins extracellular ectodomains can bind extracellular ligands and these ligands can cause conformational changes in integrins which can also aid in integrin clustering. Inside out signalling requires that intracellular cytoskeletal proteins bind the integrin cytoplasmic tail to induce conformational changes which can lead to integrin activation and increased integrin ligand binding affinity (Shattil et al., 2010). A continuous dynamic equilibrium exists between the bi-directional signalling that while both seem to regulate individual steps both work in tandem to properly regulate adhesion assemblies.

This dynamic regulation is possible because of the numerous adaptor/signalling proteins that can interact with the core adhesion proteins listed above. One of many important Signalling proteins is focal adhesion kinase (FAK) which is a non-receptor tyrosine kinase binds early on in focal adhesion sites and through autophosphorylation it can bind key structural proteins such as talin and Paxillin, notably paxillin a structural and signalling protein is required for FAK localisation at FA (Hu et al., 2014). Equally if not more importantly however FAK can bind and regulate though phosphorylation such regulating signalling molecules such as SRC kinase family proteins which can modulate numerous pathways from actin regulation through RAC and RHO GTPases, Myosin modulation and cell survival gene regulation through ERK kinase signalling (Burridge and Wennerberg, 2004).This mechanical/chemical type of regulation is decisive in stem cells as the interaction transduced from the ECM can have a direct on the outcome of

the cell in terms of morphogenic outcome, e.g. what lineage the stem cell will in differentiate into (Engler et al., 2006).

1.2 Integrins

Integrins are a heterodimeric protein that consist of non-covalently linked α and β subunits with large extracellular domains, each subunit having its transmembrane helices which then lead to individual C-terminal cytoplasmic tails. Mammals have 18α subunits and 8β units that form 24 different integrin types (Hynes, 2002) which all have varying tissue distribution such as αIIbβ3 integrins prominently found in platelets. The structure of integrins large inverted V-shaped extracellular domains is something that is key as it determines what activation state the integrin is in, three states have been observed bent-closed (inactive), extended-closed (active low ligand affinity) and extended-open (active high affinity) (Michael and Parsons, 2020). All integrin isoforms inhabit these three states, but some may be more or less likely to inhabit each state (figure 2). For example isoforms such as αvβ3 being more likely to inhabit the active state than αIIbβ3, this would depend on adaptor proteins present, ligand binding specific and isoform specific conformations (Litvinov et al., 2019). The two transmembrane helices are mediators of the varying activation conformations of integrins alongside the cytoplasmic tails discussed below. The ~20 Amino acid hydrophobic transmembrane helices interact with each other through two key interactions which keep the integrins in the more closed inactive conformations (Lau et al., 2009). An interaction in the outer leaflet of the plasma membrane allows the close packing of the two helices due to glycine packing motif GXXXG, which enables both α and β helices to pack together cooperating in keeping integrins in their inactive conformation (Russ and Engelman,

2000).This is known as the outer membrane clasp (OMC) (Lau et al., 2009) and mutations to more charged and bulky amino acids such as G to N in this region have resulted in increased integrin activation (Li et al., 2005). Another interaction aptly named the inner membrane clasp (IMC) contains a salt bridge which is positioned in the inner leaflet of the plasma membrane in proximity to the cytoplasm, which contains the highly conserved GFFKR in the α tail and HDR motif in β tails which also tend to have higher

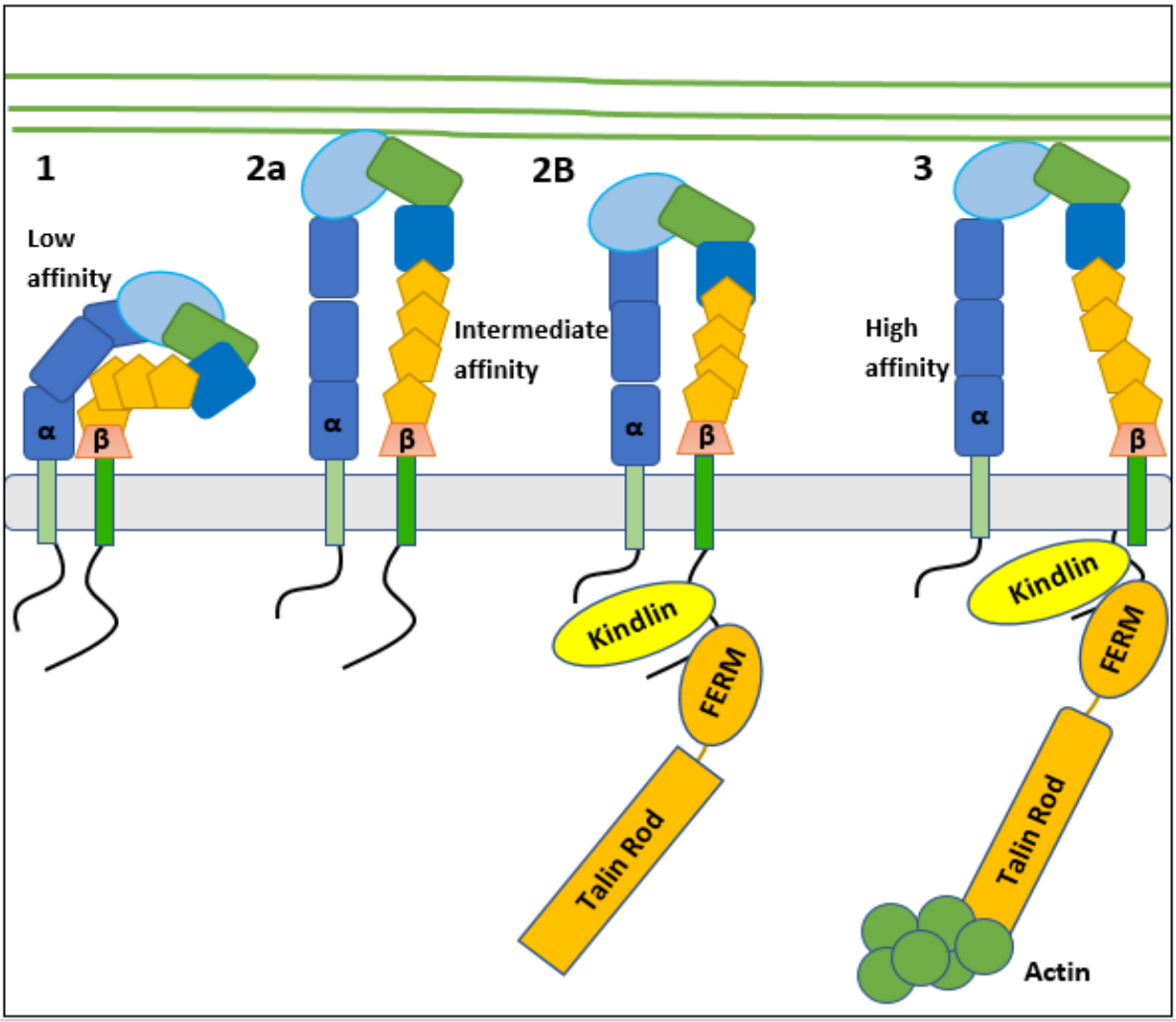

Figure 2-The different activation states of integrin molecules.1) Integrin in a low affinity conformation with no contact with ECM or intracellular proteins, 2a) an outside in signalling intermediate state with contact with the ECM, 2b) an different intermediate state showing inside out signalling with contact with intracellular proteins and 3) a high affinity state were the integrin molecule is in contact with both the ECM and intracellular proteins causing conformational changes between the α and β subunits. Redrawn from Mechanobio.info.

numbers of hydrophobic residues surrounding the motif than the α tails. In αIIbβ3 integrins this salt bridge exists between αIIb R995 and β3 D723 and again mutations to oppositely charged residues increased integrin activation (Hughes et al., 1996; Luo et al., 2005, 2004). Both these interactions are relatively weak, and both are required to keep integrins in their closed inactive conformation.

To activate integrins a combination of interactions occur between the large mechanosensitive protein talin N terminal FERM domain and the integrin β cytoplasmic tail, although many interacting proteins have roles in partially activating integrins discussed below .These interactions between talin FERM domain and β tails cause conformational changes in the extracellular ectodomains (Xiong et al., 2010) and transmembrane domains of integrins allowing the stabilising interactions mentioned above to be disrupted resulting in integrin activation (Anthis et al., 2009).

1.3 Talin

The link between integrins and the actin cytoskeleton is facilitated by a 270 kDa mechanosensitive cytoskeletal protein called talin (Burridge and Connell, 1983). Talin has a modular structure made up of 18 singular domains which can be broadly separated into two main larger domains (figure 3). The N-terminal of talin contains a FERM (4.1 protein, ezrin, radixin, moesin) domain (Chishti et al., 1998) which itself is made up of four separate domains, F0,F1,F2 and F3 (Pearson et al., 2000).This being an atypical arrangement of FERM domains because talin has a duplicated F1 domain named F0 which is shared only by Kindlin molecules and no other FERM domain containing proteins (Goult et al., 2010).

The N terminal FERM domain is connected to a large Rod domain by a short ~80 residue disordered linker region which contains a calpain protease cleavage site which is essential in the attenuation of FACs (Franco et al., 2004). The large rod domain consists of 13 4 and 5 helix bundles aptly named R1-R13, followed by a single C-terminal helix dimerization domain (DD) allowing homodimerization (Gingras et al., 2008; Goult et al., 2013a; Senetar et al., 2004).

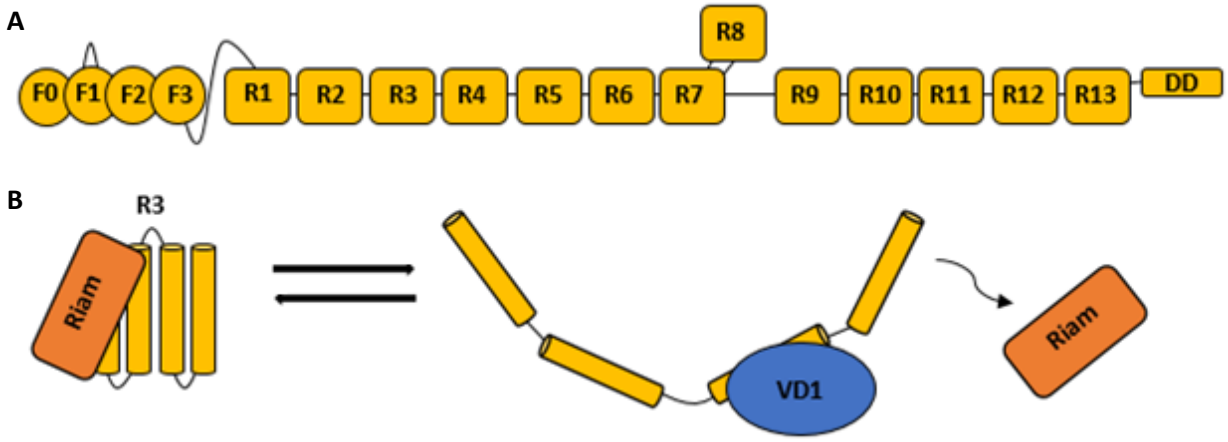

Figure 3-A)Talin the mechanosensitive adhesion protein containing the N-terminal FERM domain (F0-F3), F3 being important in integrin activation proceeding is an 80-residue disordered linker region. Attached to the linker region is the 13 alpha helical bundle Rod domains (R1-R13) which 9 out the 13 domains contain cryptic VBS (Red). At the C-terminus is a dimerization for forming homodimers between two Talin molecules. Redrawn from Khan and Goult, 2019. B) RIAM binds to the folded R3 domain talin, once tension is applied across the talin rod the R3 domain unfolds displacing RIAM and allowing VD1 to bind. Redrawn from Goult et al., 2018.

A Rap1-GTP–interacting adaptor molecule (RIAM) binds to the R2-R3 domain and recruits talin to the cell membrane allowing talin to interact with integrin cytoplasmic tails

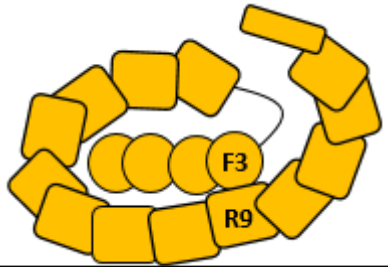

Figure 4-Talin in its autoinhibited conformation held in place through interactions between F3 and R9. Redrawn from Khan and Goult, 2019

(Lee et al., 2009).Talin exists in an autoinhibited conformation were interactions between F3 and R9 domains keep talin locked in this conformation (Dedden et al., 2019; Goult et al., 2013a, 2009; Khan and Goult, 2019) (figure 4). Freed by a combination of binding interactions between the membrane phospholipid phosphatidylinositol 4,5-bisphosphate (PIP2) binding to F1-F3 causing conformational changes that expose the IBS1 (Goksoy et al., 2008; Kelley et al., 2020; Song et al., 2012) and RIAM R2-R3 binding (Han et al., 2006).

1.3.1 Talin FERM domain

The FERM domain binds several proteins through each of its four domains for example phosphatidylinositol 4-phosphate 5-kinase 1 (PIP1 γ90) (Di Paolo et al., 2002; Ling et al., 2002) a kinase that binds to F3 that facilitates the production the aforementioned PIP2, an actin binding site (ABS) across F2-F3 and the integral integrin binding site (IBS1) in F3.Talin binds to the integrin β cytoplasmic tail through interactions between the talin F3 domain and a membrane proximal NPXY in the β cytoplasmic tail (Calderwood et al., 1999). An additional NPXY site exists in the β cytoplasmic tail at a more C-terminal position to which another FERM domain containing protein named Kindlin binds and assists in integrin activation (Harburger et al., 2009). F3 binding causes a conformational change in the membrane proximal region of integrins, the previously mentioned IMC region. Conserved lysine residues in (Talin1 324/Talin2 327) disrupt the IMC salt bridge and cause the reorientation of the integrin transmembrane helices by 20°, disrupting the OMC glycine packing also (Anthis et al., 2009). Membrane orientation patches consisting of positively charged residues present in F2 and in a loop

region in F1 help orientate the talin FERM domain to maintain integrin/talin interactions (Kalli et al., 2010).

1.3.2 Talin Rod

Each talin rod domain contains binding sites for a variety of ligands such as the Kank proteins (Bouchet et al., 2016), vinculin and actin etc. Regulation of ligand binding is something that can depend on the structural conformation of each bundle, these can be altered by post translational modifications such as phosphorylation and methylation among others (Gough and Goult, 2018) but by far the most important is mechanical force. For any mechanical force to be applied through talin it must be tethered , and this initially achieved through talin-integrin binding and talin-actin binding. Talin has three ABS, (Hemmings et al., 1996) ABS1 in F2/F3, ABS2 extending across R4-R8 (Atherton et al., 2015) and ABS3 spanning R13-DD (Gingras et al., 2008). Actin binding to any of these sites alongside actomyosin pulling on the filaments themselves will generate tension across the talin molecule. Tension across the rod domain can unfold these rod helical bundles exposing cryptic binding sites. Each domain will unfold at specific levels of pN force owing to specific residue interactions present in each helical bundle, with increasing force up to 30 pN whereupon all domains are unfolded (Yao et al., 2016). This variety in force required to unfold each domain alongside their unique ligand interactions allows talin to act as a dynamic mechanosensitive signalling hub (Goult et al., 2018), transmitting external and internal forces into both structural signals through conformational changes within talin and chemical signals that recruit signalling molecules to relay changes in the FACs. One main group of binding sites that are hidden inside these domains and are exposed upon force are vinculin binding sites

(VBS) (Atherton et al., 2015; Gingras et al., 2005) to which there are 9 helical bundles in the talin rod that contain one or two of these cryptic VBS

This change in ligand binding dependence on helical bundle conformations is exquisitely seen in the alternation between the RIAM and vinculin binding, Vinculin being a large structural actin/talin linker protein discussed in detail below. RIAM binds to R2-R3 but only when the R3 domain remains in its folded conformation, upon release of talin autoinhibition and binding to integrin and actin, tension is created across the rod domains and R3 becomes unfolded. Vinculin can now bind to the unfolded R3 domain which now has two VBS exposed, this mechanochemical switch of RIAM being exchanged for vinculin when force is applied is key for the maturation of focal complexes (Goult et al., 2013b; Yao et al., 2014a) (figure 3).The large variety of ligand binding to each rod domain is coupled to an additional dependence on each rods conformation, allowing talin to be the one of the most influential mechanosensitive regulatory proteins in the cell.

The importance of talin and its dynamic regulation in cells is seen when talin is downregulated or ablated, disruption of talin has been shown to arrest mouse embryo development early on at the gastrulation stage (Monkley et al., 2000). Talin ablation can cause defects in skeletal muscle development disrupting myotendinous junctions leading to progressive myopathies (Conti et al., 2009).Talin overexpression is associated with increased resistance to cell anoikis, increased metastasis and as such is linked to many cancers such as prostate (Zhang et al., 2015) and oral squamous cell carcinoma (Lai et al., 2011).

1.4 Vinculin

Vinculin is a 116 kDa (1066aa) mechanosensitive linker protein prominent in integrin based focal adhesions and cadherin-based cell-cell complexes. Vinculin is separated into anti-parallel α-helical bundles consisting of a large N-terminal head domain consisting of four subdomains VD1-VD4, this is followed by a disordered proline rich linker region which connects the head domain to the C terminal tail domain (VT) (figure 5). This proline linker contains binding sites for vasodilator-stimulated phosphoprotein (VASP), Vinexin (Kioka et al., 1999), Ponsin (Mandai et al., 1999) and the Actin recruiting protein 2-3 complex (Arp2/3) (DeMali et al., 2002; Golji and Mofrad, 2013; Omachi et al., 2017). The vinculin D1 domain (VD1) can bind cytoskeletal proteins such as talin (Gilmore et al., 1992), α-actinin (McGregor et al., 1994), α-catenin (Watabe-Uchida et al., 1998; Yao et al., 2014b), β-catenin (Hazan et al., 1997; Peng et al., 2010) and its own VT (Johnson and Craig, 1994). VD1 is also the target of bacterial invasive molecules such as *Shigella flexneri* IpaA invasin (Hamiaux et al., 2006) and Chlamydial translocated actin recruiting phosphoprotein (TarP) molecules (Clifton et al., 2004) which allow bacterial entry into cells.

The VT region has binding sites for actin, paxillin (Turner et al., 1990; Wood et al., 1994), PIP2 (Johnson et al., 1998) and the VD1 domain. The VT contains two ABSs (Hüttelmaier et al., 1997) that allow vinculin to link the actin cytoskeleton at its C-terminus to the cytoskeletal proteins bound at its N-terminus such as talin. Vinculin can undergo VT-VT homo-dimerisation (Bakolitsa et al., 1999) being facilitated by both PIP2 (Hüttelmaier et al., 1998) and actin (Johnson and Craig, 2000) which interacts with VT dimerization interface in the α1-α2 helices loop regions in both vinculin monomers

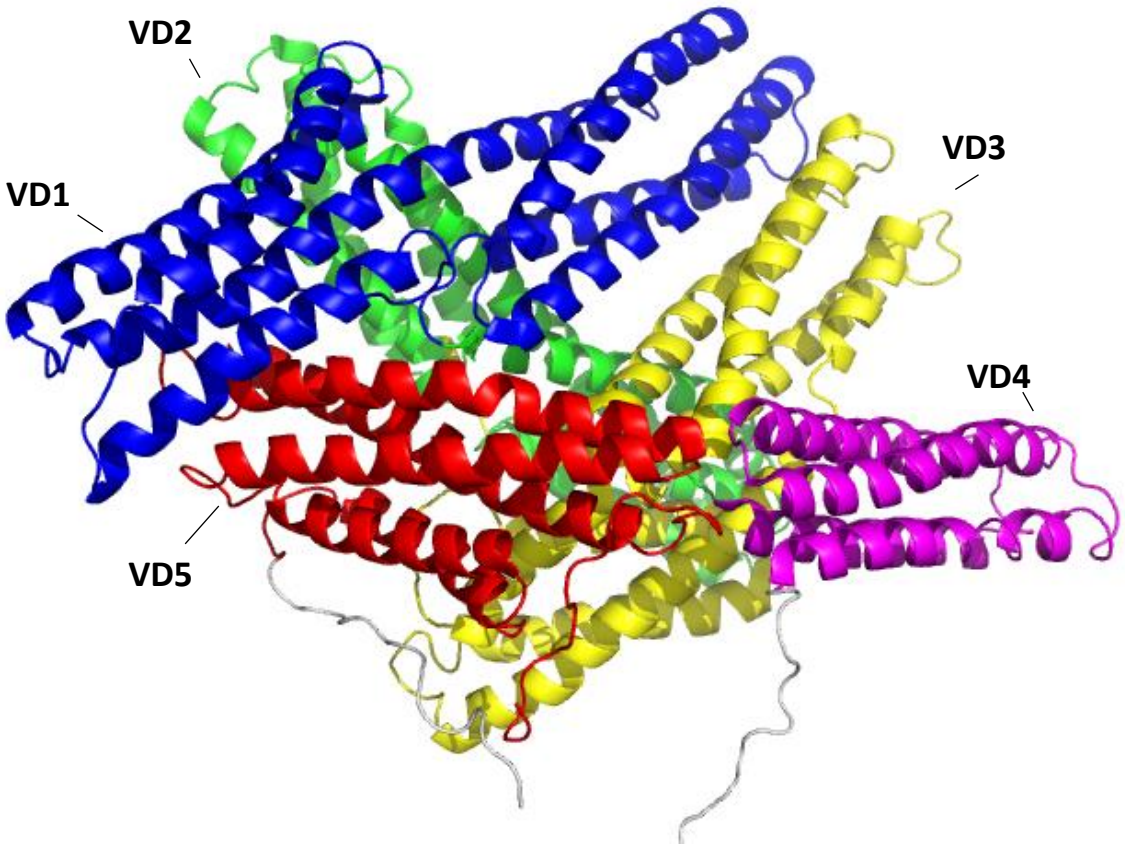

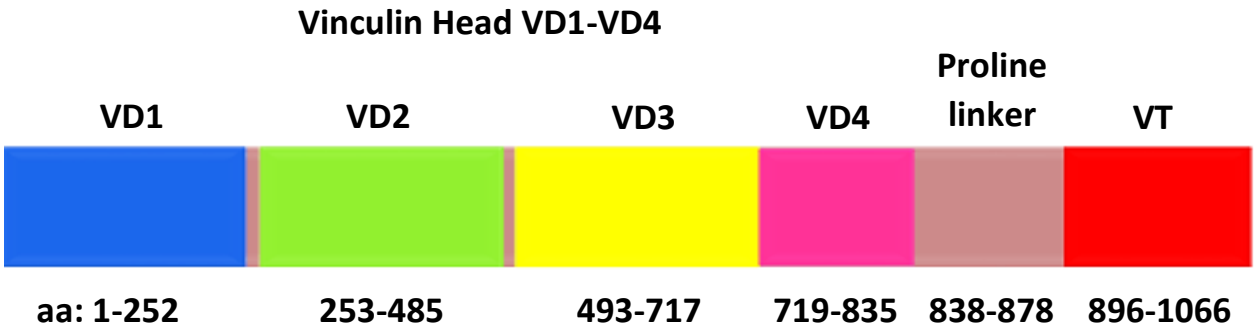

Figure 5-(Top) Structure of full-length Vinculin in its autoinhibited head-tail state showing each of its five domains VD1 blue,VD2 green, VD3 yellow, VD4 pink and VT red. PDB 1ST6 Bakolitsa et al., 2004. (Bottom) Domain boundaries VD1-5 of vinculin including proline linker region.

linking the two. Additionally, trimers can also be formed when PIP2 molecules in a dimer interacts with the α-3 helix of a vinculin monomer (Chinthalapudi et al., 2015). Vinculins linker role in these complexes is highly regulated and regulation is primarily attributed to Vinculins structural conformations.

Vinculin is maintained in an autoinhibited state via hydrophobic and hydrogen bond interactions between the VD1 domain binding to the VT (Izard et al., 2004), alongside polar interactions between VD3 and VT (Bakolitsa et al., 2004) and both ionic and hydrogen bonding interactions between VD4 and the VT (Cohen et al., 2005). The VD1 to VT interaction being the most important but the additionally interactions of both VD3 and VD4 increase the affinity by almost a hundred-fold (figure 6).

Autoinhibited vinculin is its cytoplasmic state until it is recruited into one of these adhesion complexes. To release vinculin from its autoinhibited state one hypothesis propose a combination of F-actin binding to the VT and talin VBS binding to VD1 must occur to disrupt these intramolecular interactions activating vinculin (Chen et al., 2006).

Although another hypothesis proposes that the VBS in proteins such as talin or α-actinin binding to VD1 are sufficient to activate vinculin (Bois et al., 2006; Golji and Mofrad, 2010).

The VBSs present in proteins such as talin and α-actinin participate in the activation of vinculin by binding to VD1 through the insertion of a amphipathic helix into the core of N-terminal of VD1 (Izard et al., 2004) the N-terminal consisting of four α helices (1-4) and C-terminal (4-7) (figure 7).

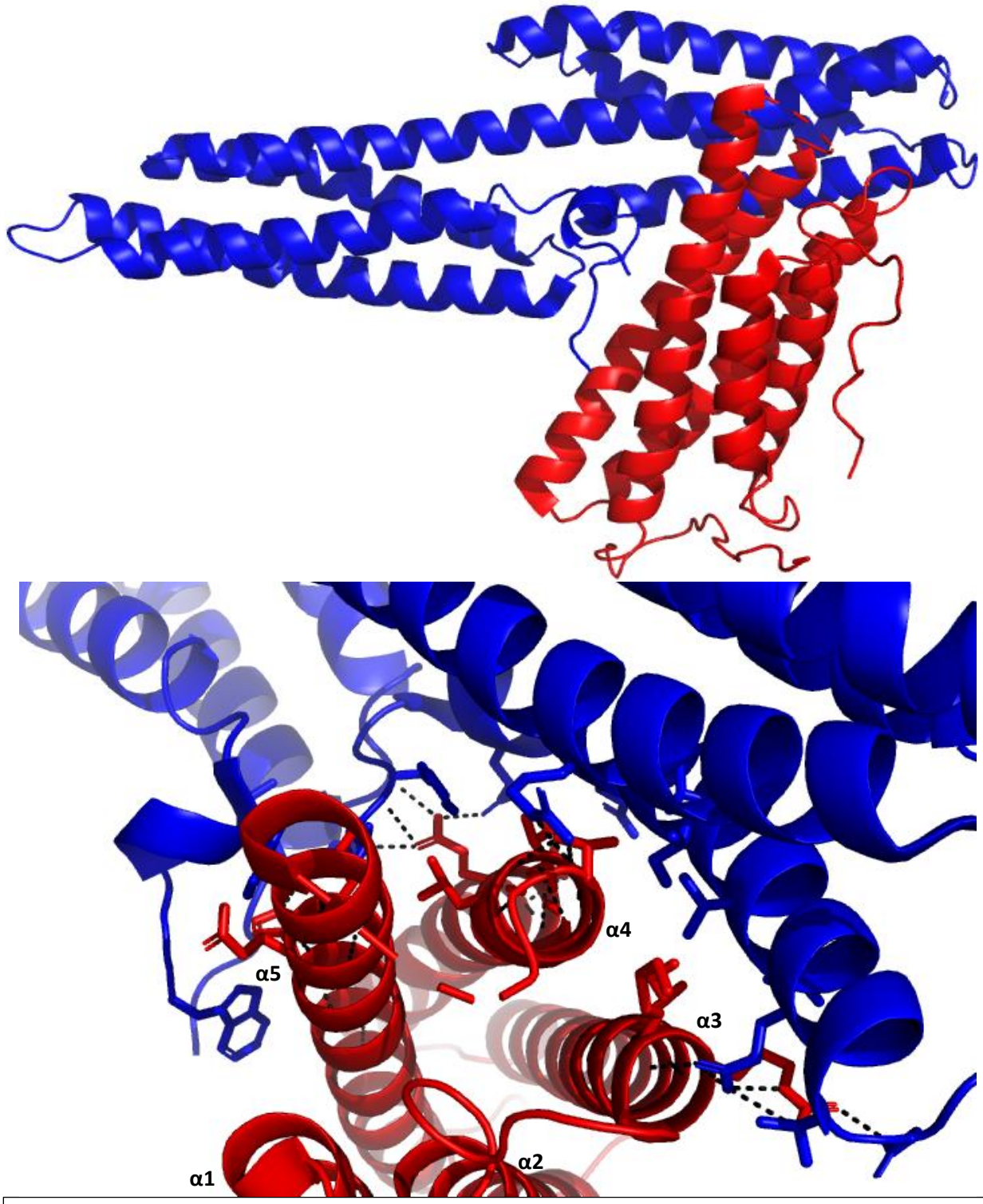

Figure 6-(Top) Structure of vinculin VD1 and VT in an autoinhibited conformation.(Bottom) Hydrogen bonds as well as hydrophobic packing maintain the VD1-VT interaction, which are subsequently disrupted upon helical insertion of VBS such as those found in talin. VT α1-5 helices. PDB 1RKE Izard et al., 2004.

This insertion occurs between the α1 and α2 helices and converts this VD1 N-terminal region into a 5-helix bundle, with the hydrophobic faces of the helix interacting the hydrophobic residues present in the core of the N-terminal bundle (Tran Van Nhieu and Izard, 2007).This helical addition causes structural rearrangements in VD1 that facilitate the weakening of the VD1-VT interaction, favouring vinculin activation.

Additionally, tension applied from the binding at the N and C termini are also important to maintain vinculin in its activated state as loss of tension across the molecule can lead to the rapid inactivation of FACs (Grashoff et al., 2010). Phosphorylation of key residues

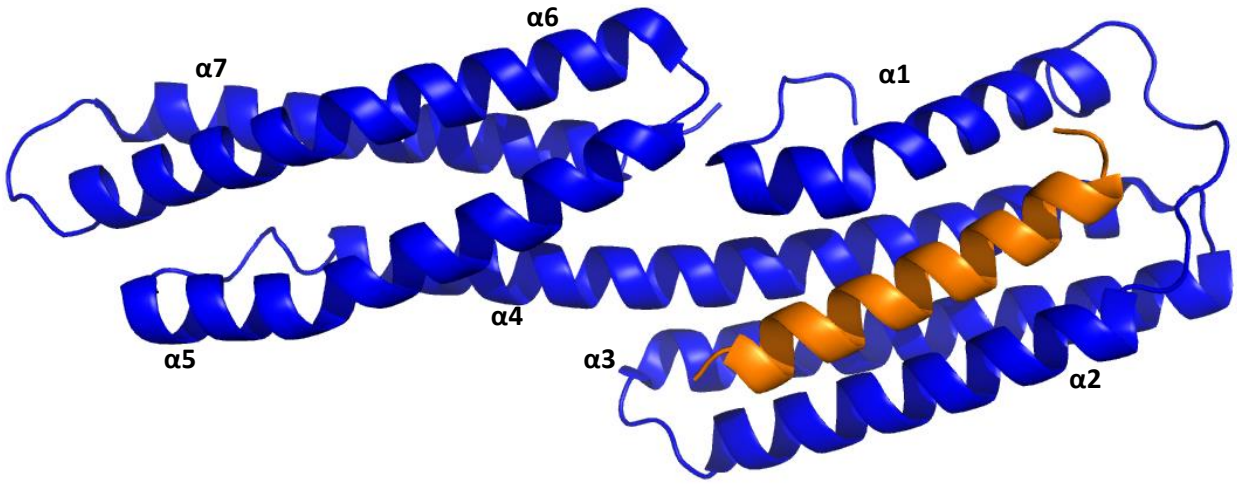

Figure 7-The insertion of the VBS (orange) helix forces the helices α1 and α2 of the N-terminal helical bundle of VD1 (blue) apart and allows the VBS to insert itself into the hydrophobic core, thus converting the 4-helix bundle to five helix bundle. This interaction disrupts VD1-VT interactions and is key to vinculin activation from its autoinhibited state. PDB 1RKC 1RKE Izard et al., 2004.

Y100, Y1065, S1033 and S1045 are also known to be important in regulating D1-VT interactions as these phosphorylations can alter charged residues orientations in D1, weakening head to tail interactions (Auernheimer and Goldmann, 2014; Golji et al., 2012; Zhang et al., 2004). The combinatorial binding of talin and actin binding appear to be needed in releasing vinculin from this autoinhibited state and the phosphorylation

Sites aid in maintaining it in the activated state. Autoinhibited vinculin is thought to be recruited to FACs by paxillin in a proposed hand off model, where increased myosin II activity increases paxillin binding to vinculin which then transports vinculin to FACs where it is 'handed' to talin (Pasapera et al., 2010). Once recruited to FACs autoinhibited vinculin replaces RIAM bound to talin R2-R3 to favour more stable adhesions and turnover and by the regulation of actin through its own ABS (Thievessen et al., 2013) and through interactions with actin regulatory proteins such as ARP2/3 (Chorev et al., 2014). Vinculin acts as a force transduction protein which transmits force from the ECM to the actin cytoskeleton and vice versa, which when under high degrees of force ultimately leads to an increase in size and stability of FACs through integrin clustering and increased links to the actin cytoskeleton (Hernandez-Varas et al., 2015). This increase in FACs stability and size caused by an increase in force means that more talin is recruited, this increase in force means more talin VBS are available for vinculin to bind and be activated by talin/actin binding.

FACs disassembly is required to allow the cell to form new adhesions and continue to migrate, a loss of force across FACs causes the loss of talin from the complex. Talin is cleaved through its calpain cleavage site found in the linker between the FERM and rod domains (Franco et al., 2004). This loss of talin alongside proposed PIP2 interactions disrupting actin-VT bonding result in loss of tension across vinculin, allowing vinculin to revert back to its high affinity autoinhibited conformation (Chandrasekar et al., 2005; Saunders et al., 2006).

1.4.1 Exploring vinculin associated interactions in the cell

Studies of vinculins many binding interactions with both structural and signalling proteins have shown how essential it is for cell migration and survival across many species. In some bacterial such as chlamydial bacteria host vinculin is considered essential for the continuation of a pathogenic cycle that sees vinculin hijacked and repurposed for bacterial invasion into a host cell. In *Drosophila* vinculin is considered non-essential in enabling embryos to grow into fully formed adults, however when vinculin is overexpressed it can result in lethality (Maartens et al., 2016). Lastly vinculin has two homologous proteins α-catenin which has a role in cell-cell adhesion complexes and α-catulin which is associated with the dystrophin associated protein complex (DAPC) which forms strong connections between the ECM and the cell interior in muscle tissues (Petrof et al., 1993). The least studied of these is α-catulin, its structural homology to vinculin could mean it shares some of the same essential binding interactions seen in vinculin. Here in this study we will investigate three separate aspects of vinculin cellular interactions.

1.To investigate a Chlamydial virulence factor that can bind and hijack vinculin to aid in the internalisation of the chlamydial bacteria

2.How vinculin mutants that can rescue *Drosophila* from hyperactive vinculin bind and interact with different talin VBS

3. Does the α-catulin vinculin homolog share some of the same key binding interactions as vinculin?

1.5 Chlamydial pathogenesis and the Vinculin recruiting virulence factor Tarp

Project 1 will look at the importance of vinculin in several cellular processes including cell motility and adhesion has led bacterial pathogens to opportunistically recruit vinculin to alter cell cytoskeletal dynamics. One bacterial pathogen family being the Chlamydia family of bacteria, which are obligate intracellular bacteria that have been found to subvert host cytoskeletal proteins to aid in its pathogenesis (Abdelrahman and Belland, 2005).

Chlamydia bacteria are responsible for the majority of sexually transmitted infections across the globe (Howie et al., 2011) and are also one of the main causes of preventable blindness (Eko et al., 2008), this ability to infect mammalian cells so well is largely due to its unique pathogenesis cycle (Elwell et al., 2016). Extracellularly Chlamydia bacteria exist as infectious elementary bodies (EB) that when encountering a suitable host cell will attach initially through low affinity heparan sulfate proteoglycans (HSPGs) on the cells surfaces (Taraktchoglou et al., 2001), then high affinity cell receptor binding with such proteins as β1 integrin (Stallmann and Hegemann, 2016), mannose 6-phosphate receptor (Puolakkainen et al., 2005) and protein disulfide isomerase (PDI), all of which have been shown to be important in chlamydia bacterial entry into cells (Conant and Stephens, 2007). The binding of the EB with these host cell receptor causes actin remodelling inside the host cell to aid in the internalisation of the EB (Carabeo et al., 2002) and enable further EB membrane interactions that can alter MEK–ERK and phosphoinositide 3-kinase (PI3K*)* host cell survival pathways (Kim et al., 2011; Subbarayal et al., 2015).The binding to host cell receptors is highly variable, differing chlamydial species and host cell tropism are seen to play their part in the large

variations in receptor bindings. Upon binding the EB injects premade virulence enhancing proteins into the host cell through a type three secretion system (T3SS) (Beeckman and Vanrompay, 2010; Slepenkin et al., 2003). These virulence factors can induce alterations in cellular signalling and cytoskeletal protein recruitment to aid in the internalisation of the EB. One such virulence factor is the TarP which has been shown to bind to both actin and vinculin and facilitates EB entry into the cell (Clifton et al., 2004).

Once the EB has been internalised in a membrane-enclosed compartment known as an inclusion, the EB inside the inclusion then undergoes differentiation into a non-infectious reticulate body (RB) (figure 8). Numerous proteins both on the surface of the inclusion and injected from the inclusion into the cytosol can allow the RB to survive in the host cells cytosol by scavenging nutrients and subverting cell apoptotic pathways . Examples being soluble N-ethylmaleimide–sensitive factor attachment protein (SNARE) proteins that associate with the inclusion membrane and scavenge nutrients from Golgi exocytotic vesicles (Lucas et al., 2015), and proteins such as cellular flice-inhibitory protein (cFLIP) that can interfere with caspase8 activation thereby controlling apoptosis (Böhme et al., 2010; Irmler et al., 1997) In later phases of infection the RB will replicate and then undergo secondary differentiation back to an Eb, at the same time expressing proteins such as the chlamydia protease-like activity factor (CPAF) (Snavely et al., 2014) that aid in the lysis of the host cell so that the EB can be free to begin another round of infection on a neighbouring host cell. Alternatively, the infected cell may

methodically exocytose EBs without lysing the cell, which requires the remodelling of the actin network through N-WASP a RhoA GTPase and Myosin II which facilitates

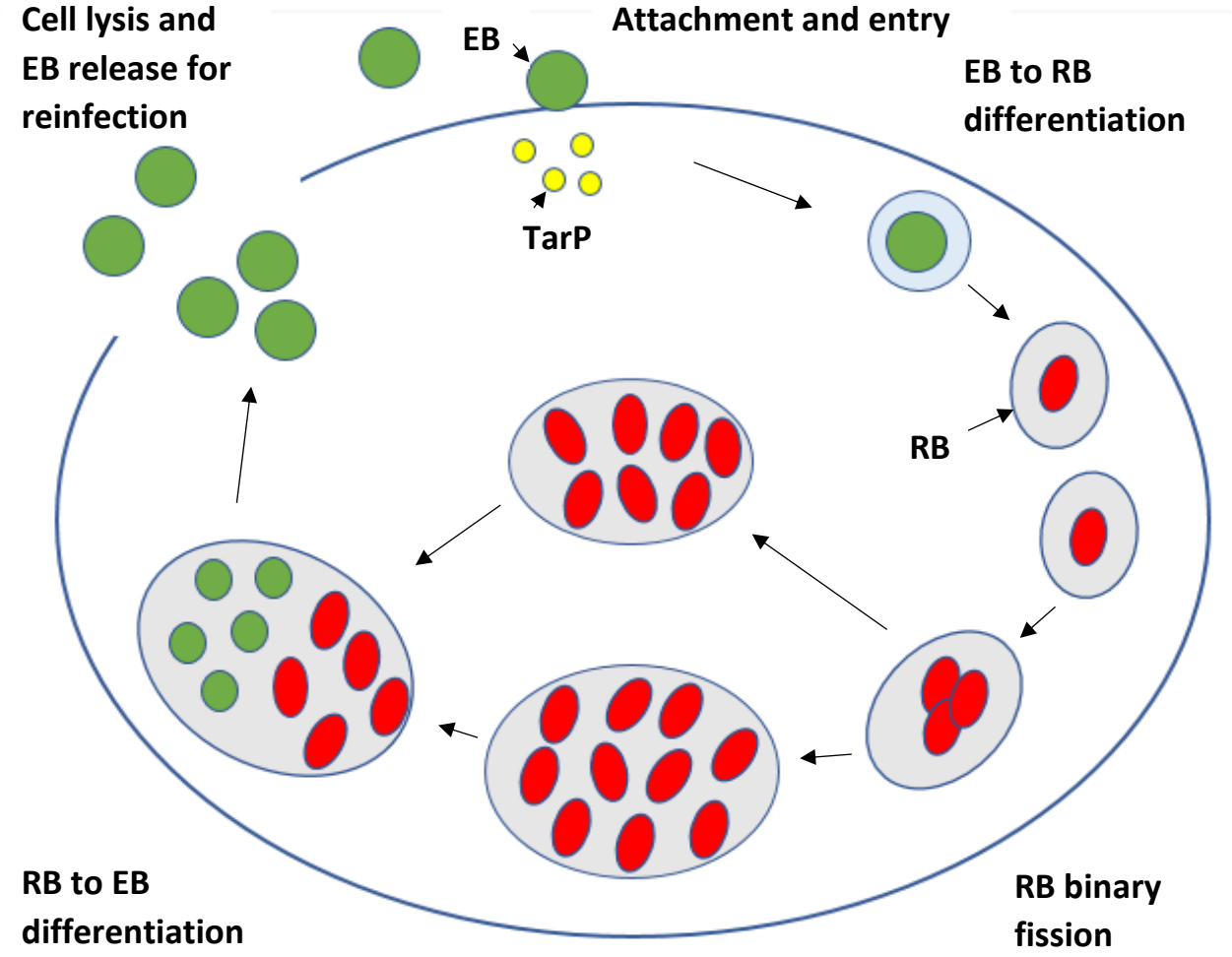

Figure 8-The chlamydial pathogenesis cycle stages from EB internalisation aided by TarP though differentiation into an RB, before multiplying and differentiating back into a EB before the cell undergoes lysis and the EB is released to invade another host cell. Redrawn from Abdelrahman and Belland, 2005

membrane pinching to release the EBs (Hybiske and Stephens, 2007). This alternative method allows the cell to maintain a continuous stream of infectious EB while limiting the hosts immune response, as there is no release of cellular debris that is detected in lysis of a cell by immune cells.

1.5.1 TarP

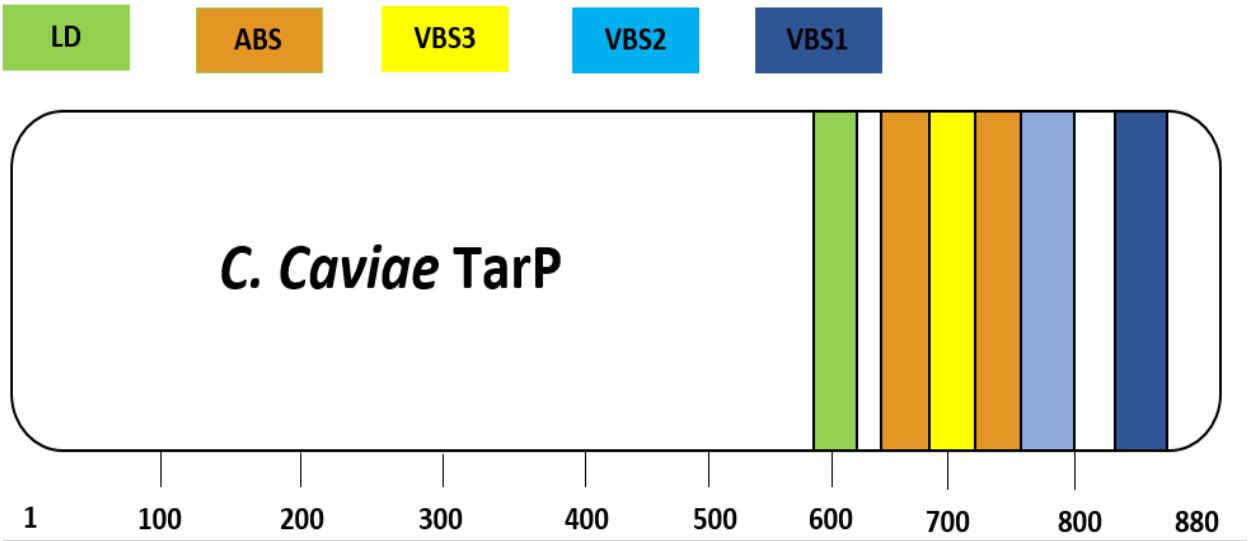

Figure 9-The *C.caviae* TarP virulence factor contains multiple binding domains primarily located at its C-terminus which aid in its remodelling of adhesion complexes for EB internalisation. *C.caviae* TarP contains one LD motif, two ABS and uniquely three VBS. Redrawn from Whitewood et al., 2018.

The intrinsically disordered TarP 90 kDa protein is key in the initial invasion of chlamydial EB largely due to its ability to bind and commandeer host vinculin (Thwaites et al., 2015) and actin (Jewett et al., 2006; Tolchard et al., 2018) and alter a host cells structural complexes to facilitate the internalisation of EBs. TarP is conserved across all the chlamydial family albeit with species specific differences. Some orthologues such as *C.trachomatis* contain an additional set of tyrosine repeats in their N-terminal domain which are missing in others (Clifton et al., 2005), these repeats can be phosphorylated and cause actin rearrangement and stimulate host survival pathways (Elwell et al., 2016) . Also, the chlamydial family shows variation in the number of both ABSs and VBSs present in each orthologue, each having a range of 1-3 ABS and 1-3 VBS (Thwaites et al., 2015). The *C.caviae* TarP ortholog consists of a single leucine/aspartic acid (LD) motif, two Wiskott-Aldrich homology 2 (WH2) ABS alongside 3 VBS at the disordered C-terminal (1-3 C-terminal to N-terminal). *C.caviae* is differs from many of

Chlamydial TarPs as it lacks an regulatory N-terminal phospho-domain that is found many TarPs (Clifton et al., 2005) as well as containing and three VBS which is unique among TarPs (Thwaites et al., 2015) (figure 9).

TarP is injected into the host cell through the T3SS and binds vinculin and actin alongside host actin regulatory proteins such as the ARP2/3 complex (Jiwani et al., 2012) as well as host signalling proteins to modulates cellular dynamics in favour of facilitating the internalisation of the EB. In *C.caviae* TarP's actin recruitment was shown

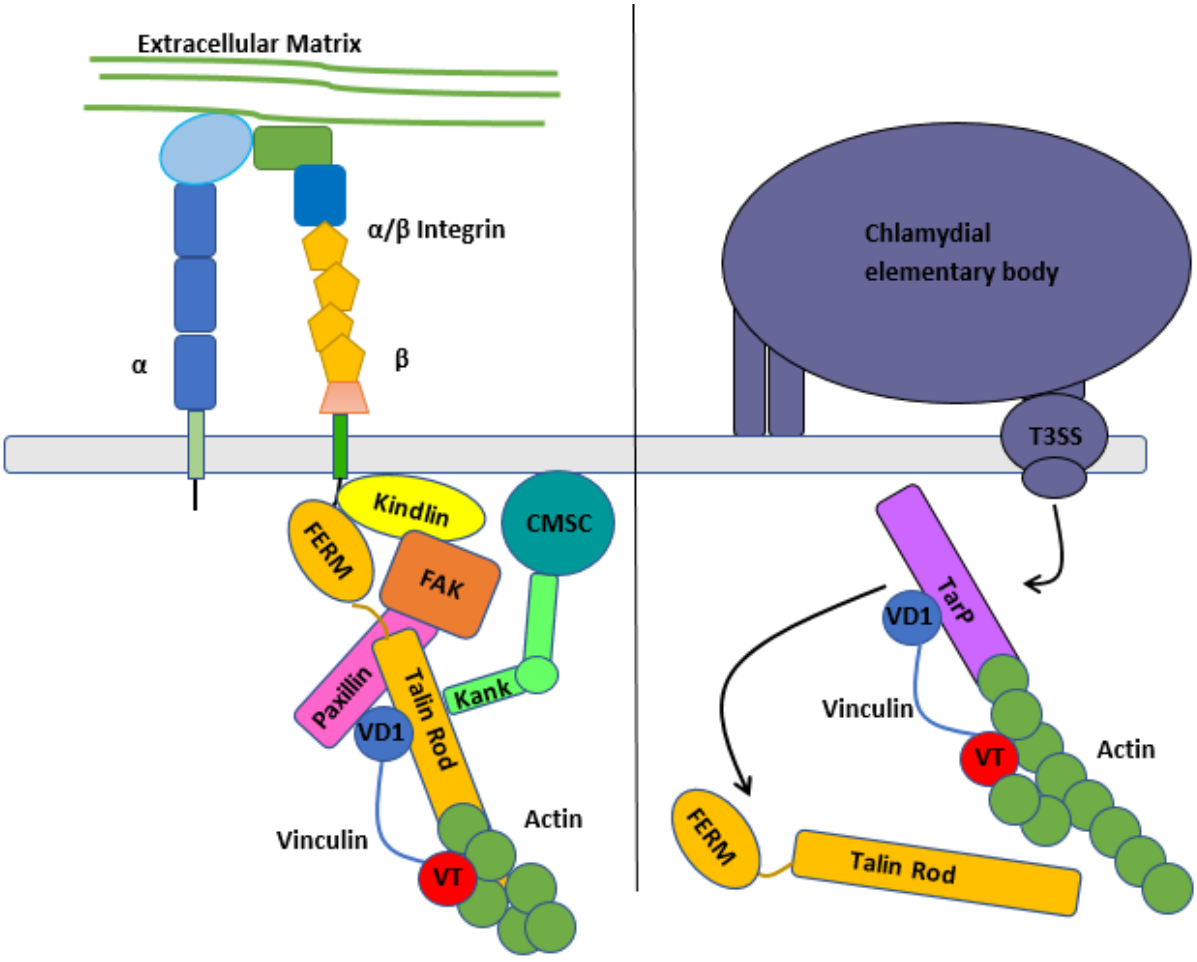

Figure 10-A comparison between an integrin based FACs (left) and an adhesion complex formed though TarP hijacking vinculin and remodelling the actin cytoskeleton to aid in the internalisation of an EB (right). Vinculin plays a role in in the formation of both complexes, its ability to bind and regulate actin remodelling as well as being a linker protein make it key for the formation of actin networks.

to be vinculin dependent (Thwaites et al., 2015) and it is proposed that the interactions

between vinculin bound to the TarP VBS regulates this actin recruitment and assembly at the cell membrane.

TarP interacts with vinculin through binding to VD1 via the same helix addition method as talin and disrupts the VD1-VT interactions, relieving it from its autoinhibited state. While isolated TarP and talin VBS both bind with similar affinities, TarP's VBSs are present in a disordered region meaning they are constitutively able to bind vinculin whereas in talin an application of force is required to uncover the cryptic VBSs inside each talin rod helical bundles (Yao et al., 2014a). This results in TarP being able to outcompete talin (Whitewood et al., 2018) in binding to free vinculin and subsequently recruit vinculin to aid in EB internalisation.

C.caviae's 3 TarP VBSs all share conservation with the VBS found in talin as well as other vinculin binding bacterial virulence factors such as *Rickettsia* surface antigen sca4 (Lee et al., 2013; Park et al., 2011a) and *Shigella IpaA* invasin (Hamiaux et al., 2006; Park et al., 2011b) which both bind vinculin and reorganise actin networks. While *C.caviae* TarP VBS1 VD1 binding data is known (Whitewood et al., 2018), less is known about the other two VBS and in this chapter we will attempt to characterise and compare them.

This projects aim is to biochemically and biophysically characterise the interactions and structure of VD1 with TarP VBS2 and 3, so as to make direct comparisons with VBS1. Also, as *C.caviae* TarP is unique in having three VBS determining the stoichiometry of vinculin molecules able to bind at any one time may enable further insight into the importance of each VBS.

1.6 Vinculin lethality rescuing mutants

Vinculins plays are large role in FACs and cadherin cell-cell complexes and regulating vinculin recruitment and activation that allows a cell to adapt to its dynamic environment (Leerberg and Yap, 2013). Vinculin's importance in embryogenesis has been shown to vary between species with some species showing higher sensitivity to its ablation and/or up regulation.

Vinculin's effects on embryogenesis have been shown in vinculin gene knockouts in several animal models. C.elegan vinculin null worms die in the larval stage due to abnormal muscle dystrophy having gone through an elongated embryogenesis (Barstead and Waterston, 1991). Vinculin null mice also show large defects in development with cardiovascular and neural tube closure defects appearing as early day as E8 followed by death at day E10 (Xu et al., 1998; Zemljic-harpf et al., 2004). In contrast in zebrafish vinculin appears to be of less importance with both isoforms (zebrafish having two vinculin isoforms VA/VB) being able to be deleted with only mild pericardial edemas (excess fluid between the heart and the sack around the heart ,the pericardium), the zebrafish grew to adulthood without major issue (Han et al., 2017). In *Drosophila* melanogaster vinculin null mutants are able to progress through embryogenesis and were still viable with only very mild defects in adult musculature. While vinculin null *Drosophila* only had mild defects (Alatortsev et al., 1997), it was shown that a constitutively open (CO) hyperactive vinculin where the autoinhibitory head to tail interactions are disrupted caused lethality (Maartens et al., 2016). CO vinculin in *Drosophila* was found at FACs but also in cytoplasmic aggregates. These subcomplexes require talin to form and addition of a singular talin VBS helix disrupted

the aggregate formation indicating talin was associated with these complexes through vinculin-talin VBS interactions. These subcomplexes do not appear to the cause of lethality and it appears the VD1 region binding talin at FACs caused the lethality. It is likely that due to CO vinculin interfering with FA turnover through constant binding to talin VBS it might disrupt the cycles of talin VBS bundles unfolding and refolding which are needed for mechano-transduction force signals (Maartens et al., 2016). This could lead to an overstimulation of FACs assembly and lifetime resulting in improper maintenance of mechanical signal transduction.

The interaction between talin's VBSs and vinculin appeared to be key to lethality, and a set of mutations in VD1 were discovered through a genetic screen, where mutations to the CO vinculin gene were made to identify if any supressed lethality. Mutations to VD1 in CO vinculin appeared to supress lethality and it was assumed that these mutations disrupted VD1 talin VBS binding. Three VD1 mutations A50I, P15L and W253X rescued *Drosophila* from lethality and the mutants showed reduced equilibrium dissociation constant (K_d) values when binding talin VBS (Data generated by Dr Karen Baker Postdoc in the Goult lab) confirming the assumption that the mutations disrupted VD1 talin VBS binding.

A talin VBS helix 50 (H50) showed only small reductions in K_d when binding the VD1 mutants when compared to wildtype (WT) VD1,and were still able to effectively bind helix 50 and rescue the *Drosophila* from lethality as was seen in the other talin VBS tested. This could indicate a different binding model may be present between A50I, P15L and W253X and talin H50.

Using x-ray crystallography, the intention is to crystallise each of the three vinculin mutants with talin H50 to identify any unique binding interactions and structural differences.

1.7 α-Catulin and the dystrophin associated protein complex

Vinculin has been shown to be a highly regulated part of FACs as well as in cadherin complexes acting as a strengthening and mechanosensitive signalling/adaptor protein. A protein with high sequence and structural homology to both vinculin and α-catenin called α-catulin has been found to be involved in another cytoskeletal adhesion complex the DAPC. The DAPC is a complex important in force transmission in muscle cells, where α-catulin too appears to play an adaptor/signalling roles.

1.7.1 DAPC

The DAPC is another large protein complex that links the ECM to the actin/microtubule cytoskeleton and plays a large role in the transmission and resistance of force in muscle tissue particularly skeletal and cardiac. Regulating and transmitting force between the sarcolemma (membrane surrounding striated muscle) and the ECM (Petrof et al., 1993). Additionally, the DAPC is vital in the formation, maturation, and maintenance of neuromuscular junctions (NMJ) (Belhasan and Akaaboune, 2020; Repository et al., 2002).

The DAPC is made up of a core collection of proteins such as Dystrophin (Deconinck et al., 1997), a dystrophin homolog utrophin (Winder et al., 1995), Dystroglycans, Sarcoglycans, Sarcospan, Syntrophins, and Dystrobrevins (Gawor and Prószyński, 2018). However, these proteins make up only the core structural complex, numerous adaptor/signalling proteins also decorate this complex. These include neuronal nitric oxide synthase (nNOS) which creates nitric oxide a neurotransmitter which regulates synaptic signalling and muscle contractions in NMJ, alongside regulating oxygen usage

in muscle sarcolemma as well as all neuromuscular tissues (Adams et al., 2008; Chang et al., 1996; Mungrue and Bredt, 2004). Other signalling proteins include the growth factor receptor-bound protein 2 (Grb2) (Yang et al., 1995a) which is involved in actin organisation as well as being involved in cellular signalling (Giubellino et al., 2008), and α-Catulin (Oh et al., 2012) which can all interact with the DAPC core proteins and aid in the regulation and transduction of physical and chemical signals.

The importance of the DAPC's role in muscle/NMJ maintenance and formation became evident when ablation of dystrophin or other core DAPC proteins can cause Duchenne muscular dystrophy (DMD) (Ervasti et al., 1990), a condition that causes muscle weakness and atrophy in skeletal and cardiac muscle (Isaac et al., 2013; Matsumura et al., 1992; Ohlendieck and Campbell, 1991). Mutations in several regulators of core proteins of the DAPC can lead to other myopathies such as Walker-Warburg syndrome (WWS) a muscular dystrophy which can cause abnormalities in the eye and brain. WWS can be caused through mutations in a glycosylation enzyme protein O-mannosyltransferase 1 (POMT1) which causes hypoglycosylation of α-dystroglycan resulting in reduced ECM binding (Van Reeuwijk et al., 2005).

The large and varied number of myopathies associated with mutations in the DAPC is due to the many overlapping interactions between DAPC proteins. Whilst dystrophin acts as the main scaffold in the DAPC there are many other protein interactions within the DAPC that regulate and maintain the whole complex and as such causes the many types of myopathy.

The key protein in the DAPC is the 427 kDa dystrophin protein, which acts as the main scaffolding/signalling hub in the DAPC much like talin in FACs. Dystrophin has a large

central 24 Spectrin like repeat domain (Koenig and Kunkel, 1990), each made up of a triple helix coiled coils giving dystrophin a more flexible linker like structure rather than a solid rod domain. Dystrophin contains multiple domains each with unique binding partners such as actin and a multitude of DAPC core proteins (figure 11). The two actin binding domains are located at the N-terminal (Rybakova et al., 1996) and within the 11-15 domain of the Spectrin like repeats (Amann et al., 1998). Dystrophin contains a binding domain at the end of the 24th Spectrin like repeat for the transmembrane receptor protein β-dystroglycan (Jung et al., 1995), that with its glycosylated α-dystroglycan partners mediate the connection between ECM ligands such as Laminin and the DAPC.

Dystrophin also contains binding domains for two adaptor proteins Syntrophin (Yang et al., 1995b) and α-dystrobrevin (Sadoulet-Puccio et al., 1997), which link dystrophin to the tetrameric transmembrane sarcoglycan proteins. Syntrophin acts by binding to dystrophin and recruiting multiple signalling proteins to the DAPC, such as nNOS (Hillier et al., 1999) and Grb2 (Oak et al., 2001).

α-dystrobrevin like syntrophin can recruit signalling and structural proteins to the DAPC such as Grb2 (phospho-dependent), α-catulin (phospho-independent) (Gingras et al., 2016) and importantly binds to transmembrane sarcoglycans (Yoshida et al., 2000). Sarcoglycans appear to strengthen the DAPC through intracellular interaction with α-dystrobrevin and extracellular interactions with α-dystroglycan through a mediating protein called Biglycan (Bowe et al., 2000; Rafii et al., 2006).

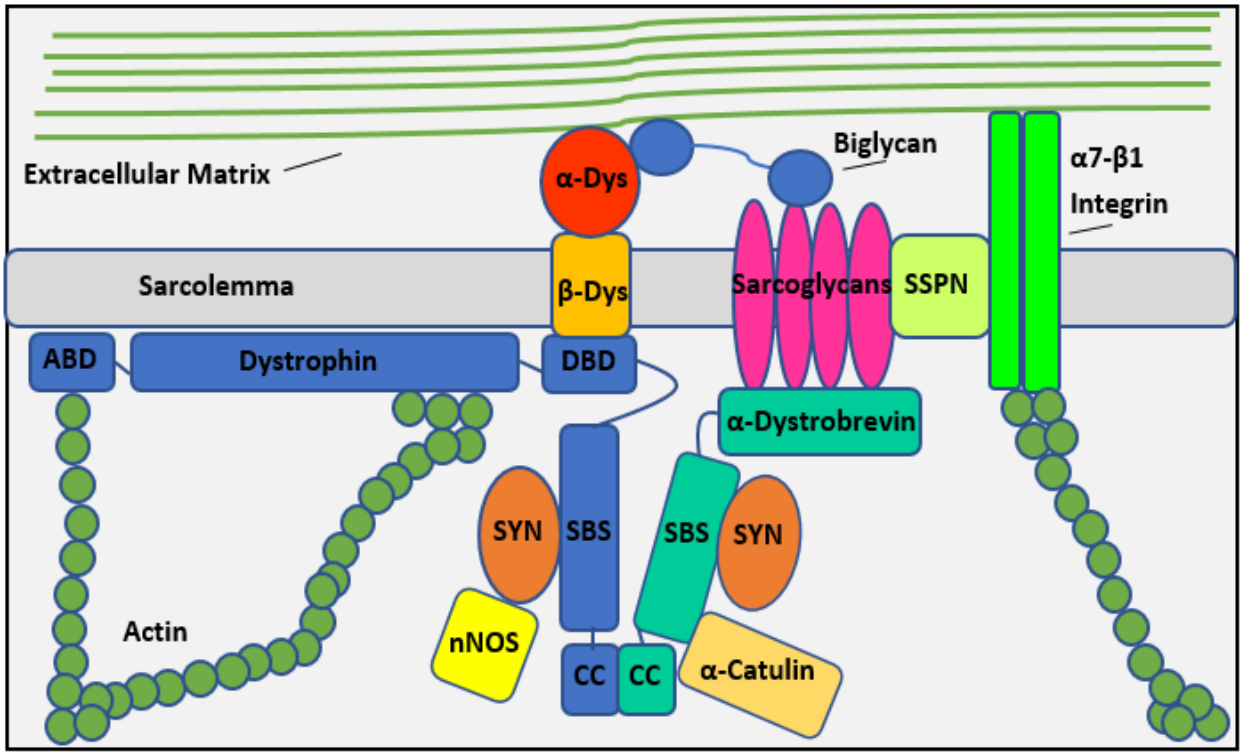

Figure 11-Dystrophin associated protein complex (DAPC) complex interaction with extracellular matrix mainly composed with Laminin and Collagen VI across the Sarcolemma membrane. Actin binding domain (ABD), dystroglycan binding domain (DBD), syntrophin binding domain (SBS), coiled coil domain(CC).α/β-Dystroglycan (α-DYS,β-DYS), neuronal nitric oxide synthase (nNOS), Sarcospan (SSPN), Syntrophin (SYN). Redrawn from Allen et al., 2015.

Sarcoglycans are also associated with another transmembrane protein Sarcospan (SSPN). Although the role of the SSPN is currently unknown in the DAPC, absence of SSPN causes autosomal recessive limb girdle muscular dystrophies which cause muscular atrophy in the hip and shoulder areas.

All these interactions maintain and regulate the DAPC integrity and disruptions in many of the core and signalling proteins result in myopathies.

1.7.2 α-Catulin

α-Catulin is an 82 kDa adaptor/signalling protein associated with the DAPC where it aids in the localisation and stability of the DAPC alongside acting as a regulatory signalling protein for the complex. α-catulin binds numerous DAPC core proteins such as α-and β-syntrophin, dystrophin, utrophin (Lyssand et al., 2010) and α-dystrobrevin, its structure and many binding partners have shown that α-catulin plays a larger role in protein localisation and cellular signalling not only in the DAPC.

α-Catulin is mainly comprised of three main domains an N-terminal α-catulin head (ACH) (1-283), a middle-coiled coil domain (307-528, CC) and a C-terminal α-catulin tail domain (ACT) (533-731) (figure 12).

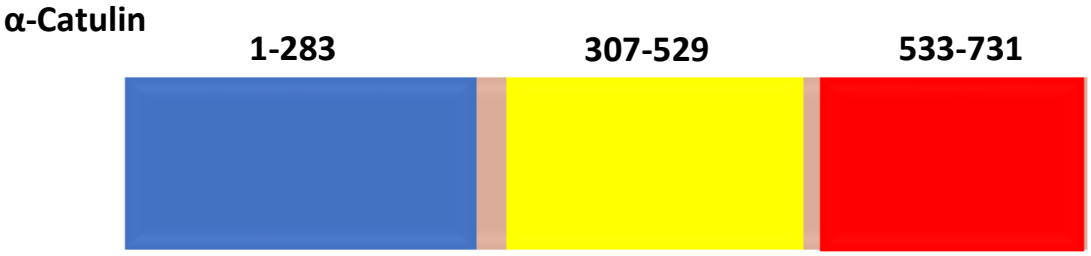

Figure 12-Full length α-Catulin domain boundaries of the ACH (blue), middle coiled coil domain (yellow) and ACT (red).

α-Catulin can bind to many DAPC core proteins, but it is the association with one specific isoform of α-dystrobrevin, α-dystrobrevin-1 contributes to DAPC localisation and stability. α-dystrobrevin-1 contains an additional 176 amino acid extension at its c terminal which contains three regulatory tyrosine residues which are required to bind proteins such as Grb2 and α-catulin (Gingras et al., 2016). α-Catulin binding to α-dystrobrevin-1 is phospho-independent, its binding region has been mapped to the very C-terminal of α-dystrobrevin-1 (468-590) a region not found in other α-dystrobrevin

isoforms and the ACH (1-377). This association between α-dystrobrevin-1 and α-catulin has been shown to be vitally important in the localisation and stabilisation of the DAPC to the cell membrane, although complexes can form from DAPC proteins they are dispersed and not localised at costameres or NMJs (Oh et al., 2012). α-catulin has also been shown to increase sensitivity of DAPC associated α1D-adrenergic receptors, key in cardiovascular functions such as blood pressure and vascular integrity and maintenance, It does this by recruiting effector proteins into the DAPC enhancing its role as a membrane associated signalling hub (Lyssand et al., 2010).

α-Catulin aids the localisation of calcium-dependent potassium (BK) channel SLO-1, channels important in the regulation of action potentials. In muscle SLO-1 channels are associated to the DAPC through a mediator protein SLO-1 interacting protein (ISLO-1) which binds through a PDZ domain to syntrophin (Kim et al., 2009). α-catulin knockouts showed a lack of SLO-1 localisation indicating α-catulin's role in DAPC stabilisation and recruitment. In neurons however α-catulin aids in SLO-1 localisation but through an independent method not linked to the DAPC (Abraham et al., 2010).

α-catulin acts as a scaffold for the Rho specific guanine nucleotide exchange factor Lbc with α-catulin (34-524) binding to Lbc (418-651) allowing α-catulin to regulate Rho signalling, which is important in cell actin/myosin based adhesion, apoptotic genes and cell differentiation (Park et al., 2002).

As α-catulin acts as a scaffold for Rho signalling its presence in the cell has been shown to increase migration significantly and siRNA knockouts of α-catulin show diminished motility. α-catulin interestingly has also been linked to neural tube closure in morphogenesis, its association with the Rho signalling pathway and in particular actin

and phosphorylated myosin Light Chain 2 (P-Mlc2) have meant α-catulin depletion from mouse embryonic stem cells (ES) leads to failure of neural tube closure and death very early in embryogenesis at day E10.5 (Karpińska et al., 2020).

α-Catulin additionally binds through a region in its tail domain (647–734) to Ik-Bb (466-756), Ik-Bb being an inhibitor of the Nf-Kb family of transcription factors (Wiesner et al., 2008). The Nf-Kb family having control over a wide range of genes including ones for ,adhesion, cell motility, cell survival, differentiation, and some adaptive and innate immune response genes.

This crosstalk between the Rho signalling pathway and the NF-Kb pathway has been linked to α-catulins role in tumorigenesis, notably in Melanomas and Squamous cell carcinomas (Cao et al., 2012; Kreiseder et al., 2015; Zhang et al., 2016). α-Catulin knockouts have been seen to arrest cell proliferation and induce senescence (Fan et al., 2011) alongside being found to be highly expressed at the tumour invasion front (Cao et al., 2012). This contributes to tumour cells transformation into a more mesenchymal state indicating α-catulin as an oncoprotein.

While α-catulin has been mostly associated with the DAPC, it plays a larger role in actin/actomyosin reorganisation and gene regulation in the cell regarding cell motility and survival. Its homology to vinculin and α-catenin (Janssens et al., 1999) may reveal additional binding interactors and perhaps indicate α-catulin has a larger role in the crosstalk of adhesion/signalling complexes.

1.7.3 Vinculin Superfamily-Vinculin/α-Catenin/α-Catulin

Vinculin shares structural and sequence homology with α-catenin (Identity 22.2% Similarity 36.4%) and α-catulin (Identity 17.6% Similarity 34.0%), α-catenin and α-catulin themselves share higher levels of homology (Identity 24.5% Similarity 40.6%) using Emboss water sequence alignment (Madeira et al., 2019). α-catenin and α-catulin are more closely related to each other phylogenetically with vinculin being more distantly related (figure 13) (Dereeper et al., 2008). All three proteins are associated with

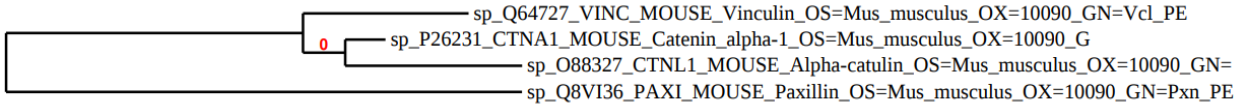

Figure 13-Phylogenetic tree of mouse (*Mus musculus*) vinculin, α-catenin, α-catulin and Paxillin (outgroup) indicating that all three-show high evolutionary homology but that vinculin is a more distant relative to both α-catenin and α-catulin. Taken from Phylogeny.fr

membrane associated adhesion/signalling complexes with vinculin in FACs, α-catenin and vinculin being associated in cadherin complexes (Watabe-Uchida et al., 1998) and α-catulin with the DAPC.

Several of vinculins domains appear to be shared between α-catenin and α-catulin, with notable exceptions as seen in the multiple sequence alignment (MSA) using T-coffee (figure 14) (Di Tommaso et al., 2011). α-Catenin shares all vinculins domains except for the VD2 domain, with α-catulin lacking the VD2 and VD4 domains (figure 15). Secondary structure prediction using PSIPRED for both ACH and VD1 secondary structures shows that both the share 8 helices structure as seen in VD1 (Note PSIPRED shows 8 helices for VD1 and ACH but from X-ray structures VD1 is known to have 7 helices not 8). The tail domains of both α-catulin and vinculin also share the characteristic 5 helices pattern making up the 5-helix bundle (Jones, 1999) (figure 16).

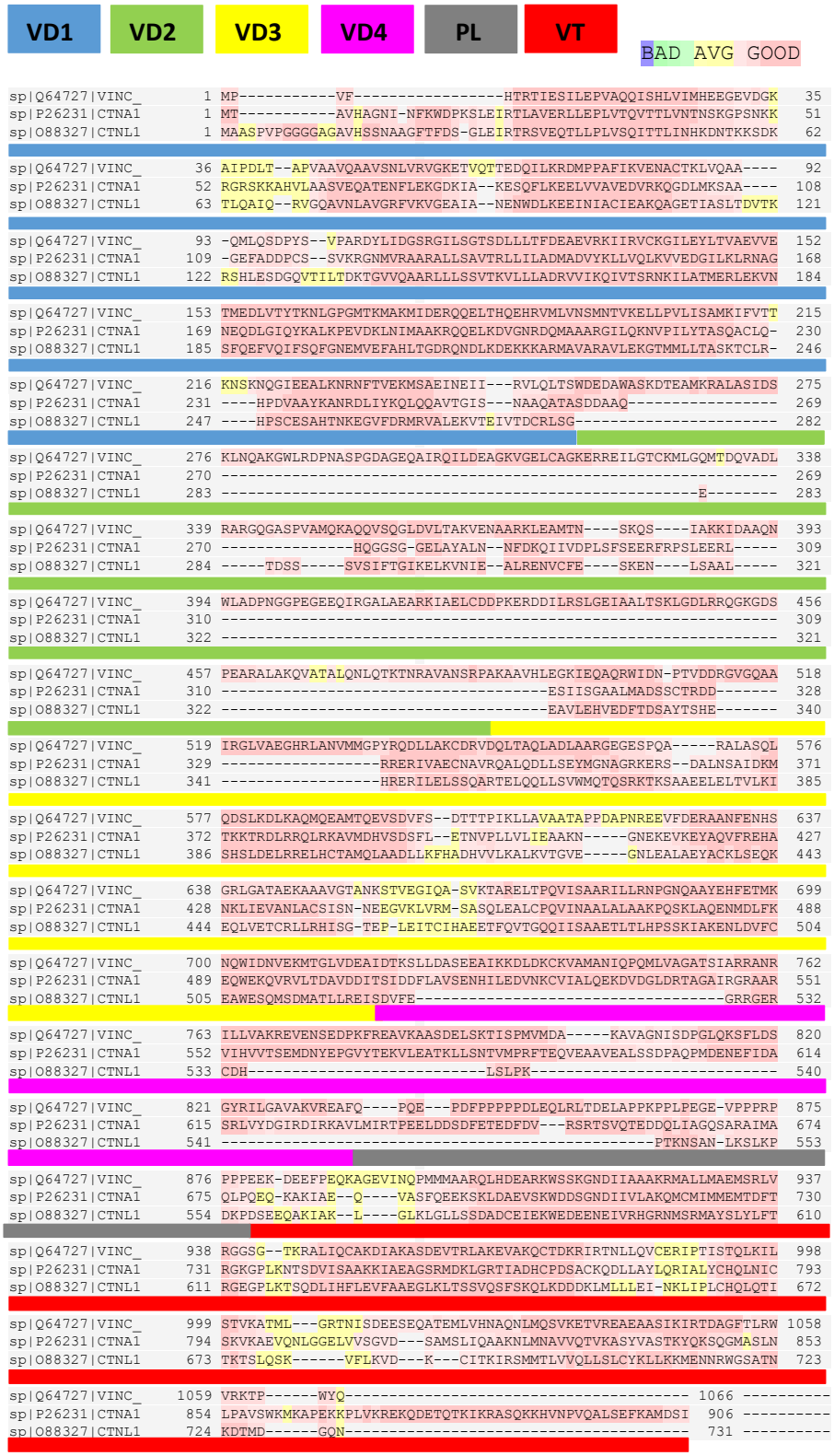

Figure 14-T-Coffee: a web server for the MSA of Vinculin=VINC, α-catenin=CTNA1, α-catulin=CTNL1 with vinculin domains overlaid, with added colour conservation.

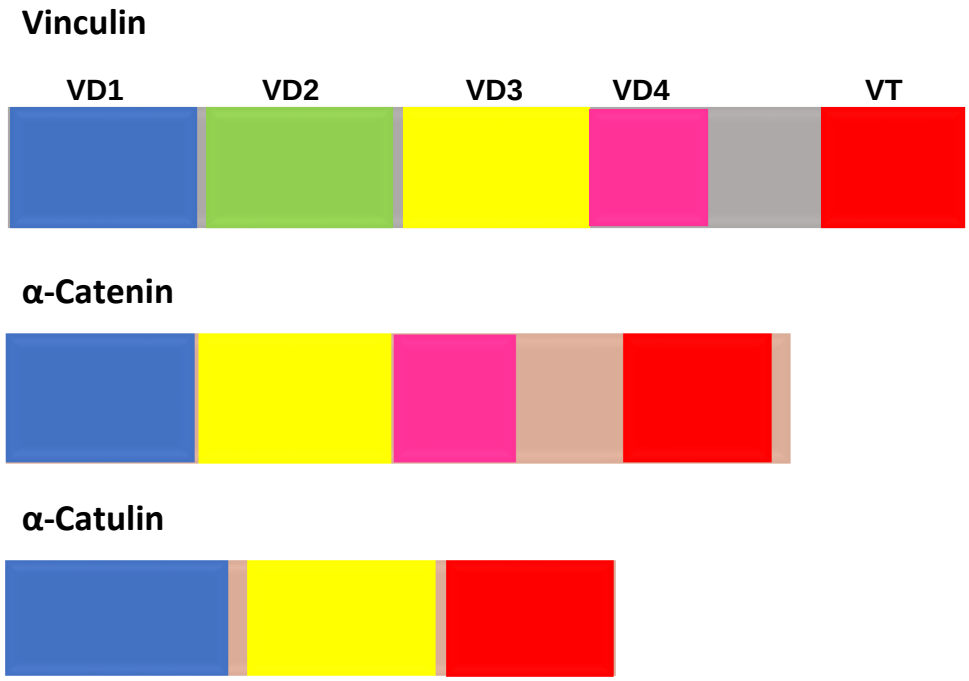

Figure 15-Domains appear to be shared between the three vinculin superfamily proteins, with α-catenin lacking VD2 and α-catulin lacking both VD2 and VD4. Notably all three conserve the VD1,VD3 and VT domains, these domains have key binding interactions across the three proteins.

In both the vinculin and α-catenin the tail has been shown to be directly involved in F-actin binding (Rimm et al., 1995) and in the case of vinculin also participates in autoinhibition (Bakolitsa et al., 2004; Izard et al., 2004). The N-terminal VD1 domain of vinculin has been shown to bind to VBS present in talin, which aid in strengthening and regulating FACs.

α-Catulin has been the least studied of the three in terms of biochemistry, the regions of high homology between α-catenin and vinculin in particular raises the possibility that α-catulin could interact with some of the vinculin binding proteins.

.

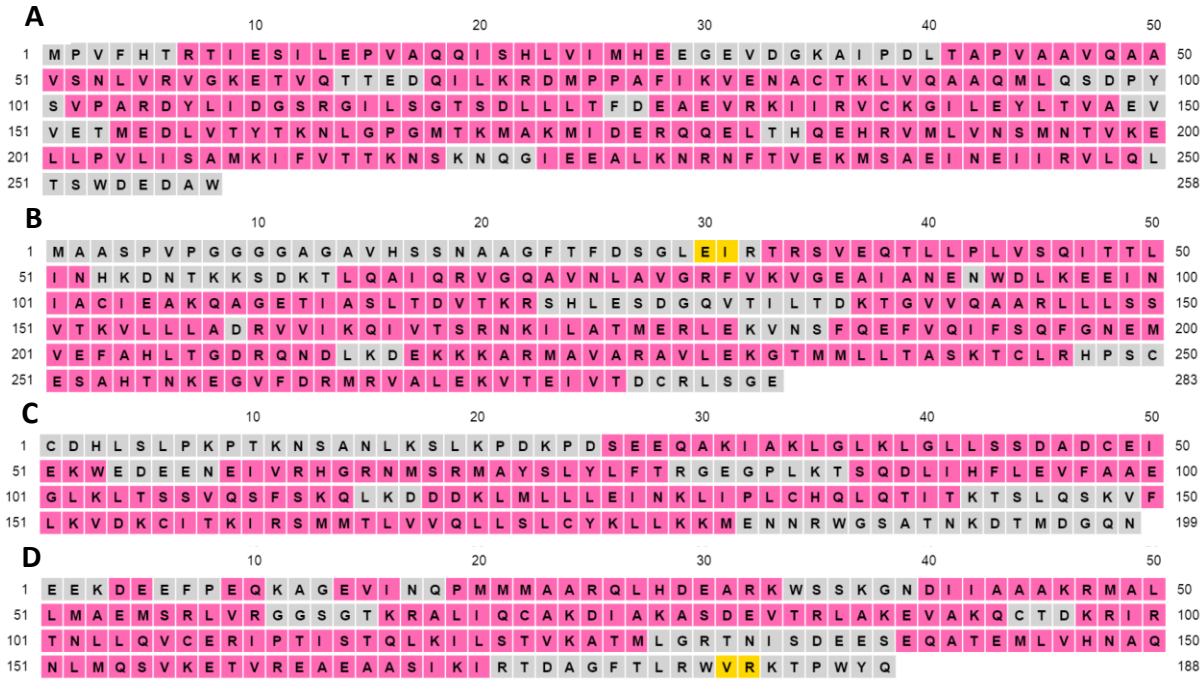

Figure 16-Secondary structure comparison using PSIPRED between VD1 (A) and the ACH (B), which show a conservation of eight α-helixes of similar length and also between the ACT (C) and the VT (D) which shows a conservation of five α-helixes again of similar length.

This project aims to biochemically characterise α-catulin and determine whether α-catulin shares binding partners associated with vinculin. Some possible interactions that are to be explored are,

1) Can the ACH interact with VBSs present within talin's helical bundles like VD1?
2) Is it possible for the ACT to enable α-catulin to exist in an autoinhibited state through ACH interactions or possibly interact with VD1 domain of vinculin?
3) Also, can the ACT domain interact with actin as is seen in both VT and α-catenin?
4) Finally, can the ACH or ACT domains interact with paxillin?

2 Materials and methods

2.1 Preparation of calcium competent Dh10β cells

DH10β cells were spread onto lysogeny Broth (LB) agar plate without antibiotics and left overnight at 37°C. A single colony was used to inoculate a 5 ml overnight culture of LB without antibiotics and left overnight shaking at 37°C. 2x 100 ml of LB were prepared in 250 ml flasks and 1 ml of overnight culture was added to each flask (1:100 dilution) without antibiotic. These were incubated at 37°C 160 rpm until an optical density (OD) (set at 595 nm) of 0.6-0.8 was reached whereupon they were removed and placed on ice for 10 minutes. The cells were centrifuged at 700 x g (2510 rpm in a Hettich Rotanta 460 R centrifuge) 4°C for 10 minutes, the supernatant was then removed, and the pellet resuspended in 10 ml of ice-cold Calcium/glycerol buffer (0.1 M CaCl2, 10% w/v glycerol, filter sterilised) and was left on ice for 15 minutes. The culture was centrifuged as above, and the cells resuspended in 1 ml of the ice-cold calcium/glycerol buffer. The cells were aliquoted into 40 µl aliquots in ice cold 1.5 ml Eppendorfs and flash frozen in liquid nitrogen and stored at -80°C.

2.2 Molecular biology-PCR/cloning

2.2.1 Primer design

Several constructs were required to be subcloned into differing vectors, be it for aiding in solubility or for the requirements of the vector plasmid. Both restriction enzyme digest and Gibson assembly types of cloning were attempted, primers for each construct were designed using ApE plasmid editor (see tables 1 and 2 respectively).

Table 1-Primers designed for restriction digest cloning using the ApE primer design software. Each construct requires both forward 5'-3' and reverse 5'-3' reverse complementary primers designed around the restriction digest sites specified by each restriction enzyme.

Restriction digest Constructs	Vector	Restriction enzymes	Forward Primer 5'-3'	Reverse Primer 5'-3' (Reverse complementary)
C. caviae TarP VBS1-3	pGEX	NheI/SalI	AA GCTAGC GATCTGCATGGTG CAGC	AA GTCGAC TTAAACTTTGCTCAGG G
ACH (1-258)	pGEX	NheI/SalI	AA GCTAGC ATGGCAGCAAGTC CG	AA GTCGAC ATTCACCGCTCAGAC G
ACH (1-258)	pET-21a	NdeI/XhoI	AA CATATGATGGCAG CAAGTCCGGTTCC AGG	AA CTCGAGTTCACCGCT CAGACGACAATCGG

Table 2-Primers for Gibson assembly cloning were designed using the ApE primer design software. Each construct requires four primers, two for the construct itself and two for the vector for which the construct is to be cloned into. The construct and vector each require forward 5'-3' and reverse 5'-3' reverse complementary primers.

Gibson assembly Constructs	Vector	Vector primer Fw 5'-3'	Vector primer Rev (5'-3' Reverse complementary)	Construct primer Fw 5'-3'	Construct primer Rev (5'-3' Reverse complementary)
α-catulin full length (1-731)	pET151-avi-2I27-mR6-2I27-spy	ACGACGGCAACCTCGAGGGGGGTGGTTCAGGACTGATTGAGGTAGAGAAAC	GAAGCGGCCATAAGCTTTCCGCTACCGCCTCCCAGCTCTTTCACTTTCAGG	GAAAGCTTATGGCCGCTTCTCCAGTCCCGG	CTCGAGGTTGCCGTCGTCCTTGAAGAAGATGGTGC
α-catulin 'VD1-3' (1-529)	pET151-avi-2I27-mR6-2I27-spy	AAGGAAGACGACTCGAGGGGGGTGGTTCAGGACTG	CGGGACTGGAGAAGCGGCCATAAGCTTTCCGCTAC	GAAAGCTTATGGCCGCTTCTCCAGTCCCGG	CTCGAGTCGTCTTCCTTCAAACACATCACTGATTTCCCTTAGCAGCGTCGCCATGTC
α-catulin 'vd3' (307-529)	pET151-avi-2I27-mR6-2I27-spy	GGAAGACGACTCGAGGGGGGTGGTTCAGGAC	GGTTCTCTTTGGACTCAAAGCAAACATTCTCAAGCTTTCCGCTACCG	GAAAGCTTGAGAATGTTTGCTTTGAGTCCAAAGAGAACCTTTC	CTCGAGTCGTCTTCCTTCAAACACATCACTGATTTCCC
α-catulin 'VBS domain' (284-615)	pET151-avi-2I27-	CTCTGTATTTATTTACTAGAGGAGAG	GTAAAAATGCTGACAGATGAGCTGTCGGTA	GCGGAAAGCTTACCGACAGCTCATCTG	CTCGAGTGGCCCCTCTCCTCTAGTAAATAA

	mR6-2I27-spy	GGGCCACTCGAGGGGGGTG	AGCTTTCCGCTACCG	TCAGCATTTTTACTG	ATACAGAGAATAGGCC

2.2.2 PCR

To amplify the insert and vector in the Gibson assembly case the DNA must be amplified using PCR, a 50 µl total mixture was used with the following components and placed in the thermal cycler (see table 3).

Table 3-The constituents of a PCR mixture, this is a standard protocol but changes to primer concentration can be made if unsuccessful.

PCR mixture Components	Volume µl (Final concentration)
Pfu DNA polymerase 10x buffer with MgSo4 (Promega)	5 (1x Final concentration)
DNTP (Invitrogen)	1 (100 mM Each)
Forward primer (IDT)	1 (Final concentration 100 µM)
Reverse primer (IDT)	1 (Final concentration 100 µM)
DNA template	1 (Final concentration 100 – 200 ng/µl)
Pfu DNA polymerase (added after DNTPs) (Promega)	1 (Final concentration 1.25µ/50µl)
Sterilised water	40

The thermal cycling conditions for each construct remain constant apart from the annealing temperatures and extension times which vary between constructs due to

differing primer annealing temperatures and the length of the constructs with larger DNA sequences to copy (see table 4).

Table 4-PCR stages and conditions for each construct, the pET151-avi-2I27-mR6-2I27-spy vector was used for each Gibson assembly construct and as required the same conditions for each

Construct	vector	Initial denaturation	Annealing	Extension	Final extension	Hold
TarP VBS1-3 (*C. caviae*)	pGEX	95°C for 1.5 min	52°C for 30 sec	73°c for 2 min	73°c for 5 min	4°C indefinitely
ACH (1-258)	pGEX	95°C for 1.5 min	65°C for 30 sec	73°C for 2 min	73°C for 5 min	4°C indefinitely
ACH (1-258)	pET-21a	95°C for 1.5 min	65°C for 30 sec	73°C for 2 min	73°C for 5 min	4°C indefinitely
α-catulin full length (1-731) construct	pET151-avi-2I27-mR6-2I27-spy	95°C for 1.5 min	65°C for 30 sec	73°C for 4 min	73°C for 5 min	4°C indefinitely
α-catulin 'VD1-3' (1-529) construct	pET151-avi-2I27-mR6-2I27-spy	95°C for 1.5 min	65°C for 30 sec	73°C for 4 min	73°C for 5 min	4°C indefinitely
α-catulin 'VD3'	pET151-avi-2I27-	95°C for 1.5 min	65°C for 30 sec	73°C for 2 min	73°C for 5 min	4°C indefinitely

(307-529) construct	mR6-2I27-spy					
α-catulin 'VBS domain' (284-615) construct	pET151-avi-2I27-mR6-2I27-spy	95°C for 1.5 min	65°C for 30 sec	73°C for 2 min	73°C for 5 min	4°C indefinitely
pET151-avi-2I27-mR6-2I27-spy vector (All Gibson assembly constructs)	pET151-avi-2I27-mR6-2I27-spy	95°C for 1.5 min	65°C for 30 sec	73°C for 14 min	73°C for 5 min	4°C indefinitely

To visualise the amplified DNA products the samples were run on a 1% agarose gel which was made by mixing 0.6 g of agarose and 60 ml of 0.5x TAE buffer (50x TAE 50 mM EDTA, 1 M Glacial Acetic acid and Tris 2 M) in a small conical flask and microwaved at full heat for 1 minute. This mixture was poured into a DNA gel box and 1000x gel stain (Ultraviolet (UV) sensitive) was added alongside a comb to create the wells, the gel was left for 30 minutes to set. To run an DNA sample 6x DNA dye was added to the sample in a ~1:6 ratio of dye to sample and load the sample into the wells left by the combs. A DNA ladder was also run to verify the sizes of the DNA bands visualised by the gel.

The gel was run for 45 minutes using the TAE setting 50 hertz (Hz) and then visualised under a UV gel dock to observe the DNA bands. The amplified DNA may contain impurities from cross contamination and as such requires purification and cleaning.

250 µl of PB buffer were added to the 50 µl PCR product and spun at 13k rpm (Thermo fisher 24x 1.5/2 ml rotor) in a QIAquick column for 60 seconds discarding the flow through. 750 µl of PE buffer was added to the QIAquick column and spun again for 60 seconds and the flow through discarded, the column was spun again to remove any residual buffer. The column was then placed into a 1.5 ml Eppendorf and 50 µl of EB was added and left for two minutes before spinning again for 60 seconds.

Table 5-Restriction digest conditions for each restriction enzyme

Component	**Final volume**	**Final concentration**
PCR DNA	X µl	Variable
Restriction buffer 10x	10 µl	1x
Restriction enzymes		
NHEI 10 u/µl (Promega)	2 µl	20u
SalI 10 u/µl (Promega)	2 µl	20u
XHOI 10 u/µl (Promega)	2 µl	20u
NDEI 10 u/µl (Promega)	2 µl	20u
Sterilised DH_2O	Make up to 100 µl	

The flow through now contained the purified PCR product, its concentration now be determined using a Nanodrop. For restriction digest cloning restriction enzymes are required to cleave the PCR vector and insert so that they able to be ligated together later. The digest mixtures were prepared in 0.5 ml Eppendorfs and mixed thoroughly as restriction enzymes tend to sit at the bottom of the Eppendorfs. The digest mixtures were left at 37°C for 3 hours, mixing them every hour to ensure the restriction enzymes have not settled (see table 5).

To visualise the digests 15 µl of 6x DNA dye was added to the mixtures and loaded across 4-5 wells of the agarose gel and run and visualised as before. The DNA was extracted from the gel using a QIAquick Gel extraction kit following manufacturer's instructions and run on an agarose gel to observe band size.

2.2.3 Ligation

The digested PCR vector and insert were ligated together using the components listed in table 6, the concentrations of both the vector and insert were measured using the Nanodrop, the insert to vector ratio should be roughly 3:1 although the ratios can be altered if needed (see table 6). The ligation mixture was then left at 4°C overnight, then the next day the mixture was transformed into DH10β E.coli cells as explained above. At the end of the next day a 5 ml LB + chosen antibiotic (100 mg/ml)+a single colony was left overnight, the next morning a QIAprep spin Miniprep Kit (Qiagen) miniprep was used to extract the DNA according to manufacturer's instructions and the DNA stored at -20°C.The DNA was tested through a test restriction digest or sent for Sanger sequencing using a forward and/or reverse primer to fully sequence the new plasmid.

Table 6-Ligation conditions, each construct will have differing DNA concentration depending on how successful the PCR was. A ratio of 3:1 insert to vector should be used and altered if unsuccessful.

Component	Volume	Concentration
T4 DNA ligase 3 u/µl (Promega)	1 µl	3 u
10x Ligase buffer (Promega)	1 µl	1X
Insert	Variable	Variable
Vector	Variable	Variable
Sterilised DH_2O	Make up to 10 µl	

2.2.4 Gibson assembly

Gibson assembly is a cloning technique that does not rely on specific restriction sites to enable the insert to be ligated into the new vector. Gibson uses multiple overlapping DNA fragments in this case two for each of the insert and vector alongside three enzymes T5 Exonuclease, Phusion DNA Polymerase and Taq DNA Ligase to fully ligate the insert into the new vector. Gibson assembly was attempted on the constructs listed in table 2, using the Gibson Assembly® Protocol (E5510) (NEB) following the manufacturer's instructions.

2.3 Cell culture

2.3.1 Expression of recombinant polypeptide constructs

Both Ampicillin and isopropyl β-D-1-thiogalactopyranoside (IPTG) were used at a final concentration of 100 mg/L from 1000x stock 0.2 µm filter sterilised.

To express all the recombinant protein constructs (see table 7) 2 µl of DNA was added to 20 µl of BL21(DE3) competent E.coli cells and left on ice for 30 minutes. The BL21

cells were placed in a 42°C water bath for 40 seconds and placed back on ice for 2 minutes. 200 µl of LB was added to the BL21 cells and left at 37°C for one hour. 100 µl of the BL21 cells can be plated onto LB Agar plates (10 g tryptone,5 g yeast extract 5 g NaCl,15 g agar made up to 1 litre with Milli Q water) with ampicillin for antibiotic selection and left in a non-shaking incubator overnight at 37°C. The remaining 100 µl of BL21 cells can be added to 10 ml of LB in a 50 ml falcon tube containing ampicillin at a final concentration of 100 mg/l and incubated at 37°C 160 rpm in a shaking incubator overnight. 750 µl of overnight LB was added to 300 µl of 60% glycerol stock, vortexed and stored at -80°C. The remaining 9.25 ml of overnight starter culture can be used to inoculate two 500 ml autoclaved LB flasks.

Table 7-Recombinat polypeptide constructs which were transformed into BL21(DE3) E.coli cells and glycerol stocks made for storage at -80°C.

Constructs	Residues	Plasmid
Mouse VD1	1-258	pET151
Mouse VD1 A50I	1-258	pET151
Mouse VD1 P15L	1-258	pET151
Mouse VD1 W253X	1-252	pET151
Mouse ACH	1-283	pET151
Mouse ACT	533-731	pET151
Mouse VTΔlinker	879-1066	pET151
TarP VBS1-3 (*C. caviae*)	745-868	pET151
TarP VBS1-3 GST (*C. caviae*)	745-868	pGEX

2.3.2 Growth of cell cultures

Ampicillin was added to autoclaved LB flasks and 4-5 ml of overnight LB starter culture was used to inoculate 500 ml of LB. These were incubated at 37°C 160 rpm for approximately 4 hours, checking the OD_{595} once per hour using a spectrophotometer until OD_{595} 0.6-0.8 was achieved. Once reaching OD_{595} 0.6-0.8, IPTG was added to the flasks to induce protein production. 500 µl samples were taken once an OD_{595} of 0.6-0.8 was reached and again each hour for 3 hours. Each sample was centrifuged for five minutes at 13k rpm (Thermo fisher 24x 1.5/2 ml rotor) and the supernatant discarded, 50 µl of reducing sample buffer (RSB) was added and heated at 90°C for 3-5 minutes and placed in a freezer at -20°C or room temperature to be used for Sodium dodecyl sulphate (SDS) Polyacrylamide gel electrophoresis (PAGE) analysis.

2.3.3 Harvesting of cell cultures

After the induction period the cultures were poured into 500 ml centrifuge tubes and spun at 2831 x g (4000 rpm in a Beckman JA-10 rotor) for 15 minutes at 4°C. The supernatant was removed, the bacterial pellets were resuspended in 25 ml of an appropriate buffer and stored in a 50 ml falcon tube at -20°C.

2.3.4 Isotopically labelled protein expression

Samples that that were to run be in multidimensional NMR experiments were required to be isotopically labelled with ^{15}N Ammonium chloride. The cells were required to be grown in 2M9 minimal media (see table 8).

Table 8-(Top) Components of the 10x M9 salts, (bottom) Composition of M9 minimal media for isotopic protein expression.

Composition of 10x M9 salts solution pH 7.2 Autoclaved

Salt	**g of salt per litre of water**
$Na_2HPO_4.2H_2O$	66
KH_2PO_4	33
NaCl	5.5

Composition of M9 minimal media 0.2 µm sterile filtered

Component	**ml of solution per L of medium**
Milli-Q water (autoclaved)	887
10x M9 salts	100
1M $MgSO_4$ (autoclaved)	1
0.1M $CaCl_2$ (Autoclaved)	1
BME vitamins	1
Glucose	4g per litre

To maximise the growth of cells and to reduce the overall labelled compound used a condensation method was used that utilised the growing of unlabelled cells which were then condensed and transferred for growth in labelled media. A 4:1 condensation ratio of unlabelled media to labelled was used. 2x 10 ml Unlabelled LB overnight cultures were set up as previously mentioned with a scraping of the protein of interest glycerol stock alongside ampicillin. 5 ml of overnight culture was added per 500 ml autoclaved

LB media containing ampicillin. The cells were placed in an incubator at 37°C 160 rpm until an OD_{595} of between 0.6-0.8 was reached. Once the OD_{595} was reached the cells were centrifuged (3000 x g, 5 min at 4 °C) and then resuspended in 200 ml 10x M9 salts solution, centrifugation was repeated to wash the bacterial pellets of any remaining LB. The pellet was resuspended in 1 L of M9 minimal media and 1 g of ^{15}N Ammonium chloride (NH_4Cl) was added, (Note the NH_4Cl was purposely not included in the 10x M9 salts solution as it would require 11 g instead of 1 g, poignant if only performing limited numbers of experiments). The resuspended cells were left to acclimatise in M9 minimal media for 1 hour at 20°C, IPTG was then added, and the cells left incubating for approximately 15-20 hours at 18°C 160 rpm. Harvesting of the cells was performed as previously mentioned and the cells were resuspended in 25 ml of appropriate buffer and stored at -20°C.

2.3.5 Lysis of cells by sonication

The resuspended frozen bacterial pellets were thawed and lysed using 5 rounds of sonication using 30 second pulses at an amplitude 50% (14 Amps) for 5 minutes while continually being kept on ice. Length of sonication time may be in/decreased depending on the density of the bacterial cell pellet, but caution when increasing as overheating the cell lysate can occur degrading any protein present. Post sonication the lysed cells are poured into 50 ml centrifuge tubes and spun at ~48,000 x g at 4 °C for 30 min. The supernatant was stored in a 50 ml falcon whilst the bacterial pellet was discarded, 500 µl samples were taken of both supernatant and pellet as made as mentioned above.

2.4 Protein purification

2.4.1 Nickel ion affinity chromatography

2.4.2 Nickel Batch method

Nickel ion Affinity chromatography was used to purify any constructs tagged with a histidine tag (His-tag). HisPur™ Ni-NTA Superflow agarose slurry beads were added to a 50 ml falcon tube and washed with 20 ml of Nickel buffer A (20 mM tris, 500 mM NaCl, 20 mM imidazole pH 8) and centrifuged at 700 x g (2510 rpm in a Hettich Rotanta 460 R centrifuge) at 4°C for 2 minutes. Using a ratio of 1 mL HisPur™ Ni-NTA Superflow agarose slurry per litre of bacterial culture. The soluble cell lysate was added to the beads and left on a rocker to incubate for 20 minutes at room temperature, then centrifuged at 700 x g (2510 rpm in a Hettich Rotanta 460 R centrifuge) at 4°c for 3 minutes. The supernatant was removed, and the pellet resuspended with 20 ml of Nickel buffer A and centrifuged at 700 x g (2510 rpm in a Hettich Rotanta 460 R centrifuge) at 4 °c for 3 minutes. This process was repeated five times and subsequently once with wash buffer (20 mM Tris, 500 mM NaCl, 50 mM imidazole pH8). After this final wash 10 ml of the supernatant was kept and the rest discarded, the beads were resuspended in nickel buffer A and poured into an empty gravity flow column (Bio-Rad).The flow through may be collected and a sample taken to run on an SDS-page gel to ensure the protein of interest hasn’t been lost after the higher imidazole wash buffer. Nickel buffer B (20 mM Tris, 500 mM NaCl, 500 mM imidazole pH8) was added to the column and three 1 ml elutions were collected. Throughout the batch method samples were taken at specific steps for further SDS-PAGE analysis, 1, 2) after first Nickel buffer A wash both the supernatant and beads, 3, 4) after fifth Nickel

buffer A wash both the supernatant and beads, 5) after Wash buffer just supernatant and 6, 7, 8) each of the three 1 ml elutions.

2.4.3 Immobilised Nickel ion affinity chromatography

Nickel ion purification was also performed using an ÄKTA fast protein liquid chromatography (FPLC) system. Using the FPLC system a 5 mL HisTrap HP column was washed and equilibrated using Nickel buffer A and Nickel buffer B. The sample supernatant was loaded onto the column using a peristaltic sample pump and subsequently washed with 20 ml of Nickel buffer A. An imidazole gradient of Nickel buffer B was used to gradually reach a Nickel buffer B percentage that eluted the protein of interest. Samples of each elution can be taken and run on an SDS-PAGE for analysis if the elution peaks appear undefined or to check purity. The 5 mL HisTrap HP column was then washed with Nickel buffer A and stored in 20% ethanol.

2.4.4 Dialysis

If the proteins are required to be further purified through ion exchange chromatography dialysis into a lower salt buffer was required. The elutions were dialysed using Thermo Scientific SnakeSkin dialysis tubing (7000 MWCO) into five litres of Q-buffer A (20 mM Tris-HCl, 50 mM NaCl pH8) for proteins with an isoelectric point (pI) below 7, or S buffer A (20 mM phosphate, 50 mM NaCl, pH 6.5) for proteins with a pI of above 7. These were left overnight at 4°C with stirring, additionally if the His-tags were to be cleaved a TEV-protease was added.

2.4.5 PD-10 desalting column

An alternative to lengthy dialysis is a buffer exchange using a pd-10 desalting which can be used to quickly exchange a protein from one buffer to another, especially in removing one from a high imidazole after a nickel ion purification. A PD-10 column was equilibrated with 25 ml of an appropriate buffer and the flow through discarded. 2.5 ml of sample was added to the column (if under 2.5 ml use buffer to make up to 2.5 ml) and the flow through discarded. 3.5 ml of the buffer to be exchanged into was added and the flow through collected.

2.4.6 Batch GST-purification

Protein constructs containing a Glutathione *S*-transferase (GST) tag were purified using a batch method like the previously mentioned hit-tag method. Per 1 litre bacterial culture ~1 ml of Pierce™ Glutathione Superflow agarose slurry was added to a 50 ml falcon tube and the beads washed with 20 ml of 1x phosphate buffered saline (PBS) (10x stock concentration 100 mM NA_2HPO_4, 18 mM KH_2PO_4, 1.4 M NaCl pH 7.4) by mixing gently. This was centrifuged at 700 x g (2510 rpm in a Hettich Rotanta 460 R centrifuge) for 3 minutes at 4°C and the supernatant discarded.

The soluble cell lysate was then added to the washed beads and left to incubate for 1-2 hours at room temperature or if the protein is prone to degradation the same incubation period can be done at 4°C. Once fully incubated the sample is centrifuged at 700 x g (2510 rpm in a Hettich Rotanta 460 R centrifuge) for 3 minutes at 4°C and the supernatant removed, a sample of the supernatant was taken at this point for SDS-PAGE analysis. 25 ml of 1x PBS was added and the sample was centrifuged at 700 x g

(2510 rpm in a Hettich Rotanta 460 R centrifuge)) for 3 minutes at 4°C and the supernatant removed. This wash step was repeated 5 more times and a sample was taken after the last wash of both the supernatant and beads for SDS-page analysis. The beads were resuspended in 1x PBS and were now ready to use for a GST-pulldown experiment if required. If the GST tag is to be removed from the sample, a TEV protease was added and left agitating overnight at 4°C. The sample was then poured through a gravity column and the flow through collected as this now contained the protein of interest if the TEV protease had fully cleaved the protein from the beads. A sample for SDS-PAGE analysis was taken to confirm this. Note the TEV should also be in flow through.

2.4.7 Ion exchange chromatography

FPLC automated ion exchange chromatography was also performed to separate the proteins based on their charge. Each individual protein will have a unique pI at which the protein will have a net charge of zero. Inputting the amino acid sequence into ExPASy ProtParam (Wilkins et al., 1999) allowed the pI to be determined for each protein. If the protein had a pI of <7 then a negatively charged cation exchanger (Q-column) was used with Q-buffer A (20 mM Tris , 50 mM NaCl, pH8) and Q-buffer B (20 mM Tris, 1M NaCl,pH8). If the pI was 7> then an anion exchanger (S-column) was used with S-buffer A (20 mM phosphate pH 6.5, 50 mM NaCl) and S-buffer B (20 mM phosphate pH 6.5, 1 M NaCl).Note for proteins with a pI above 8 which were used for crystallography a MES-buffer A (20 mM MES-Hydrate pH 6.5, 50 mM NaCl) and MES-buffer B (20 mM MES-Hydrate pH 6.5, 1 M NaCl) was used to exclude phosphate ions. A Q-column can remove the TEV-protease and cleaved His-tag if used as they both

flow into waste and do not stick to the column. An S-column binds TEV-protease and as such the peaks were analysed and run on a gel to determine which fractions contain just the protein of interest.

Using the same FPLC procedure as the immobilised Nickel chromatography, the protein was loaded onto the column and an increasing salt concentration that eluted the protein of interest in 3 ml fractions. The fractions were analysed using SDS-PAGE. The proteins were either dialysed/buffer exchanged into another buffer, aliquoted out to be used or flash frozen with and kept at -20°C.

2.4.8 SDS-PAGE

10% SDS-PAGE gels of samples collected were run with SDS MOP buffer in a SureLock gel tank, set at 200 volts and 400 amps for 1 hour. Gels were stained with Coomassie blue and left for 1 hour, Coomassie blue destain was added to counterstain the gels and left for 1 hour. Coomassie destain was repeated twice before visualizing the gels.

2.5 Biochemical/biophysical assays

2.5.1 Fluorescently Labelling peptides

Peptides were labelled with fluorescein for use in fluorescence polarisation experiments.100 µM of the peptide was mixed together with 25 µl of fluorescein-5-maleimide dye, 5 µl TCEP (1 M stock), 2.5 µl of 20% Triton X and made up to 1 ml with 1x PBS. The mixture was covered in foil to block UV light and then left mixing for 2 hours at room temperature. A PD-10 column was equilibrated with 25 ml of 1x PBS and the labelled peptide was added, and the excess equilibration buffer allowed to flow

through. 2.5 ml of 1x PBS was then added to elute the labelled peptides and the flow through was collected, the labelled peptides typically eluted after the first 1 ml. The labelled peptides were prepared in 10 µl aliquots and flash frozen using liquid nitrogen and stored at -20°C.

2.5.2 Size exclusion chromatography-Gel filtration

Size exclusion chromatography (SEC) is a technique that allows separation of molecules based primarily on the molecular weight, shape, and hydrodynamic properties of the molecule. The Hydrodynamic properties of a molecule being solvent associated with the molecule. SEC works on the principal that molecules are passed through a column filled which contains a gel matrix of porous beads that have a very specific size arrangement. The separation of molecules occurs through the porous beads as large molecules do not diffuse into the porous matrix and are eluted early on, whereas small molecules diffuse into the porous matrix and are retained for longer periods resulting in later elution. Consequently, larger molecules being eluted before smaller molecules enables the molecules to be separated by size. Gel filtration is a specific type of SEC which uses a hydrophilic filled column with an aqueous mobile phase to elute the molecules.

Gel filtration was performed using a Superdex-200 size exclusion chromatography column (GE healthcare). 1x PBS buffer was set at a flow rate of 0.75 ml min^{-1} to equilibrate the column, 500 µl VD1 and ACT samples were both run individually at 56 µM. VD1 and ACT both at 56 µM were then incubated together at room temperature for 45 mins in a 1:1 ratio before being loaded.

2.5.3 Size exclusion chromatography with multiangle light scattering

To analyse the stoichiometry of the of the TarP VBS1-3 with VD1 SEC with multiangle light scattering (SEC-MALS), utilising SEC as explained above to separate the proteins according to size whilst the MALS detects light scattered by the proteins after they are eluted from the column allowing the proteins precise molecular weights to be determined. This technique can be used for determining the stoichiometry of multiple monomers binding to a single secondary protein.

The Superdex-200 size exclusion chromatography column (Ge healthcare) and MALS machine (Viscotek SEC-MALS 9 and Viscotek RI detector VE3580 (Malvern Panalytical) was equilibrated with 1x PBS buffer at a flow rate of 0.75 ml min^{-1}, the making sure the flow is continuous for at least three hours before running any samples to allow MALS and RI (refractive index) signals to stabilise. 40 µM VD1 was run singularly and then with TarP VBS1-3. VD1 and TarP VBS1-3 were then incubated for one hour at room temperature. (The concentration of the TarP VBS1-3 was estimated based on protein concentration determined on agarose gels (as it contains no UV absorbing residues) alongside serial dilutions of VD1). This was done as to achieve a 1:3 ratio between TarP VBS1-3 and VD1 respectively to allow the full extent of the stoichiometry of the TarP VBS1-3 VD1 binding sites to be apparent. 40 µM VD1 was determined to be in excess of this 1:3 ratio with TarP VBS1-3. Both samples were run at the same constant 0.75 ml and eluted in 500 ml aliquots. The elution profile was then analysed using the OMNISEC software to identify individual protein peaks and possible complexes.

2.5.4 GST-Pulldowns

To identify any binding partners for a GST-tagged protein a technique known as a GST-pulldown was attempted which utilised the Glutathione bound GST tagged proteins previously purified and a query protein to identify any interactions while the GST-protein is still attached to the Glutathione beads. If interactions are seen, different ratios 1:1, 1:2 etc can aid in determining any stoichiometry in binding when it is shown a protein may have multiple binding sites for the same protein. 50 µl of the TarP VBS1-3 GST loaded beads in 1x PBS was mixed with 150 µl of VD1 in an Eppendorf at 5 µM 1:1 ratio, 10 µM 1:2 and 1:3 15 µM, the 5 µM 1:1 ratio was predicted through optimisation with varying concentrations of VD1 to the TarP VBS1-3 GST on an SDS-page gel. The Eppendorfs were left to incubate on a rocker at 25°C for one hour. The samples were spun in a tabletop centrifuge at 700 x g (2510 rpm in a Hettich Rotanta 460 R centrifuge) for 5 minutes at 4°C and 50 µl of the supernatant was taken. The GST pellet was washed twice more with 1x PBS at 700 x g (2510 rpm in a Hettich Rotanta 460 R centrifuge)for 3 minutes at 4°C and the supernatant removed. A 10 µl sample of both the GST beads and the supernatant were taken and run of an SDS-PAGE as explained above.

2.5.5 Circular Dichroism

Far UV circular dichroism (CD) is an ideal technique for visualising secondary structures such as α-Helices, β-sheets, βTurns and random loops of proteins. The basis of CD is that proteins differently absorb right and left circularised polarised light through chiral chromophores that are present throughout amides groups along the polypeptide backbone of the protein. A proteins thermal stability can also be determined by

performing a melting curve, the change in CD signal can be followed over a temperature gradient. The binding of ligands to proteins can also be visualised as changes in protein secondary structure are evident in many binding events.

Analysis of ACT and VTΔlinker using CD was performed on a JASCO J-715 spectropolarimeter equipped with a JASCO PTC-423S temperature control unit. A Far UV CD spectrum was performed on both ACT and VTΔlinker at wavelengths 190-260 nm. Each protein was run at 20°C, 4 µM concentration dissolved in 1x PBS. A temperature melting curve was performed at temperatures ranging from 20-90°C with 1°C per minute increments. Both samples were blanked with 1x PBS buffer. All experiments were carried out using a 0.1 cm pathlength quartz cell.

2.5.6 Nuclear Magnetic Resonance spectroscopy

Nuclear magnetic resonance (NMR) is a technique that exploits the quantum nuclear spin properties of atoms when under a strong magnetic field. Using short radiofrequency pulses followed by relaxation periods it is possible to pass magnetisation from one nuclei to another and record the changes in environment. For 1D experiments the ^{1}H present in the backbone and chemical groups found throughout the protein are recorded, each peak corresponding to a unique ^{1}H environment. For 2D NMR experiments the protein is required to be isotopically labelled with either ^{15}N or ^{13}C. In ^{15}N labelled proteins each peak corresponds to a unique magnetic environment between the backbone amide ^{15}N and ^{1}H, alongside sidechain NH and NH_2 groups. Changes in the environment be it denaturation or ligand binding can be seen by shifts in a peaks position, important in determining the exact residues involved in ligand binding sites.

An ^{15}N ACT sample was grown up using the condensation method of isotopically labelled proteins as explained above and purified using nickel ion affinity and ion exchange FPLC. The sample was dialysed into phosphate buffer (50 mM NaCl, 20 mM sodium phosphate, 2 mM DTT pH 6.5). The NMR spectra were obtained using a Bruker AVANCE III 600 MHz spectrophotometer with Cryo Probe set at 298K. A 450 µl ACT sample which included 5% D2O was added to a Shigemi NMR tube and run at 50 µM concentration. 1D and 2D heteronuclear single quantum correlation (HSQC) experiments were performed to analyse ACT.

2.5.7 Fluorescence polarisation assays

A fluorescence polarisation assay works on the basis that when a fluorescently tagged peptide is excited by polarised light the light that is emitted is also polarised. A fluorescently labelled protein in solution tumbles however and causes a drop in the emission of polarised light. If when in solution however the fluorescently tagged peptide binds to a protein the peptide will tumble at a reduced rate and as such an increase in polarised in one direction is detected. This change in polarisation alongside a series of increasing protein concentrations can enable binding affinities to be generated.

Three peptides were coupled to a thiol reactive fluorescein tag to a C-terminal cysteine residue present in each peptide, the three peptides being paxillin LD2, TarP VBS1 and TarP VBS3. (Note TarP VBS2 peptide aggregated in solution so was not coupled).

Paxillin_LD2 (NLSELDRLLLELNC) *Homo sapiens* residues 141-153

TarP_VBS1 (LLEAARNTTTMLSKTLSKV-C) *C. caviae* residues 850–868

TarP_VBS3 (DLHGAAKGVADSLSNLLQAATP-C) *C. caviae* residues 745–766

The paxillin LD2 peptide were tested with the ACT and VTΔlinker sample and prepared in 1X PBS (140 mM NaCl, 100 mM Na_2HPO_4, 18 mM KH_2PO_4) and run at a stock concentration of 300 µM. TarP VBS1 and 3 were tested with VD1, prepared in 1X PBS and run at a stock concentration of 200 µM.

Each sample was titrated in 1x PBS using a constant 1 µM concentration of fluorescein-coupled peptide, with increasing protein concentration culminating in a final 100 µl final well volume. Each experiment was run at 25°C and in triplicate. The Data was recorded on a BMG LabTech CLARIOstar plate reader and the K_d calculated using GraphPad Prism software based on the one-site binding model.

2.5.8 X-ray crystallography

Multiple crystal screens were attempted for VD1 lethality rescuing mutants A50I, P15L, W253X and the ACT, all performed at room temperature, screened with concentrations ranging from 4-20 mg/ml and encompassing protein to peptide ratios (where applicable) between 1:1 and 1:3. Successful crystal formation conditions are listed below in table 9.

All screens were processed using the Mosquito® XTal3 utilising a hanging drop vapour diffusion method.

Vinculin W253X and Talin helix 50 complexes

Crystal screening for the Vinculin mutant (*Mus musculus)* W253X-H50 (*Mus musculus)* complex were performed at room temperature, the W253X concentration at 214 µM inm (20 mM Tris, 50 mM NaCl, 1 mM DTT pH8) with Talin H50 at a concentration of 430 µM at a 1:2 protein to peptide ratio.

Table 9-Conditions for each successful crystal formation and if successfully diffracted at Diamond light source.

Protein	Protein concentration mg/ml	Peptide (if applicable)	Protein to peptide ratio	Screen	Condition	Diffraction
A50I	(JCSG+96) 12 (Wizard classic) 12	Talin H50	1:3	JCSG+ 96 and Wizard classic	(JCSG+ 96) G12 (Wizard classic) G11	Awaiting Synchrotron time
W253X	6.4	Talin H50	1:2	JCSG+ 96	H7	Diffracted
ACT	12.5	NA	Na	JCSG+ 96	E8	Awaiting Synchrotron time
VD1	15	TarP VBS3	1:3	JCSG+ 96	H3	Diffracted

The mix was then left to incubate for 2 hours at room temperature. JCSG+ 96 well screening plates were used to identify optimal conditions for crystal growth and left for five days at room temperature (22°c). Crystals growth was observed in condition H7 which was comprised of 0.2 M ammonium sulphate salt, 0.1 M Bis/tris, pH 5.5 with 25% w/v PEG 3350. A 24 well optimisation screen was prepared using the H7 condition varying the ammonium sulphate 0.1 M-0.2 M, the PEG 3350 25%-29% and pH 5.4-5.7.

Optimisation proved unsuccessful, so the crystals were taken from the JCSG+ 96 plate and cryoprotected in liquid nitrogen.

Vinculin VD1 and TarP VBS3 complex

Previously Crystal screening for the (*Gallus gallus)* VD1-TarP VBS3 (*C.Caviae)* complex had been performed and resulted in diffraction of the crystals. The crystal screenings were carried out at room temperature, the VD1 concentration was 500 µM in (20 mM Tris, 50 mM NaCl, 1 mM DTT pH8) with TarP VBS3 at 1500 µM in 1:3 protein to peptide ratio. The mix was then left to incubate for 2 hours at room temperature. JCSG+ 96 well screening plates were used to identify optimal conditions for crystal growth and left for five days at room temperature (22°c). Crystal growth was observed in condition H3 which was comprised of no salt, 0.1 M Bis/tris, pH 5.5 with 25% w/v PEG 3350. A 24 well optimisation screen was prepared using the H3 conditions varying the PEG 3350 21%-31% and pH 5.3-5.6. Optimisation proved successful, crystals were taken from the optimisation plate and cryoprotected in liquid nitrogen. Note this set of crystals was produced with help from Dr.Austin whitewood.

Both W253X-H50 and VD1-TarP VBS3 diffraction data was collected at Diamond Light Source (Didcot, UK) using beamline i04-1 and the data was automatically processed using autoPROC for W253X-H50 and Dials-Xia2 for VD1-TarP VBS3 which both utilise XDS, Pointless, Aimless and Staraniso for subsequent integration, scaling and merging of the collected data. Determination of both structures was carried out utilising PHASER molecular replacement using (PDB:4DJ9) for W253X-H50 and (PDB:3ZDL) for VD1-TarP VBS3. The structures were manually remodelled and refined using COOT and REFMAC and validation was carried out using MOLPROBITY.

3 Results

3.1. Project 1:*C.caviae* TarP vinculin binding site structure and stoichiometry

C.caviae TarP is unique among TarPs in that it has three VBSs, most other species having two or one. Here we have explored if all three VBS are required, if there is a hierarchy between them in terms of binding affinity and how important is each to the invasion process?

TarP VBS3 binding data and structure were acquired and compared with the TarP VBS1 data (Whitewood et al., 2018). Also, the stoichiometry of the TarP VBS1-3 region binding to VD1 molecules was determined, also inadvertently giving some indications as to whether the TarP VBS2 may bind to VD1 as well.

3.1.1 TarP VBS3 binds to VD1 with higher affinity than TarP VBS1

To obtain TarP VBS3 binding data an in vitro FP assay was performed with TarP VBS1 as a positive control and comparison. The TarP VBS3 peptide bound VD1 tightly with a K_d of 81 nM, binding with higher affinity than the TarP VBS1 peptide tested here at 223 nM and also with the previous binding data for TarP VBS1 129 nM (Whitewood et al., 2018).

This higher affinity seen in TarP VBS3 may indicate that TarP VBS3 may have a more prominent role than stated previously (Thwaites et al., 2015) where the TarP VBS1 was hypothesised to be key to invasion with TarP VBS2 and 3 being dispensable.

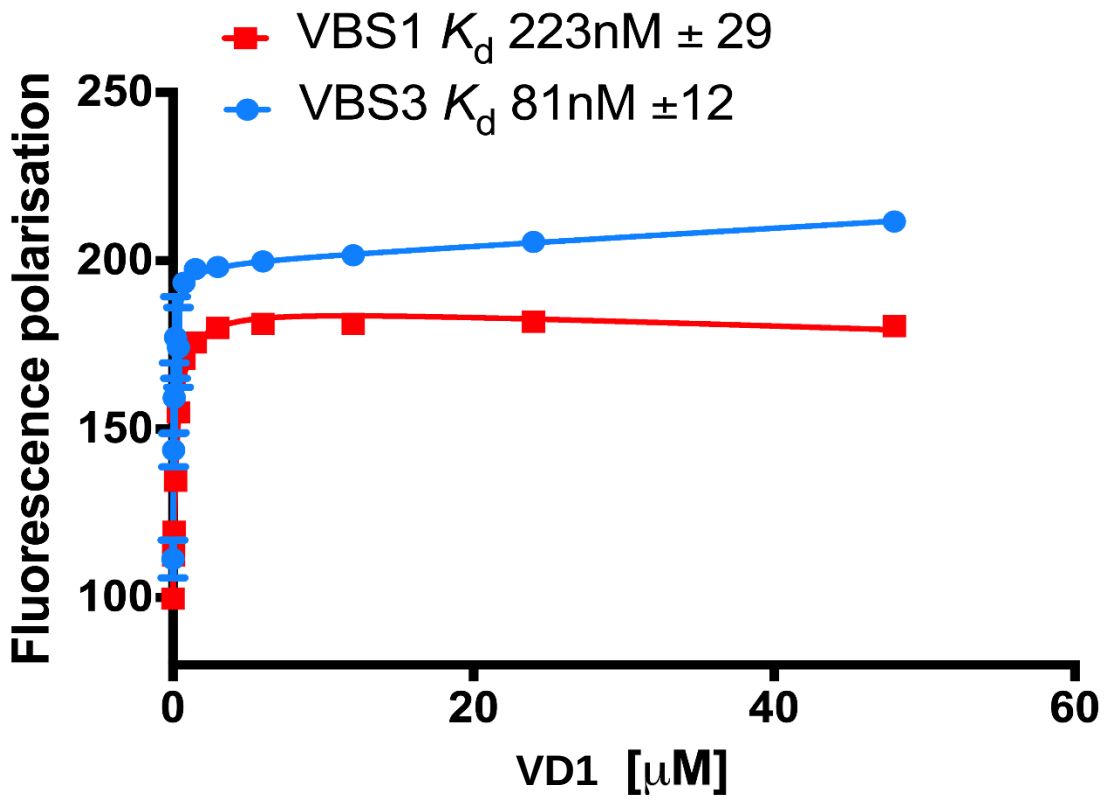

Figure 17-FP binding data between VD1 and both TarP VBS1 and VBS3, the TarP VBS3 K_d value of 81 nM indicates it has a higher binding affinity than TarP VBS1 having K_d value of 223 nM. Data presented using GraphPad Prism software (SE values are shown in the legend), all experiments were run in triplicate and with two biological replicates.

3.1.2 Cloning TarP VBS 1-3 into pGEX GST vector

TarP VBS1-3 in pET151 N-terminal His-tag vector appeared to aggregate after lysing the BL21 cells and optimisation using high concentration urea to alleviate the aggregation was unsuccessful. It was then subsequently successfully cloned into a pGEX GST vector to aid in solubility, expression and for use in techniques such as GST-pulldowns.

3.1.3 GST-Pulldown using TarP VBS1-3 to determine stoichiometry of VD1 binding

C.caviae TarP contains three VBS and VBS1 and 3 have been shown to bind to VD1 with high nanomolar affinity though FP, with VBS2 seemingly unable to stay in solution without aggregation. *C.caviae* TarP is unique in having three VBSs, as all other TarPs have one or two depending on the species, the stoichiometry of VD1 binding to *C.caviae* TarP is something that is unknown. By performing a GST pulldown with a determined 5 µM bead bound TarP VBS1-3 GST (MW 39 kDa) mixed with either 5 µM, 10 µM or 15 µM VD1 (MW 29 kDa), would allow us to identify if the TarP VBS1-3 GST bound VD1 in a 1:1, 1:2 or 1:3 ratio. (Note the TarP VBS1-3 GST concentration was determined to be 5 µM by serial dilution of 5 µM, 10 µM, 15 µM VD1 against TarP VBS1-3 GST, see figure 18). This would allow the analysis of the number of VBSs

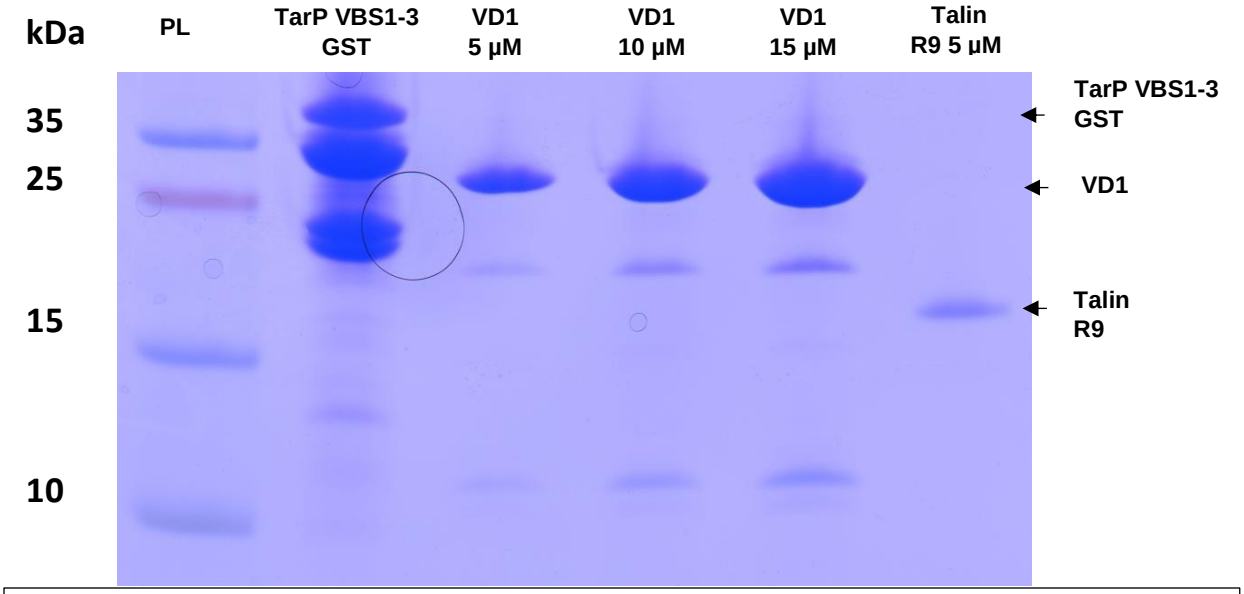

Figure 18-SDS gel to determine the concentration of TarP VBS1-3 GST. Lane 1 protein ladder (PL), lane 2 TarP VBS 1-3 GST, lane 3-5 VD1 5 µM, 10 µM, 15 µM respectively and lane 6 talin R9 5 µM. TarP VBS 1-3 GST was determined to resemble the VD1 at 5 µM (lane3). Pulldown assay was performed with three biological replicates.

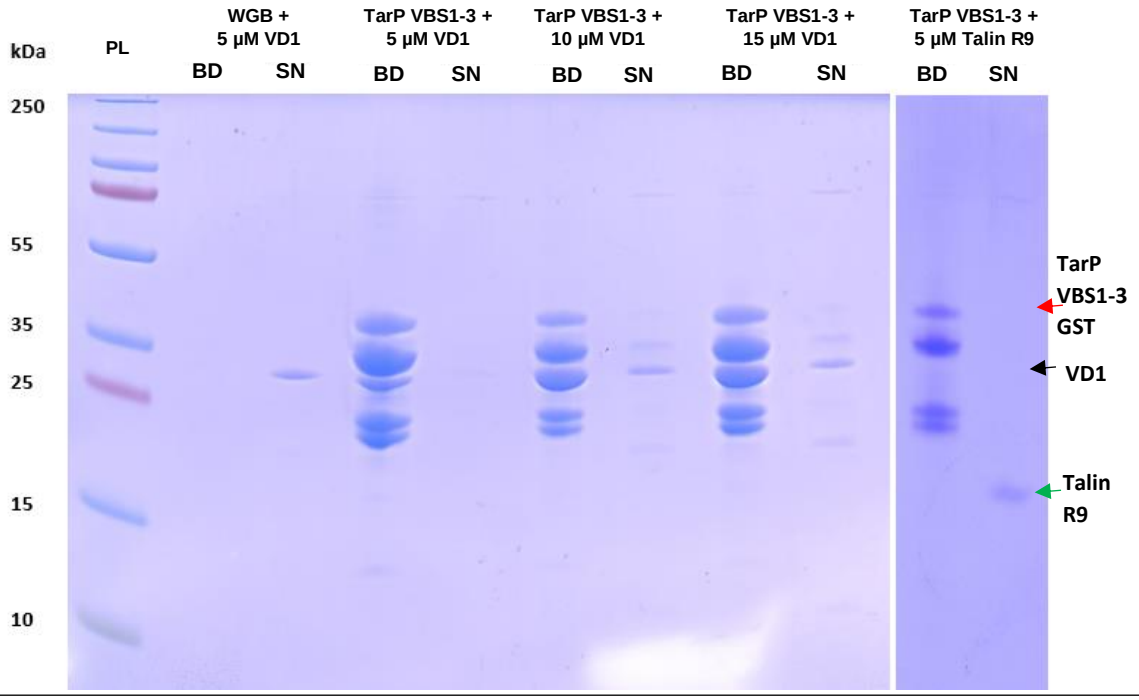

Figure 19- SDS gel of GST-pulldown of TarP VBS1-3 GST with 5 µM, 10 µM and 15 µM VD1, alongside TarP VBS1-3 GST with 5 µM talin R9 (control) and washed glutathione beads (WGB) with 5 µM VD1 (control). PL=protein ladder, BD=beads, SN=supernatant. Red arrow TarP VBS1-3 GST (39 kDa), Black arrow VD1 (29 kDa) and green arrow talin R9 (17 kDa). Note VD1 kDa in beads appears lower down due to higher concentration present when compared to supernatant. Pulldown assay was performed with three biological replicates.

that can be occupied at any one time, adding the possibility whether structural restraints restrict VD1 bindings. All protein concentrations in the GST-pulldown (figure 19) resemble the concentrations seen in figure 18. Viewing the GST-pulldown (figure 19), 5 µM, 10 µM and 15 µM VD1 all appear in the bead samples when mixed with TarP VBS1-3 GST, indicating VD1 association with bead bound TarP VBS1-3 GST. The 10 µM and 15 µM VD1 samples when mixed with TarP VBS1-3 GST additionally showing trace amounts of VD1 in the supernatant, indicating that they are possibly not exact 1:2 and 1:3 ratios and the concentrations perhaps are slightly too high. However, the majority of VD1 is present in bead sample of TarP VBS1-3 GST mixed with the 15 µM VD1 concentration, which indicates that TarP VBS1-3 could possibly bind VD1 up to a potential 1:3 ratio, further attempts to optimise the concentration would still need to be

attempted. Controls of washed glutathione beads with 5 µM VD1 which showed VD1 in the SN and not in the BD indicating no interaction with the washed glutathione beads. Additionally, a control of bead bound TarP VBS1-3 GST with 5 µM talin R9 (MW 17 kDa) was used as a negative control, R9 was found in the supernatant indicating no interaction with the bead bound TarP VBS1-3 GST.

3.1.4 SEC-MALS analysis of the stoichiometry of VD1 binding to TarP VBS1-3

To aid in confirming the stoichiometry between TarP VBS1-3 and VD1, a SEC-MALS assay was performed to more accurately determine how many VD1 monomers associate with the TarP VBS1-3. The SEC-MALS experiment will allow a visualisation of

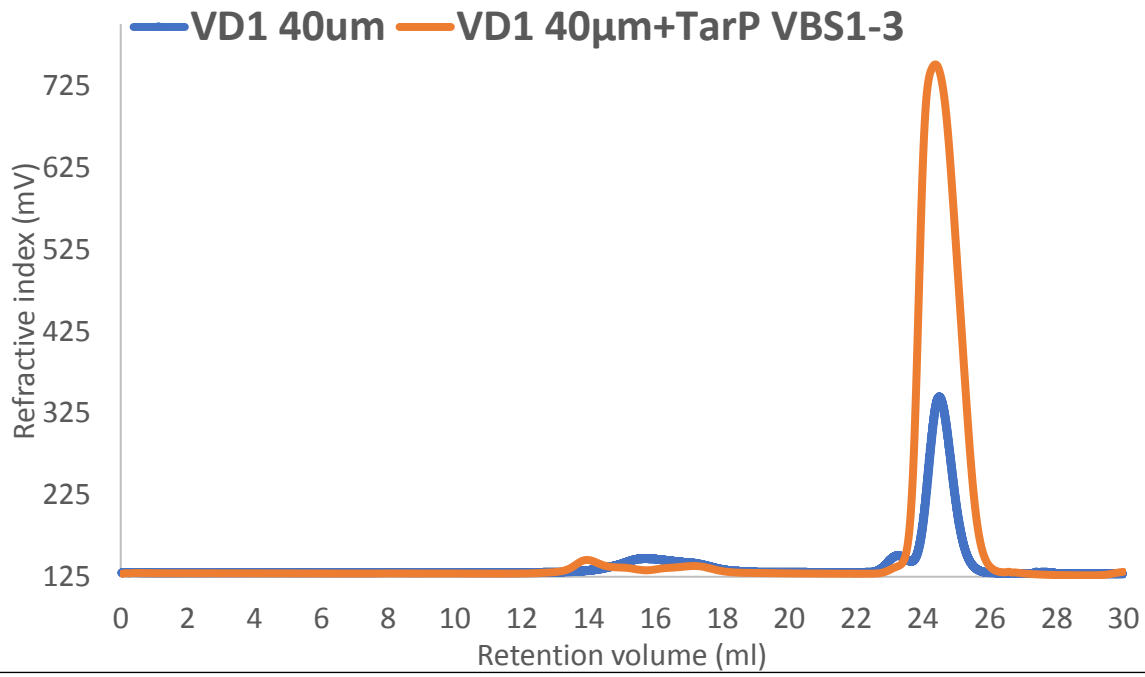

Figure 20- SEC-MALS data indicating the lack of association between the TarP VBS1-3 and VD1. Each VD1 sample was run 40 µm, although fluctuations in sample volume with the variation in peak height in between the VD1 apo and VD1+TarP VBS1-3 runs is present. SEC-MALS was performed with one biological replicate.

stoichiometry of VD1 binding to TarP VBS1-3 by analysing shifts in peaks to smaller retention volumes if any VD1 binds to the TarP VBS1-3, with SEC-MALS the MW of any

complexes can be accurately determined to discover the stoichiometry of VD1 binding (figure 20).

A 40 µM apo VD1 sample was run and is seen forming a characteristic double peak with the monomer eluting at ~24.5 ml and the dimer at ~23 ml. In the 40 µM VD1:TarP VBS1-3 mix the VD1 eluted at ~24.5 ml again although the dimer of VD1 at ~23 ml is not present, the peak itself is much larger than the VD1 sample and again the problem is attributed to over concentration the VD1:TarP VBS1-3 before loading. What is not seen however are any peaks at smaller retention volumes appearing from supposed VD1:TarP VBS1-3 complexes, while the TarP VBS1-3 has been seen to interact with VD1 in the GST pulldown section 3.1.3 that was when still attached to a GST tag. The lack of any complexes forming indicates that the TarP VBS 1-3 when cleaved from its GST tag as is the case here, may aggregate and as such not effectively bind VD1. The TarP VBS1-3 is a disordered protein, and a GST-tag was necessary for it to be soluble and able to be purified, by cleaving the GST-tag after purification may again render it insoluble. An attempt was made to use reduced glutathione to remove the TarP VBS1-3 GST tagged protein from the Glutathione Superflow agarose slurry beads but was unsuccessful due to aggregation on addition of the reduced glutathione. While unsuccessful, a repeat of this experiment with optimisation in the removal of the TarP VBS1-3 GST tagged protein from the Glutathione Superflow agarose slurry beads leaving the GST tag attached, as well as controls of VD1:VT as positive control and VD1:talin R9 and VD1:apo GST tag as negative controls would give a more definitive answer to what is seen in the GST pulldown in section 3.1.3.

3.1.5 VD1:TarP VBS3 crystal structure

The VD1:TarP VBS3 was determined at 2.08 Å in a P21212 orthorhombic space group with 1 molecule being present in the asymmetric unit (Au) with a probability of 99% using Matthews coefficient. Using Pisa analysis, it was seen that 57.4% of the TarP VBS3 is buried in the complex interface with VD1, further details of validation and quality analysis can be seen in figure 20. The TarP VBS3 peptide has two residues proline 870 and cysteine 871 that are not visible in the electron density, due to being present in a disordered loop region.

The TarP VBS3 can be seen to interact with VD1 in the same helical bundle insertion into the N-terminal helical bundle of VD1 as seen in talin VBSs. Helices α1 and α2 can be seen to be separated by the TarP VBS3 which then positions itself in the hydrophobic core of the N-terminal helical bundle of VD1 (figure 21).

==========Summary ==========

Ramachandran outliers	=	0.00 %
favored = 99.63 %		
Rotamer outliers	=	6.20 %
C-beta deviations	=	2
Clashscore	=	15.86
RMS(bonds)	=	0.0118
RMS(angles)	=	1.79
MolProbity score	=	2.31
Resolution	=	2.00
R-work	=	0.2848
R-free	=	0.3146
Refinement program	=	REFMAC

Figure 21-Structural statistics of the TarP VBS3-VD1 crystal structure as determined in CCP4i2 REFMAC program.

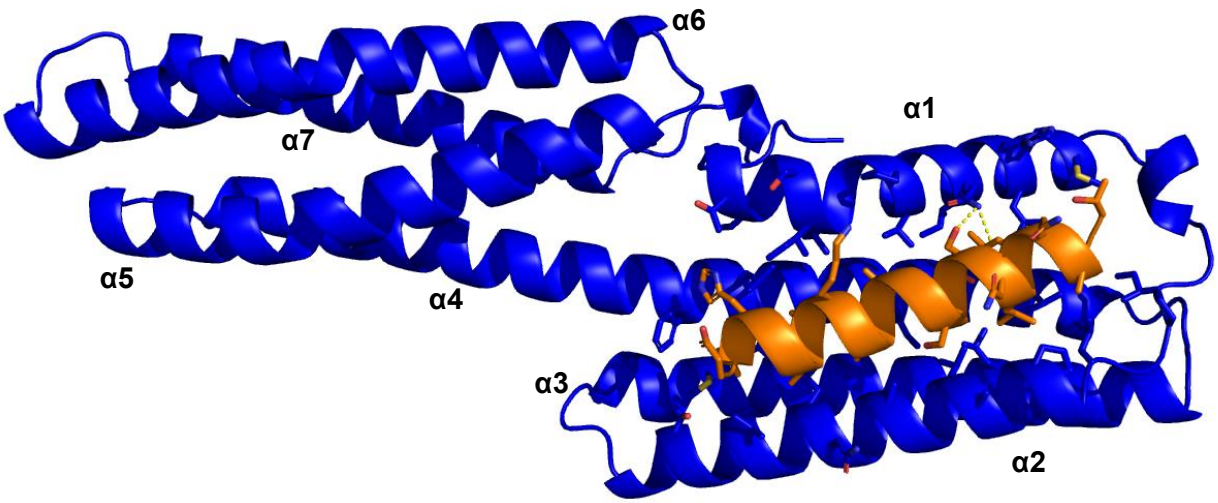

Figure 22-TarP VBS3-VD1 structure modelled in PyMOL showing the helical insertion of the TarP VBS3 peptide between the α1 and α2 helices of VD1. Interface residues side chains are modelled using the interfaceresidues.py script in PyMOL.

A Hydrogen bond is present between VD1 Glutamine 19 to TarP VBS3 serine 758 which is mostly conserved between VBSs with regards to residue and bond distances (figure 22B).

The structure shows that hydrophobic residues line the primary interface side of the TarP VBS3 peptide and look to enable its tight association within the hydrophobic core of the helical bundle (figure 22A). Differences between the TarP VBS1 and 3 residues in this hydrophobic interface are present, TarP VBS1 appears to differ from TarP VBS3 at two key residues T857 and T864, which in TarP VBS3 are V753 and L760 at the same positions (figure 22 C, D, E). While TarP VBS1 has two other hydrophobic residues in its VBS namely L850 and L851, these are either not modelled with L850 due to being at the end of the peptide as such it's difficult to determine precise orientation but is conserved so is most likely also important in binding much like its conserved residues in the same position in other VBS. L851 presence seems non-essential in binding as there is no consensus in that position among VBS .

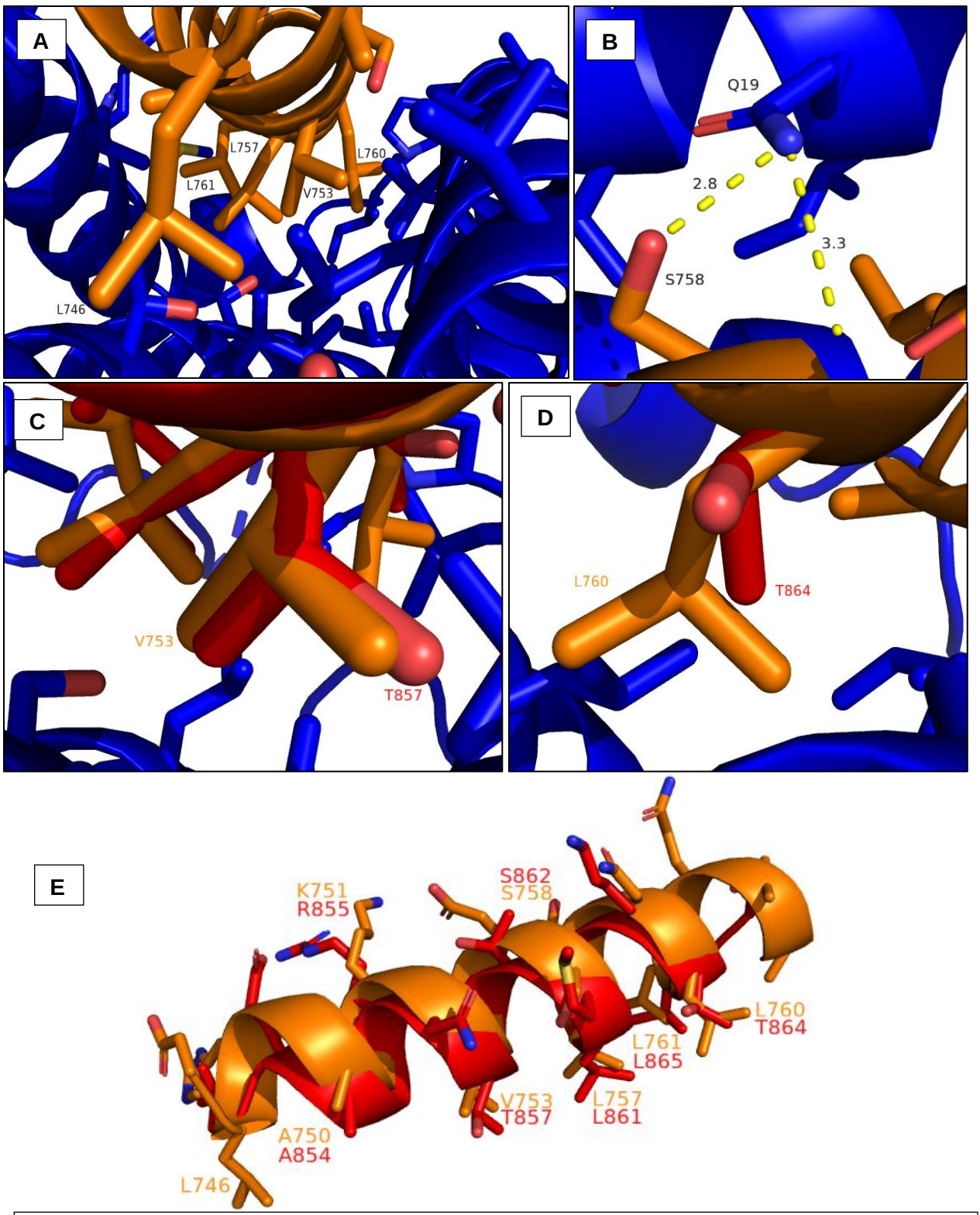

Figure 23-(A) TarP VBS3 hydrophobic residues interacting with the hydrophobic core of VD1. (B) Hydrogen bond between VD1 Q19 and TarP VBS S758. (C) Overlay of TarP VBS3 V753 (orange) and TarP VBS1 T857(red). (D) Overlay of TarP VBS3 L760 and TarP VBS1 T864.(E) TarP VBS3 and TarP VBS1 overlaid with all consensus residues labelled with side chains.

A methionine M860 is present in the TarP VBS1 but it is positioned away from the hydrophobic core interface. An additional hydrogen bond is present in TarP VBS1 between VD1 S11 and TarP VBS1 R855 but is not seen in the TarP VBS3, this ubiquitously conserved residue appearing as either arginine/lysine/asparagine. However, although the residue is conserved this hydrogen bond is rarely seen in any VD1-VBS complexes and as seems unimportant in binding affinity.

Comparing the TarP VBS1 and 3 structures, the inclusion of the extra two hydrophobic residues V753, L760 in TarP VBS3 which interact with the VD1 hydrophobic core appear to be the cause for the increase in affinity seen in figure 17.

3.2. Project 2: Analysis of lethality rescuing VD1 mutants with talin H50

As seen in the interaction between TarP VBSs with VD1, the binding of a VBS to VD1 may follow a certain consensus of residues in order to bind effectively, but with small variations in sequence and structure of the VD1-VBS interface region having drastic effects on binding affinity. The Vinculin lethality supressing mutants (discovered through a genetic screen, unpublished data) A50I, P15L and W253X showed that small mutations can result in reduced binding affinities, although the W253X mutant exhibited K_d values consistent with the WT while somehow rescuing the *Drosophila* from lethality .These mutants can disrupt talin VBS-VD1 binding and as such rescue *Drosophila* from lethality caused by CO vinculin. This disruption of talin VBS-VD1 binding was mostly consistent across tested talin VBS (helixes 6,27,33,36 and 50) (Data generated by Dr Karen baker Postdoc Goult lab), however H50 exhibited only mild increases in K_d and was the only helix tested to actively bind all three of the mutants including the A50I mutant which was reported to disrupt the talin: vinculin interaction. Crystal structures of each VD1 mutant with H50 would allow direct analysis as to how and why H50 allows the binding of these VD1 mutants. While numerous attempts were made as seen in section 2.5.8 to acquire crystals for each complex only the W253X-H50 complex successfully diffracted and as such the only structure available for direct analysis of any unique binding interactions or structural changes.

3.2.1 VD1 mutant W253X with talin helix 50 structure

The W253X-H50 was determined at a resolution of 2.11Å in an P21 monoclinic space group with one molecule of the complex in the Au with a probability of 100% using

```
================== Summary ==================

Ramachandran outliers =    0.00 %
              favored =   99.22 %
Rotamer outliers      =    5.60 %
C-beta deviations     =       8
Clashscore            =   15.35
RMS(bonds)            =    0.0105
RMS(angles)           =    2.06
MolProbity score      =    2.26
Resolution            =    2.11
R-work                =    0.2688
R-free                =    0.3214
Refinement program    = REFMAC
```

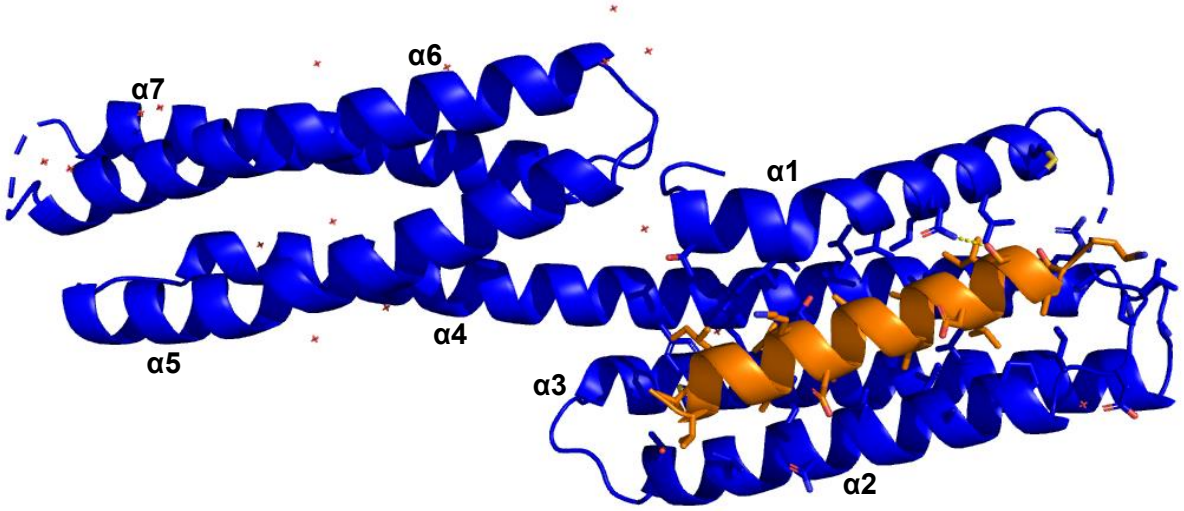

Figure 24-(Top) Structural statistics of the W253X (blue) -H50 (orange) crystal structure as determined in CCP4i2 REFMAC program. (Bottom) TarP W253X-H50 structure modelled in PyMOL showing the helical insertion of the H50 peptide between helices α1 and α2 of VD1. Interface residues side chains are modelled using the interfaceresidues.py script in PyMOL.

Matthews coefficient. Pisa analysis shows that 48.5% of the H50 peptide is buried in the complex interface, further details of validation and quality analysis can be seen in figure 23. VD1 residues 1-3, 34-35 and 221-225 are missing as well as H50 residues 2075-2078 and 2100-2103, these residues are all present in disordered loop regions. The same helical bundling insertion is seen with hydrophobic interactions inside the

core of the N-terminal helical bundle of the W253X mutant. Comparing the W253X-H50 with the WT-H50 (PDB 4DJ9,(Yogesha et al., 2012), the semi-conserved hydrogen bond between VD1 glutamine 19 and serine 2096 as seen in both TarP VBS1 (Whitewood et al., 2018) and 3 is present but not in wildtype VD1 with H50 as seen in section 3.1.5. Although both the W253X and WT complexes share a hydrogen bond in between VD1 Q19 and G2092 (figure 24C). The hydrogen bond mention from W253X Q19 to H50 S2096 is not seen in the WT, however this hydrogen bond can be formed in the WT structure simply by altering the S2096 into a different but still acceptable rotamer. Possibly the WT VD1 may favour the serine in a non-hydrogen bonding rotamer while the W253X favours a hydrogen bonding serine rotamer.

The W253X-H50 and WT-H50 structures overlaid reveal that all the residues appear to conserve their positions apart from the hydrogen bond mentioned and one other minor difference. In the WT-H50 structure a lysine in the H50 Peptide K2099 is pointed towards a positively charged Histidine H27 in the α1 helix of VD1. In the W253X-H50 structure this lysine is pointed away from the α1 helix and the W253X H50 interface region, this difference may be the reason why the α1 helix in W253X appears to shift slightly towards the H50 peptide (figure 24 A, B). The six C-terminal residues removed in the W253X mutant are in a unstructured loop region that interconnect the region between VD1 and VD2, their deletion appears not to intrinsically interfere with the binding of the H50 peptide to the W253X mutant when compared the WT interaction. These small structural differences between the two structures do not answer the question as to how the W253X mutant still is able to rescue the *Drosophila* lethality phenotype.

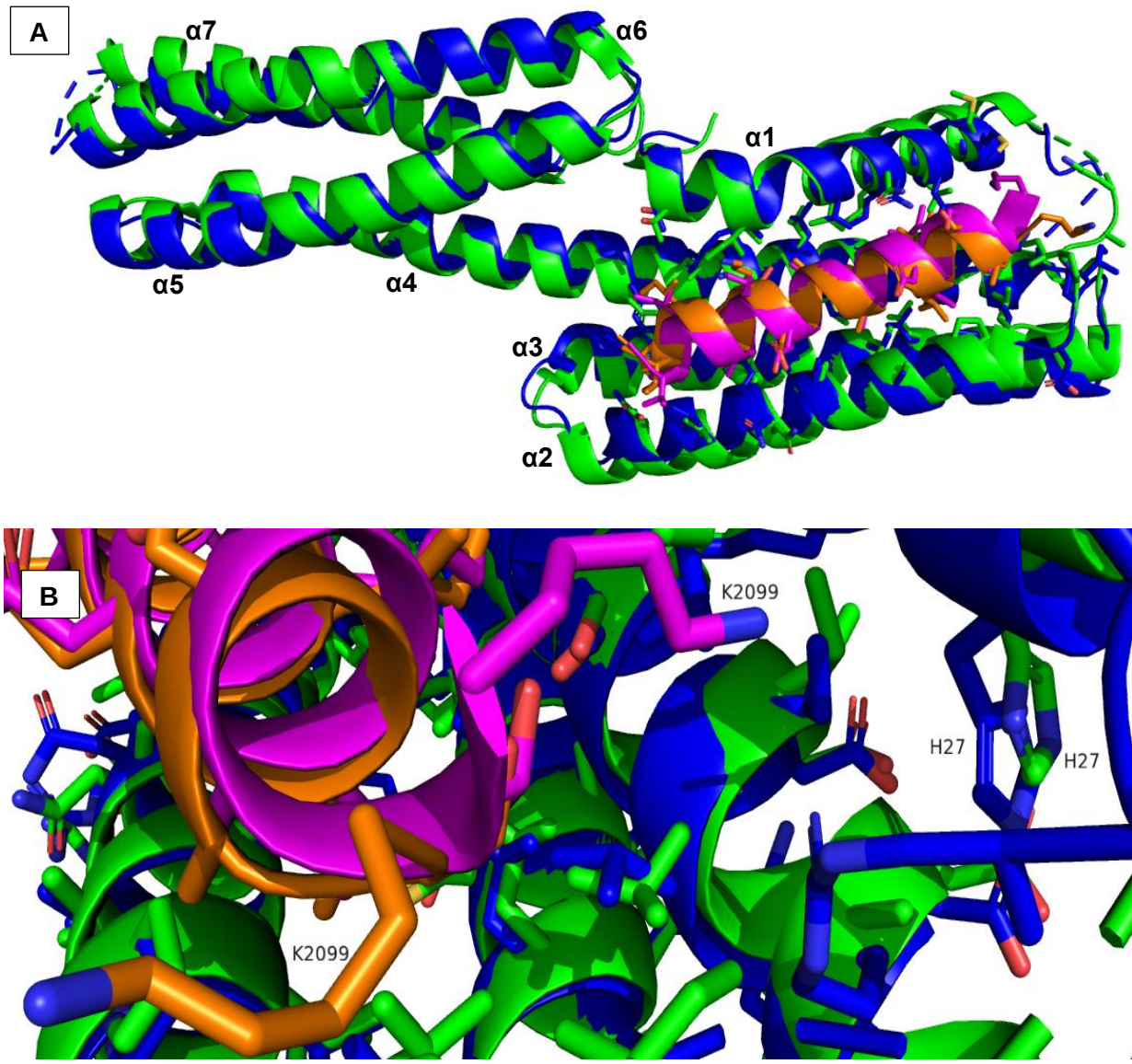

Figure 25-(A) The W253X-H50 (blue, orange) structure overlaid on the WT VD1-H50 (green, pink) structure with Interface residues side chains are modelled using the interfaceresidues.py script in PyMOL.

(B) K2099 reorientates in the W253X-H50 complex to face away from the positively charged H27, compared to the WT VD1-H50 where it faces towards the VD1 helix 1.

(C) The W253X-H50 structure shows VD1 Q19 able to hydrogen bond to both S2096 and G2092, whereas the WT VD1-H50 is only able to hydrogen bond to G2092.

3.3. Project 3:α-catulin structural characterisation and its homology to Vinculin

Biochemical/biophysical techniques were performed to identify any structural similarities between vinculin and α-catulin, as well as explore whether binding interactions seen in vinculin are also present in α-catulin. Also utilising bioinformatic techniques to analyse sequence similarities between vinculin and α-catulin.

3.3.1 Cloning α-catulin constructs into new vectors

The N-terminal ACH (1-283) did not express from the pET151 N-terminal His-tag vector and attempts to clone the ACH into both a C-terminal HIS-Tag vector (pET 21a) and a pGEX GST vector, were both unsuccessful. Attempts to clone α-catulin full length (1-731), α-catulin 'VD1-3' (1-529), α-catulin 'VD3' (307-529) and α-catulin 'VBS domain' (284-615) into a pET151-avi-2I27-mR6-2I27-spy vector also proved unsuccessful. However, the C-terminal ACT (533-731) expressed and purified well and was used in the following assays.

3.3.2 NMR spectra of the ACT

The predicted high structural similarity between VT and ACT region meant that potential binding interactions seen in VT may also bind to ACT. Paxillin's LD2 domain has been shown to bind both VD1 and VT (albeit weakly) (Wood et al., 1994), so we used 2D NMR to identify if this was observed for the ACT.

^{1}H 1D and ^{1}H -^{15}N 2D transverse relaxation optimised spectroscopy (TROSY) NMR spectra were performed on the ACT to acquire a fingerprint spectrum. Both spectra were run with the same 50 µM ^{15}N labelled ACT sample loaded at 350 µl into Shigemi NMR tubes with 5% D_2O.

The 1D spectra indicates the presence of protein with peaks present in the amide/backbone region (6-10 ppm) but the peaks are broad indicating that protein concentration appears to be insufficient or forming a higher order species (aggregated). Normally a concentration of 100 µM-1 mM is required for a clear signal and higher defined peaks. This together with the lack distinct methyl group peaks (0-1.5 ppm), which in a higher concentration may indicate the protein is unfolded but, in this case it was more likely the concentration was simply not high enough for clear definition. The TROSY experiments showed poorly defined peaks owing most likely to low 50 µm concentration mirroring what was shown in the 1D experiment. The poorly defined peaks in the spectra however indicated a possibility that the ACT was behaving like a protein of a higher MW, as MW increases definition decreases and the peaks become broader. The ACT sample showed no clear sign of aggregation, but it was possible that it was forming a dimer (possibly confirmed in gel filtration see below) or aggregating and as such the spectra given was one of a much larger protein and as such much less defined. (Note the His-tag was not cleaved due to concern the small concentration might be lost through the addition of TEV).This lack of definition of the peaks meant subsequent experiments with peptides such as the paxillin LD2 could not be performed as shifts seen in VT and Paxillin are extremely subtle and as such in the ACT would not be seen. While the spectra gave a fingerprint of the ACT, the poor definition precludes further experiments and requires further optimisation. The concentration used could be on reason while the spectra is highly defined, but also the ACT forming aggregates could be another reason. Optimising expression of the ACT for higher concentrations,

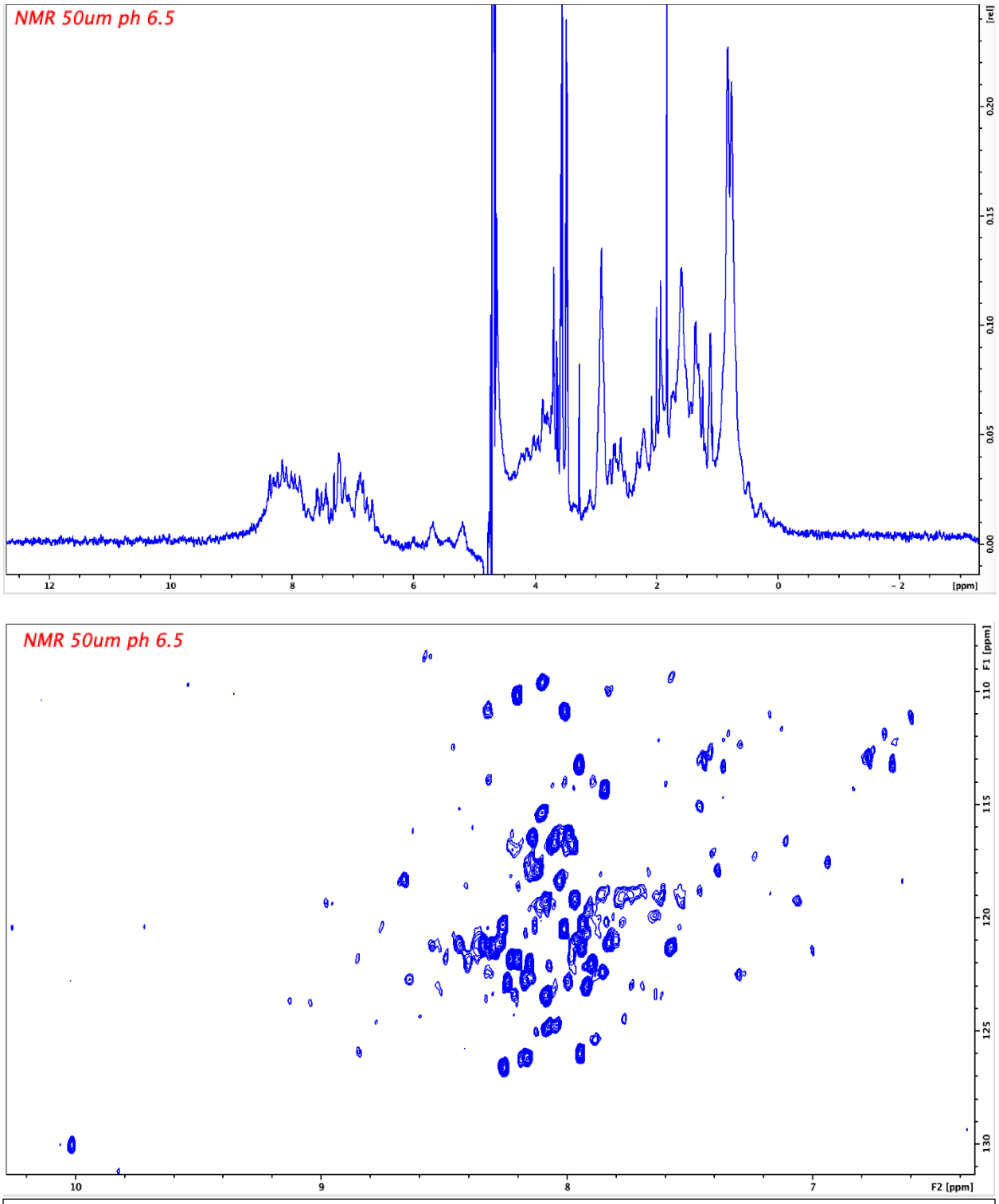

Figure 26-(Top) A 1D NMR spectra of the ACT show the presence of protein from peaks in the amide regions (chemical shifts 6-10 ppm). (Bottom) 2D TROSY spectra of the ACT, the TROSY data peaks are not well defined due to the low 50 µM concentration. NMR spectra performed with one biological replicate.

finding conditions in which aggregation may not occur would, alongside cleaving the His-tag would all aid in refining the spectra.

3.3.3 CD comparison between ACT and VT

The secondary structure of the ACT was analysed using Far UV as well as using a melting curve to determine the overall thermal stability of the protein. This was run alongside the VTΔlinker for a direct comparison. The Far UV spectrum of the ACT was run at 4.4 µM in 1x PBS indicates an alpha helical structural as shown by the prominent 'double dip' trace seen between wavelengths ~208 and ~227.

The spectra for the VTΔlinker mirrors that of the ACT with the double dip present also indicating an alpha helical structure (figure 26A). The melting curve for the ACT run at 20-90°C shows high levels of thermal stability with a melting temperature (TM) of ~85°C, although no real change occurs until ~90°C whereupon its folded structure appears to be truly disrupted. The spectra of the VTΔlinker again mirrors the ACT with both sharing the same~85°C TM and the full disruption of the folded structure at ~90°C (figure 27B). While the VT has been clearly shown to be a 5 helix bundle as seen in crystal structures (PDB 1QKR, (Bakolitsa et al., 1999), the ACT has only been predicted through online structural programs that predict secondary structure based on protein homology databases such as Phyre2 and T-Coffee MSA. All spectra were blanked using 1x PBS buffer.

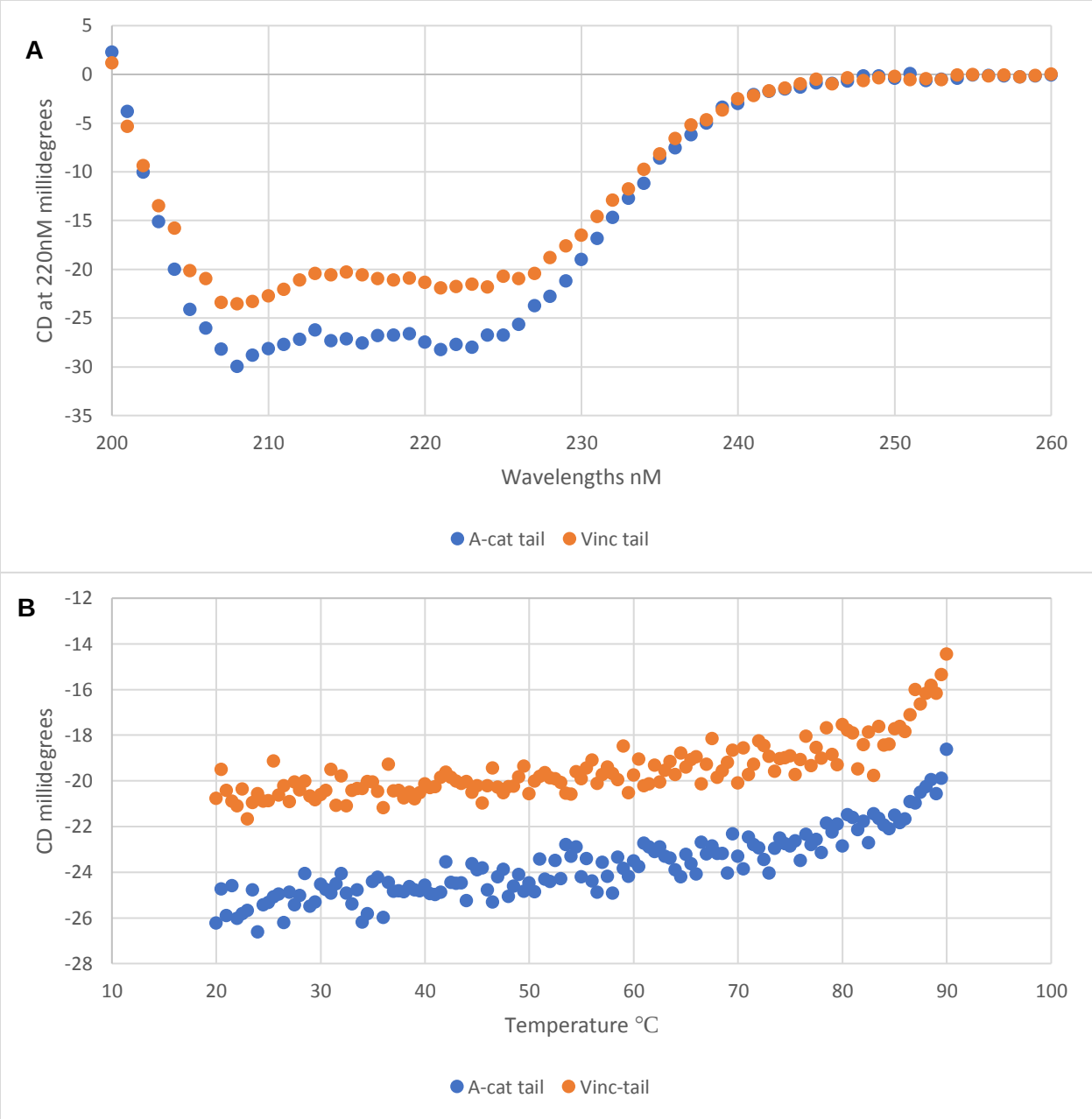

Figure 27-A) Far UV comparison between the ACT and VT indicating both share a largely α-helical secondary structure as visualised by the characteristic double dip shape of the spectra. B)The melting curve spectra shows that both the ACT and VT share high stability, unfolding occurring at ~85°C for both. Both far UV and melting curve CD assays performed with 3 biological replicates.

3.3.4 Analysis of ACT association with VD1 using gel filtration

The structural homology between the ACT and the VT suggests that the ACT may associate with VD1, as VT binds to VD1 in its autoinhibited state. Perhaps ACT may bind to VD1 and indicate a mechanism for a possible vinculin-α-catulin complex. Gel filtration SEC was carried out to determine whether ACT (22 kDa) associated with VD1 (29 kDa). Each protein eluted at separate retention volumes with the larger peaks of both VD1 and ACT eluting at 15 ml and 16 ml, respectively. Both also showed secondary peaks at 13 ml for VD1 and 14 ml for ACT which could indicate dimerisation for VD1 and possible dimerization for the ACT, possibly indicating another similarity between the two. The ACT:VD1 mix appears to show no new peaks when compared to the Apo proteins, although the peaks for the Apo proteins appear lower this is likely due to concentration fluctuations in the sample due to loss of sample volume while loading.

The somewhat similar MW of both VD1 and ACT mean that substantial overlap occurs around 14-16 ml however all peaks for both VD1 and ACT remain at the same retention volume albeit with higher UV values. If an association of VD1 and ACT had occurred a new peak would be present between the VD1 dimer peak at 13 ml and the ACT possible dimer at 14.5 ml, which is not seen. While this gives some indication that there is no association between VD1 and the ACT, overall, with concentrations not being equal between the apo and mix samples I would say this interaction so far is inconclusive. Also, no control run was performed which would have been VD1 with the VT, which would have also defined if the VD1 was properly folded etc that would have then shown a negative association across all runs including the ACT run as seen.

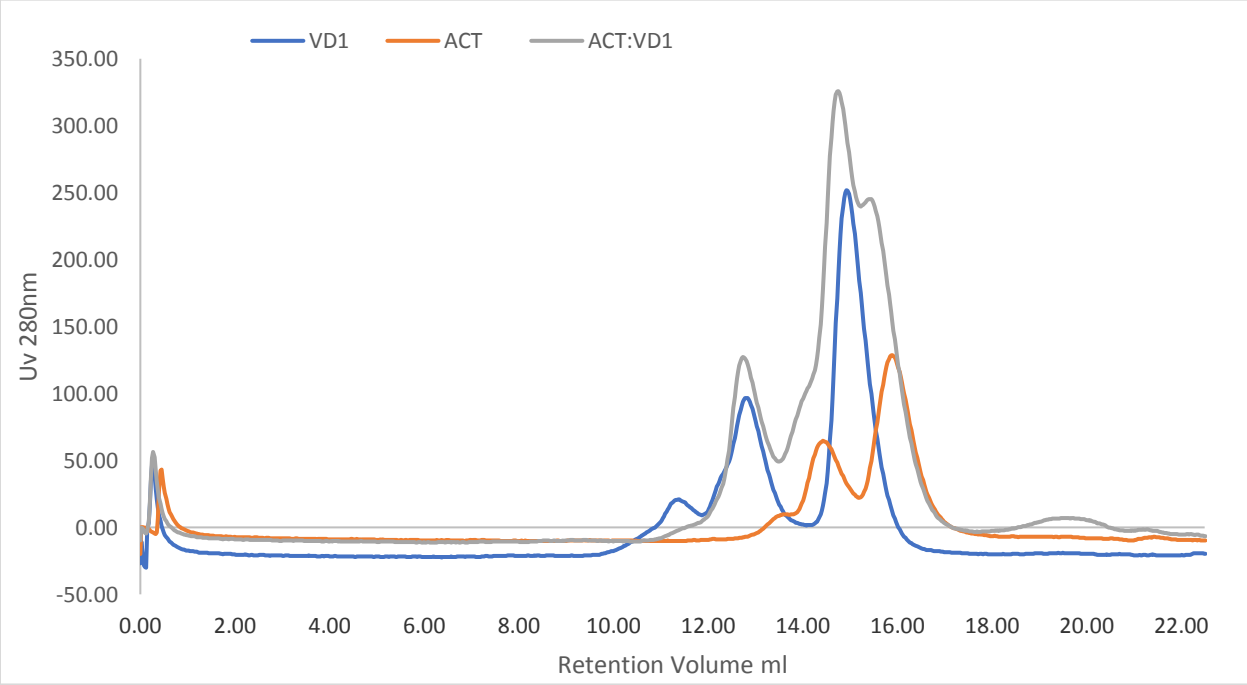

Figure 28-Gel filtration SEC data indicating the lack of association between the ACT and VD1 domain. Each sample was run 56 µm, although fluctuations in sample volume with the variation in peak height in both ACT and VD1 apo runs is present. GF SEC assay performed with 2 biological replicates.

3.3.5 FP of the ACT with Paxillin LD2

The VT has been shown to interact weakly with paxillin's LD2 domain, as ACT shares homology with the VT an FP assay was performed to identify whether this interaction with LD2 might also occur for α-catulin. Paxillin's LD2 domain has been shown to be important in the recruitment of both vinculin and talin to FACs (Pasapera et al., 2010), an interaction between paxillin's LD2 and α-catulin could indicate that possibly α-catulin is also recruited to FACs or perhaps that paxillin is then associated with the DAPC.

While the FP assay shows that ACT has a very similar binding curve as VTΔlinker the K_d was unable to be determined much the same as the FP assay between VTΔlinker and LD2. As mentioned in section 3.3.2 a TROSY NMR experiment with the ACT and

paxillin LD2 would have helped to confirm this interaction but as mentioned was not possible. While this interaction could indicate that ACT could possibly interact with paxillin through the LD2 domain the interaction is very weak and could possibly just be non-specific binding due to high concentrations of each protein used in the FP assay.

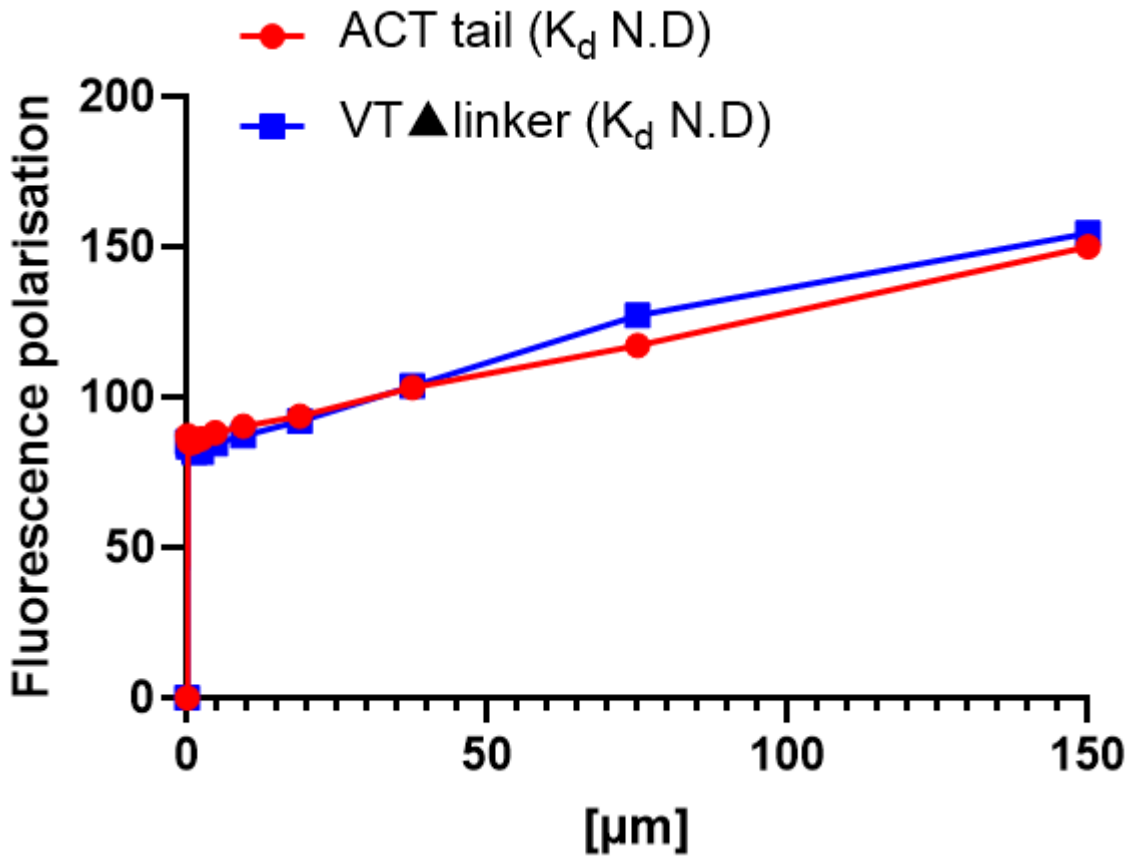

Figure 29-FP shows that the ACT binds weakly to paxillin's LD2 domain much like the VT, the VT has been shown to bind to paxillin's LD2 domain and even though the K_d cannot be determined for either in this study it suggest an interaction between the ACT and paxillin is possible. FP was performed with two biological replicates.

If the ACT were optimised for NMR an interaction with LD2 could be proved this would help to corroborate the FP data shown (figure 29). This alongside expressing constructs of full length or multidomain parts of α-catulin, may also help to prove that perhaps paxillin's interaction with the α-catulin may not be exclusive to the ACT. Paxillin may bind α-

catulin across multiple domains, the apparent weak binding seen between the ACT and the LD2 domain may only be one part of a stronger interaction between paxillin and α-catulin that is spread across multiple domains.

4 Discussion

4.1. Project 1:TarP vinculin binding site structure and stoichiometry

Vinculins ability to recruit and bundle actin to FACs (Wen et al., 2009) as well as cadherin cell-cell junctions (Leerberg and Yap, 2013) plays a key part in cellular migration as well as cellular homeostasis. This has led to bacterial pathogens obtaining virulence factor proteins that contain VBS motifs that hijack vinculin to facilitate their entry into host cells. Bacteria such as Rickettsia which uses a cell surface antigen Sca4, Shigella with its IpaA invasion protein and Chlamydia with its T3SS protein TarP. Each virulence protein being able to recruit vinculin though VBS-VD1 interactions and repurpose vinculin for their pathogenesis cycle.

This study attempted to examine the specific binding interactions between the three VBS present in *C.caviae* TarP and vinculin. Biochemical and biophysical techniques were used to determine these binding affinities and structural interactions between the three VBS and VD1 alongside determining the stoichiometry of VD1 bound to the *C.caviae* TarP three VBSs concurrently.

4.1.1 A structural Comparison between the three TarP VBS bound to VD1

C.caviae TarP VBS1 had previously been shown to bind to VD1 using the same helical bundling method as seen with talin VBSs and had actively outcompeted talin in binding to VD1 with Tarp VBS1-VD1 showing a high K_d value of 1290 nM, (Whitewood et al., 2018). By using an FP assay, we have been able to determine the K_d for the TarP VBS3 and determined that its binds to VD1 with a higher binding affinity than TarP VBS1. By testing both TarP VBS1 and VBS3 it is shown that TarP VBS1 binds with an affinity of

223 nM whereas TarP VBS3 binds with an affinity of 81 nM. A hypothesis on what causes the difference in binding affinity between the two VBS can be made by comparing the previously solved TarP VBS1-VD1 structure (6FQ4,(Whitewood et al., 2018) and the TarP VBS3-VD1 structure solved here.

In section 3.1.5 the structure of the TarP VBS3-VD1 shows that TarP VBS3 binds VD1 in much of the same way that TarP VBS1 does with interactions between a lane of hydrophobic residues in TarP VBS3 with the hydrophobic core of the N-terminal helical bundle of VD1. A difference in hydrophobic residues is seen between TarP VBS1 and TarP VBS3 however, TarP VBS1 as has two polar residues T857 and T864 in contact with the VD1 hydrophobic core whereas TarP VBS3 has a L753 and V760 at the same positions. This inclusion of a L753 and V760 TarP VBS3 results in it having two extra hydrophobic residues that can interact with the hydrophobic core of VD1 and as such could be the reason for the enhanced binding affinity shown by the FP data of the TarP VBS1 compared to 3.

```
C.caviae_VBS1|850-868      ------------LLEAARNTTTMLSKTLSKV----------      19
C.caviae_VBS2|805-829      ------------GIPGAAANVTATLSSVANKIALFEK-----      25
C.caviae_VBS3|745-769      ------------DLHGAAKGVADSLSNLLQAATPSTT-----      25
Talin_VBS1|607-636         ------------PLLQAAKGLAGAVSELLRSAQPASAEPRQN      30
Talin_VBS33|1512-1546      ASARTANPTAKRQFVQSAKEVANSTANLVKTIKA--------      34
Talin_VBS36|1628-1652      --------PRWSVLAGHSRTVSDSIKKLITSMR---------      25
Sca4_VBS|810-834           -----------DDIYNKAREVINAVNPVIEALEKSK------      25
IpaA_VBS2|566-584           ------------IYEKAKEVSSALSKVLSKI----------      19
```

Figure 30-MSA of the conserved VBS residues in talin as well as bacterial virulence factors TarP,Sca4 and IpaA. Redrawn with Clustal Omega using sequences from Whitewood et al., 2018.

While the affinity of TarP VBS2 could not be determined due to solubility issues with the peptide, using PyMOL the residues of the TarP VBS3 peptide were mutated to the TarP VBS2 sequence and a prediction can be made onto its affinity using the consensus sequence alongside the model (figure 29, 30). The TarP VBS2 sequence shows high homology with the consensus sequence with two small deviations, TarP VBS2 has

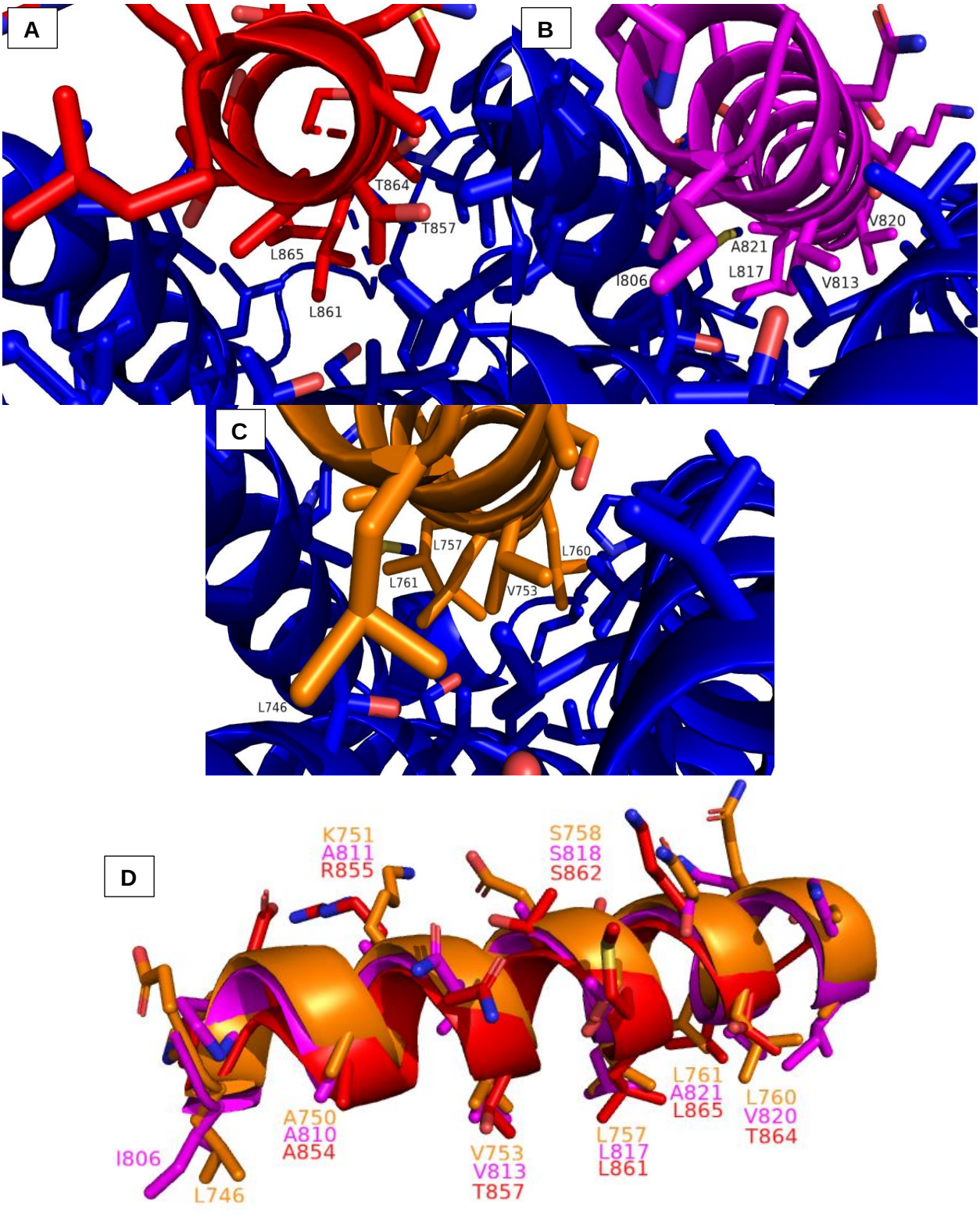

Figure 31-A) Conserved hydrophobic residues for the TarP VBS1, B) TarP VBS2 and C) TarP VBS3. D) Overlay of all the conserved residues between all three of TarP's three VBSs. Note TarP VBS1 is missing its L850 from the structure and as such is not modelled, which would overlay with TarP VBS2 I806 and TarP VBS3 L746.

an alanine A821 in place of a Leucine found in both TarP VBS1 and 3 and while alanine is hydrophobic its reduced capacity for hydrophobic interactions may cause some reduction in affinity. Additionally, it has an alanine A826 in place of the conserved Arginine/lysine, while a hydrogen bond was seen in the TarP VBS1 involving the arginine it was not seen in other VBS-VD1 complexes and deemed not important in binding although conserved. These slight differences might imply that TarP VBS2 may bind weaker than TarP VBS3 but stronger that TarP VBS1 which as mentioned is lacking two key hydrophobic residues. Indicating that perhaps *C.caviae* TarP VBSs have a VBS3>VBS2>VBS1 hierarchy in terms of affinity for vinculin.

When looking at sequence consensus between the three TarP VBS it appears that VBS1 and 2 share portions of homology in residues that appear not in the consensus sequence, VBS1 N856 and VBS2 N812 are shared alongside VBS1 T859 and VBS2 T814 and VBS1 K867 and VBS2 K823. All three of these are not seen in VBS3. While perhaps not immediately apparent this does give rise to the theory that VBS1 is the original VBS in TarP and through duplication mutations occur in VBS2 and again until reaching VBS3 which then shows the highest affinity so far. This works in tandem with as shown above VBS1 has fewer key hydrophobic residues in the core interface region and this amount increases in VBS2 until VBS3 where key hydrophobic residues appear to give the highest affinity. This indicates that perhaps TarP VBS1 was the original TarP VBS and through duplication mutations, each subsequent VBS increases in number of key hydrophobic residues and subsequently an increase in affinity for vinculin. This increase in affinity could have enhanced TarP's ability to form complexes needed for the internalisation of the EB.

4.1.2 The stoichiometry of Vinculin binding to TarP VBS1-3

The binding data for TarP VBS3 proved that multiple high affinity VBS are present in *C.caviae* TarP C-terminal, but as all of the TarP VBS are present in close proximity to each other the question arose of how many VBS could be bound to vinculin at one time. By performing a GST pulldown, we found that TarP VBS1-3 GST could associate with VD1 in a 1:3 ratio (figure 19), indicating that each VBS can bind one VD1 monomer concurrently. While the GST pulldown did show some traces of VD1 in the supernatant the vast majority of the VD1 associated with the TarP VBS1-3 GST attached to the glutathione beads in the pellet. While this result shows a good confirmation that the stoichiometry of TarP VBS1-3 GST to VD1 ratio is 1:3 the SEC-MALS assay would have proved this ratio by measuring the MW accurately to see if three VD1 monomers do truly associate with the TarP VBS1-3 GST-tagged. The SEC-MALS however were unsuccessful due to reasons explained in section 3.1.4 and would need to be repeated to corroborate the GST-pulldown data.

The size of the regions separating the three TarP VBS at the C-terminal region of TarP is something that could possibly influence the predicted 1:3 ratio of TarP VBS1-3 to VD1, if the regions between each VBS are too short for example this could physically inhibit the binding of multiple vinculin. While no structure of the entire TarP VBS1-3 region exists, a structural model was made using residues 745-868 with the linker regions between each TarP VBS added. Note the linker region between TarP VBS3 and 2 is a ~44aa disordered loop, while the TarP VBS2 has an additional short helical region after the consensus VBS and a short ~6 aa disordered loop region connecting it to TarP VBS1. The secondary structure prediction software PSIPRED was used to determine

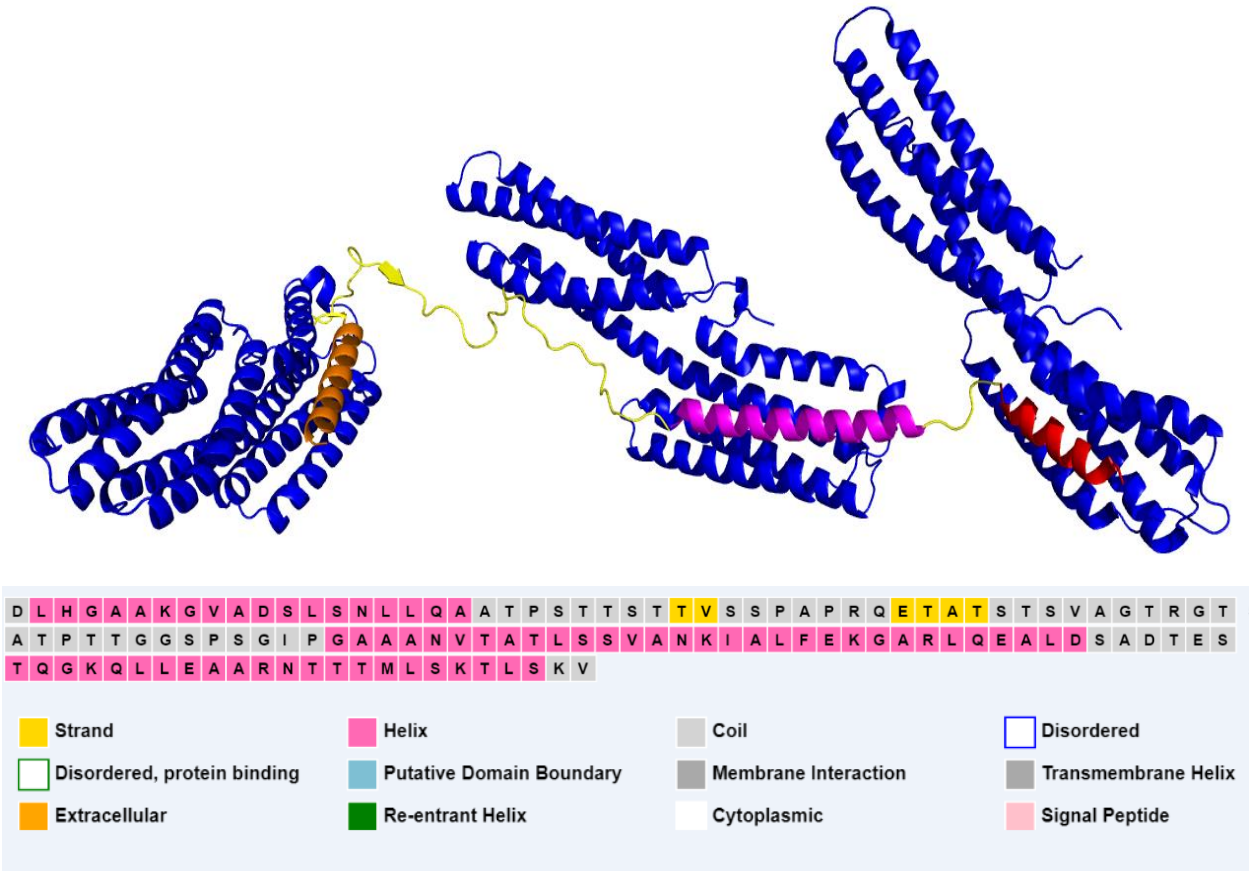

Figure 32-(Top) PyMOL model of TarP VBS1-3 (745-868) with three VD1 molecules to indicate in the linkers physically allow this 1:3 binding stoichiometry. TarP VBS1 red, TarP VBS2 pink, TarP VBS3 orange with the linkers in yellow. (Bottom) PSIPRED secondary structure analysis of TarP VBS1-3 residues 745-868 showing each TarP VBS (pink) and the two linker regions between them.

these linkers (figure 31). Viewing the model, it seems possible that all three TarP VBS can bind a VD1 monomer, although the linker region between TarP VBS2 to VBS1 is only 6 residues it appears that the VD1 monomers are able to bind each TarP without being physically blocked. Additionally, although not modelled the remaining residues in the TarP protein are primarily disordered and as such may not appear to interfere as much with the VBS region in comparison to fully formed helical or β-sheet domains.

While the model suggests that three VD1 monomers can bind concurrently to TarP VBS1-3, in vivo the TarP will be binding to full length vinculin not just VD1. The difference between TarP VBS1-3 binding to three VD1 monomers and binding to three

full length vinculin monomers, in terms of the physical spacing between protein chains will certainly be substantially different.

4.1.3 Does TarP VBS stoichiometry change throughout the chlamydial pathogenesis cycle?

In a recent study by Pedrosa et al they suggest that TarP has a post invasion role after the internalisation of the Chlamydial EB (Pedrosa et al., 2020). This post-invasion role for TarP see it modulating the dynamics and organization of host cell focal adhesions This post invasion role envisions TarP molecules being inserted into FACs and actively reorganising and stabilising them, this results in more FACs being formed and reducing he motility of the infected cells through higher numbers of cell-ECM contacts. This higher number of cell-ECM contacts appears to suggest that higher contact between the cell and the ECM will reduce apoptotic signals associated with cell detachment (Frisch and Francis, 1994; Gudipaty et al., 2018).This post invasion role differs considerably from the actin recruiting and remodelling for EB internalisation seen early in invasion and expands a theory that each VBS present in TarP may be used at differing times throughout the chlamydial pathogenesis cycle, as both the roles that TarP exhibits rely on the TarP VBS domains interaction with vinculin. So perhaps in initial invasion a certain TarP VBS or number of VBSs are needed to facilitate invasion while in the post invasion role a different configuration of VBS interactions may be required. Previously a study by Thwaites et al. suggested that the TarP VBS1 in *C.caviae* was essential in the initial invasion stage where it bound and recruited vinculin, with both TarP VBS2 and 3 being deemed dispensable (Thwaites et al., 2015). In the study Thwaites mentions however that if investigated TarP VBS2 and 3 may appear to have roles in stabilisation

and maturation of the protein complex although no data is presented for this. The data collected throughout this study may help to corroborate the link between Pedrosa's post invasions role for TarP and Thwaites study of TarP VBS1 being essential for invasion. Possibly during initial invasion, the C-terminal TarP VBS1 is all that is required to bind and recruit Vinculin for invasion while TarP VBS 2 and 3 are dispensable. However, when the TarP is then integrated into FACs post invasion all three VBS might be utilised to bind multiple vinculin molecules rearranging and stabilising FACs connection to the ECM. The higher binding affinity seen in TarP VBS3 to VD1 may also indicate that its role is required more in stabilisation rather than the recruitment role seen in TarP VBS1 which exhibits a slightly lower binding affinity to VD1. While speculation the data collected in this study possibly supports the idea that there could be varying configurations of TarP VBS bound to vinculin throughout different stages of the chlamydial pathogenesis cycle.

4.2 Project 2: Lethality rescuing VD1 mutants' unique interactions with talin H50

This study aimed to analyse the binding interactions between the three A501, P15L and W253X with the VD1 mutants and talin H50, binding interactions proved by FP (Data generated by Dr Karen Baker Postdoc Goult lab) showed high levels of disruption in VBS and mutant VD1 binding in the tested VBS. This disruption of talin vinculin interactions in *Drosophila* lead to the rescue from lethality when hyper-active CO vinculin was introduced. While disruption seemed mostly uniform across the VBS, H50 in talin showed considerably less disruption in binding with the VD1 mutants. Uniquely H50 was able to bind the A50I mutant with a K_d of 1.015 µM, whereas in other talin VBS the binding was disrupted giving affinity values between K_d 14 µM and 38 µM.

In this study the W253X-H50 structure was solved and the binding interactions analysed to determine why the W253X deletions of the last six residues of VD1 can rescue the *Drosophila* lethality phenotype.

4.2.1 The structural comparison between the W253X-H50 and the WT VD1-H50 structures indicates subtle differences in interactions and helix placement

In section 3.2.1 the W253X-H50 was compared to the WT VD1-H50 structure (4DJ9) the two complexes overlaid appeared structurally conserved apart from an additional hydrogen bond VD1 Q19 to H50 S2096 and the position of H50 lysine K2099. In W253X-H50 K2099 is orientated away from the binding interface whereas in the WT VD1-H50 its orientated spatially towards a histidine in the VD1 α1 helix, one positively charged residue repulsing another and causing a slight shift in WT VD1 α1 helix. This displacement of α1 helix in VD1 is by this lysine residue as mentioned in WT VD1-H50

study (Yogesha et al., 2012) however they attribute a different histidine (H22) that could be repulsing the lysine residue, however H27 positions seems more indicative of interacting with K2099 and displacing the α1 helix of VD1, however is most likely a combination of the two. This results in the WT VD1 α1 helix being shifted away from the H50 peptide by a small degree, in the W253X-H50 structure this shift is still present but to a lesser degree suggesting the lysine's position is not solely responsible for this helix shift but plays a large role.

This change of K2099 orientation is only seen in W253X-H50 complex and the deletion of the last six residues somehow causes this change, a theory to why this occurs could be that an interaction/spatial restraint between the last six residues in α7 and the first 5 in α1 of VD1 may cause this slight shift in the α1 helix. This interaction is not completely modelled in either H50 structure, but can be seen in the Shigella IpaA-VBS3 in complex with human VD1 structure (PDB 3RF3 (Watabe-Uchida et al., 1998). Note that both the last six residues and the first five residues are disordered loops. The presence of the

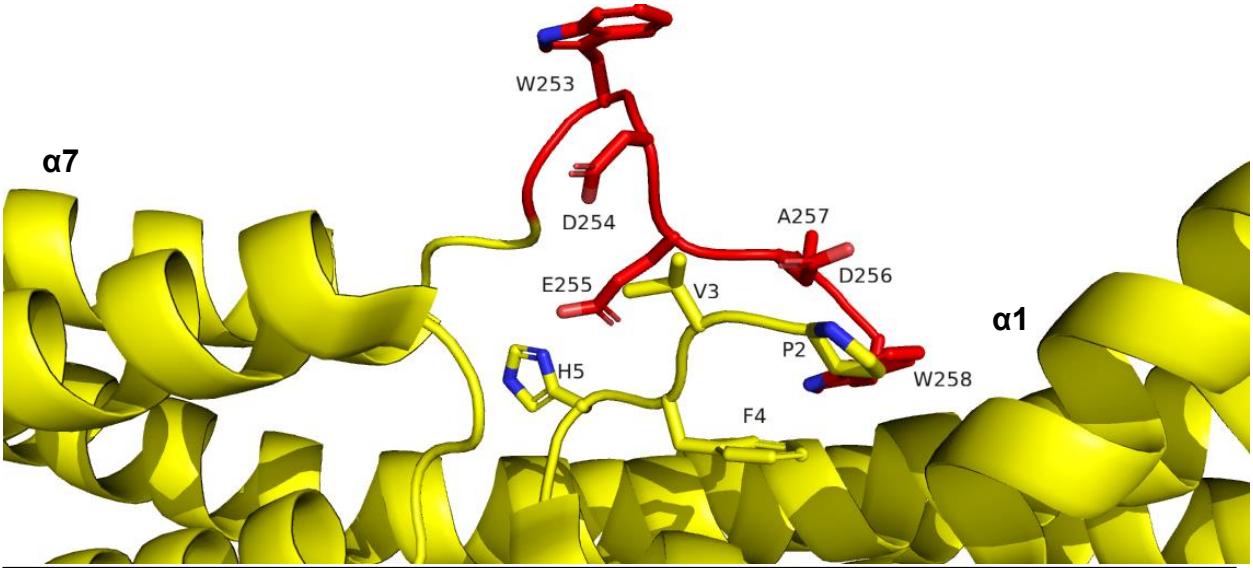

Figure 33-PyMOL model of residues 1-5 (yellow) region of VD1 in contact with residues 253-258 (red) of VD1 both present in disordered loops. PDB 3RF3 Watabe-Uchida et al., 1998.

last six residues of VD1 could possibly constrain the first five residues of VD1 to a small degree, this constraint leads to a VD1 phenylalanine F4 to interact with three hydrophobic residues I9, L13 and A17 in the VD1 α1 helix, maintaining the α1 helix at an angle. This interaction in combination with the K2099 repulsion of the histidine H22 could maintain α1 in its shifted position away from the H50 peptide in the WT VD1-H50 complex. In the W253X-H50 complex the last six residues are deleted and the F4 interactions with I9, L13 and A17 are disrupted. This alteration could possibly cause the α1 helix to shift back towards the H50 peptide and in the process the repulsion from the positively charged H22 and H27 in the a1 helix causes K2099 to adopt a new

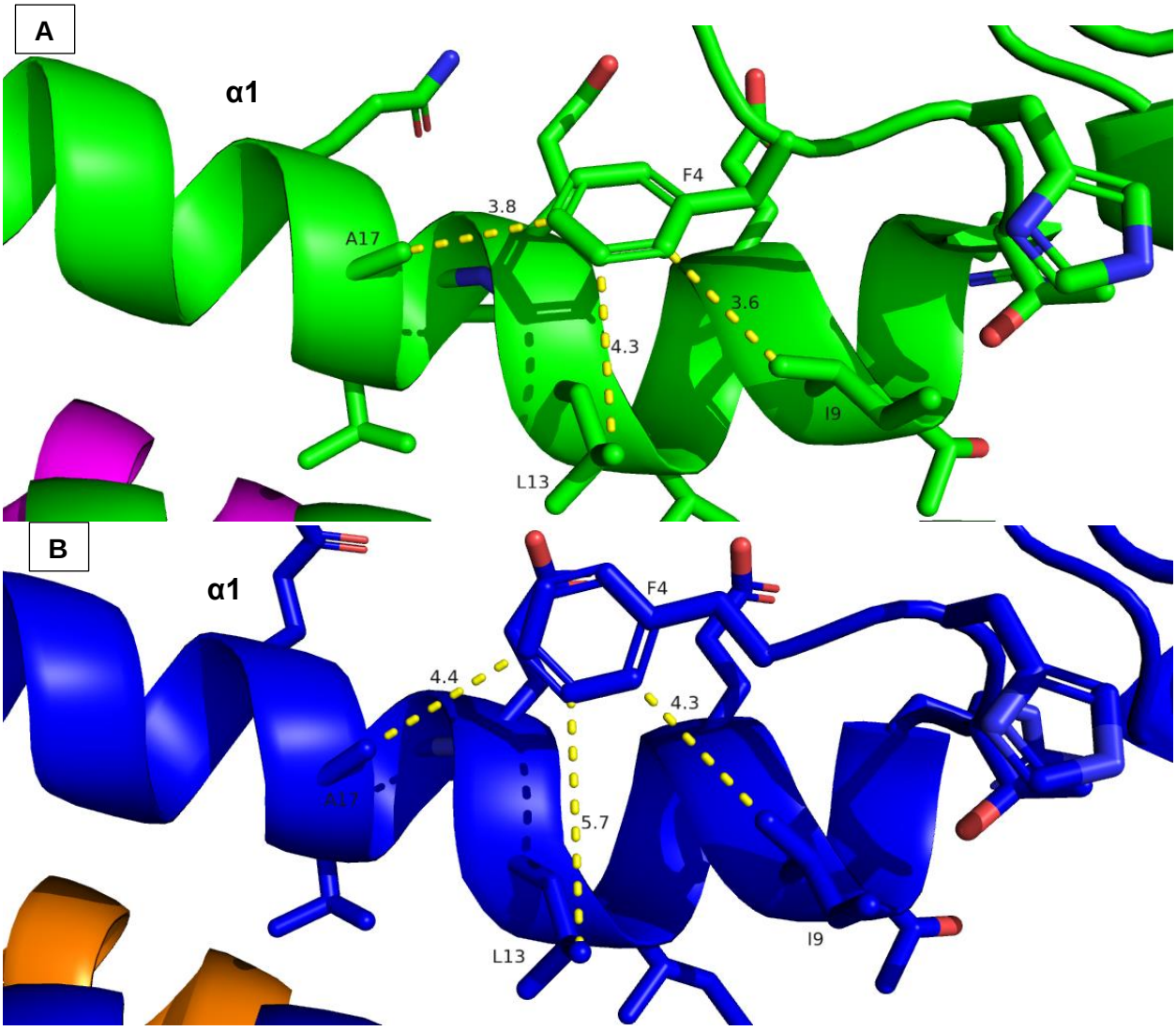

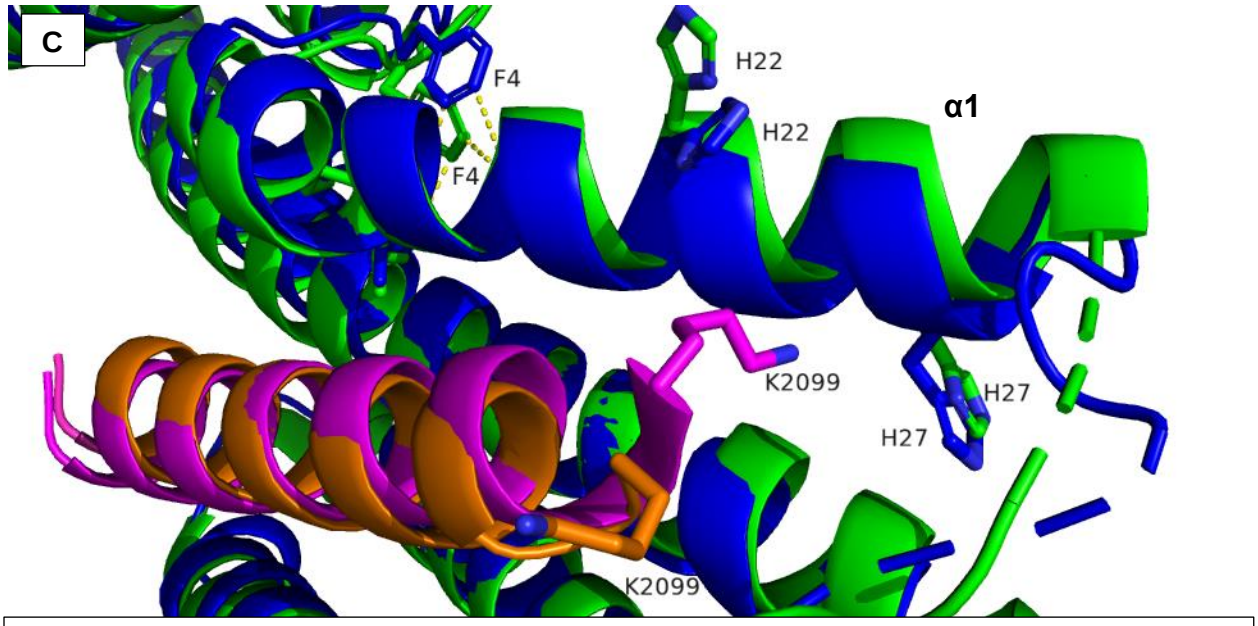

Figure 34-A) In the WT VD1-H50 (green, pink) structure F4 appears to be close enough to establish hydrophobic interactions with I9,L13 and A17 keeping the α1 helix in its shifted conformation away from H50. B) In the W253X-H50 (blue, orange) structure F4 appears to favour a different rotamer and appears not to interact with I9, L13 and A17 as closely which could possibly cause the shift in the α1 helix of VD1 to shift towards the H50 peptide. C) Overview of the F4 interactions linked with the shift in the α1 helix one of VD1 and the displacement of K2099 in the W253X-H50 structure, perhaps through repulsive interactions from H22 and H27 caused by the shift in the α1 helix.

orientation away from the binding interface altogether. Unfortunately, the last six and first five residues are in disordered loops and not fully modelled in either the W253X or WT VD1 models and the theory of their interaction and thus lack of it causing this shift in the α1 helix, is at the moment conjecture based on several different. VD1-VBS complexes and further data is required to make a more conclusive analysis. The lysine orientation, additional hydrogen bond and α1 helix shift towards the H50 however do result in a slight difference in binding affinity between the WT VD1-H50 and W253X-H50 with each showing K_d values of 610 nM and 515 nM respectively (figure 34). Indicating that the deletion of the last six residues in W253X mutant does have small effects on the binding affinity.

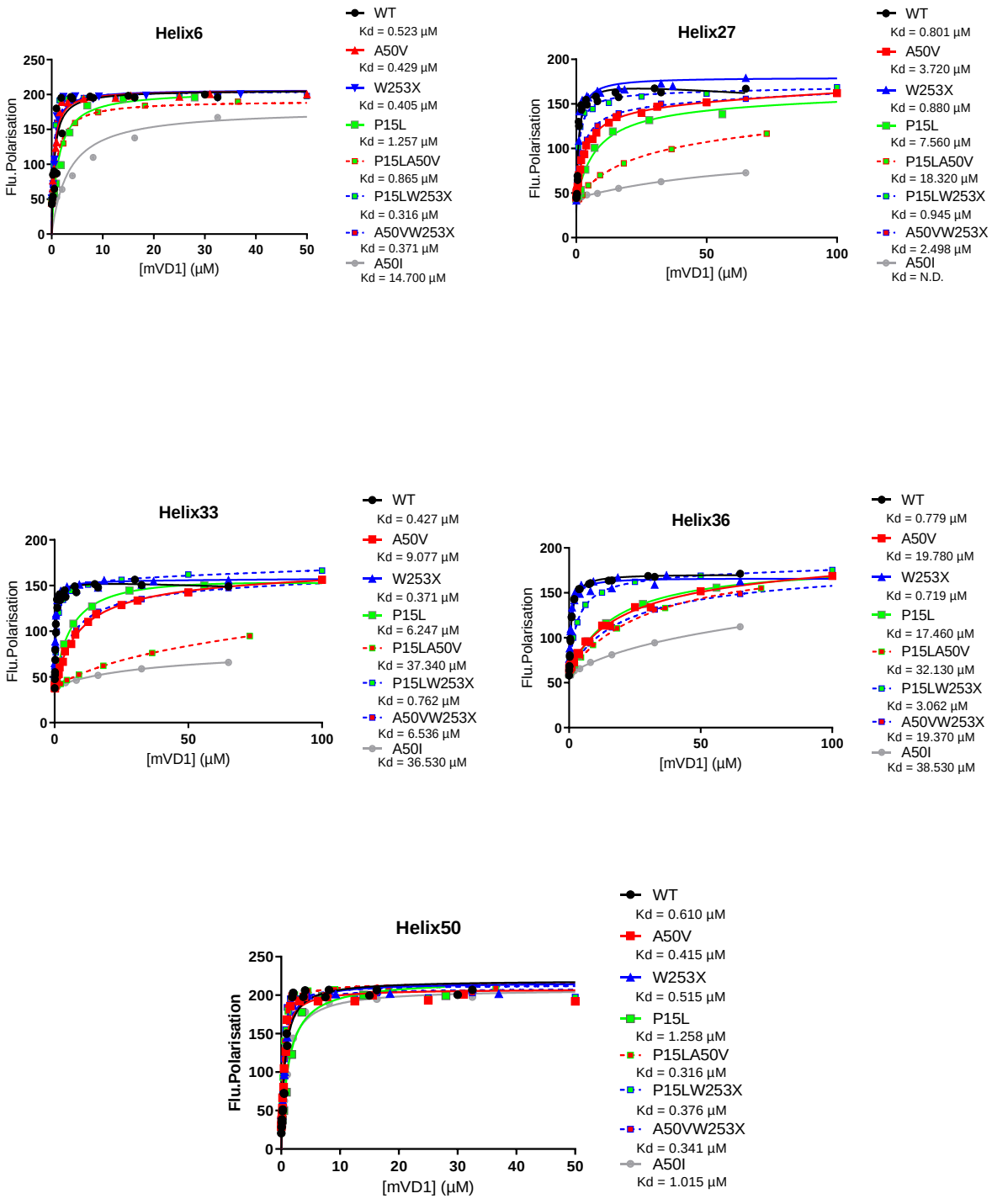

Figure 35-FP data of lethality rescuing VD1 mutants being tested against talin helixes 6, 27, 33, 36 and 50.The VD1 mutants are A50V, W253X, P15L, A50I and double mutants P15LA50V, P15LW253X and A50VW253X. (Data generated by Dr Karen Baker Postdoc Goult lab).

4.2.2 What causes the W253X mutant to rescue *Drosophila* from lethality

Why the W253X mutant results in rescuing *Drosophila* from lethality is something that from the structure or biochemical analyses is not apparent, as the deletion of the last 6 residues is all that differs from the WT VD1. These residues could possibly interact with other proteins to cause this phenotype, as from the structure they do not negatively interact with VBS binding, when compared to the A50I and P15L mutants. Figure 34 shows that the deletion of these residues only strengthens the binding affinity, this strengthening of binding affinity caused by the W253X mutant is not unique to H50 as all the tested talin VBS shared this increase in binding affinity. Additionally, double mutants of P15LW253X show large increases in affinity compared to the single P15L mutant.

One possibility is that the last six residues may be important in forming VD1:talin aggregates, although these aggregates have been shown not to be essential for the lethality phenotype their involvement has not been ruled out (Maartens et al., 2016). VD1 it is known to dimerise after time in vitro, perhaps VD1 dimerisation plays a role in aggregate formation and by deleting the last six residues this is disrupted and the *Drosophila* are rescued from lethality phenotype. This is just a possibility and until more structures of these VD1 mutants in complex with H50, especially double mutants like the P15LW253X, why the W253X mutant rescue *Drosophila* will remain conjecture.

4.2.3 How is the H50 able to bind to both the A501 and P15L VD1 mutants

Both the A50I and P15L (figure 35) mutations caused complete disruption in binding in the majority of talin VBSs tested, an outlier was seen when binding to H50 K_d values

where A50I bound with 1015 nM and P15L with 1258 nM. This points to a unique interaction between H50 and both A50I and P15L. While the A50I-H50 and P15L-H50 structures aren't available, by comparing the WT VD1-H50 to another VD1-talin VBS structure for example the VD1-talin helix 33 (H33) structure (PDB 3S90,(Yogesha et al., 2011) we may identify why H50 binds to both these VD1 mutants.

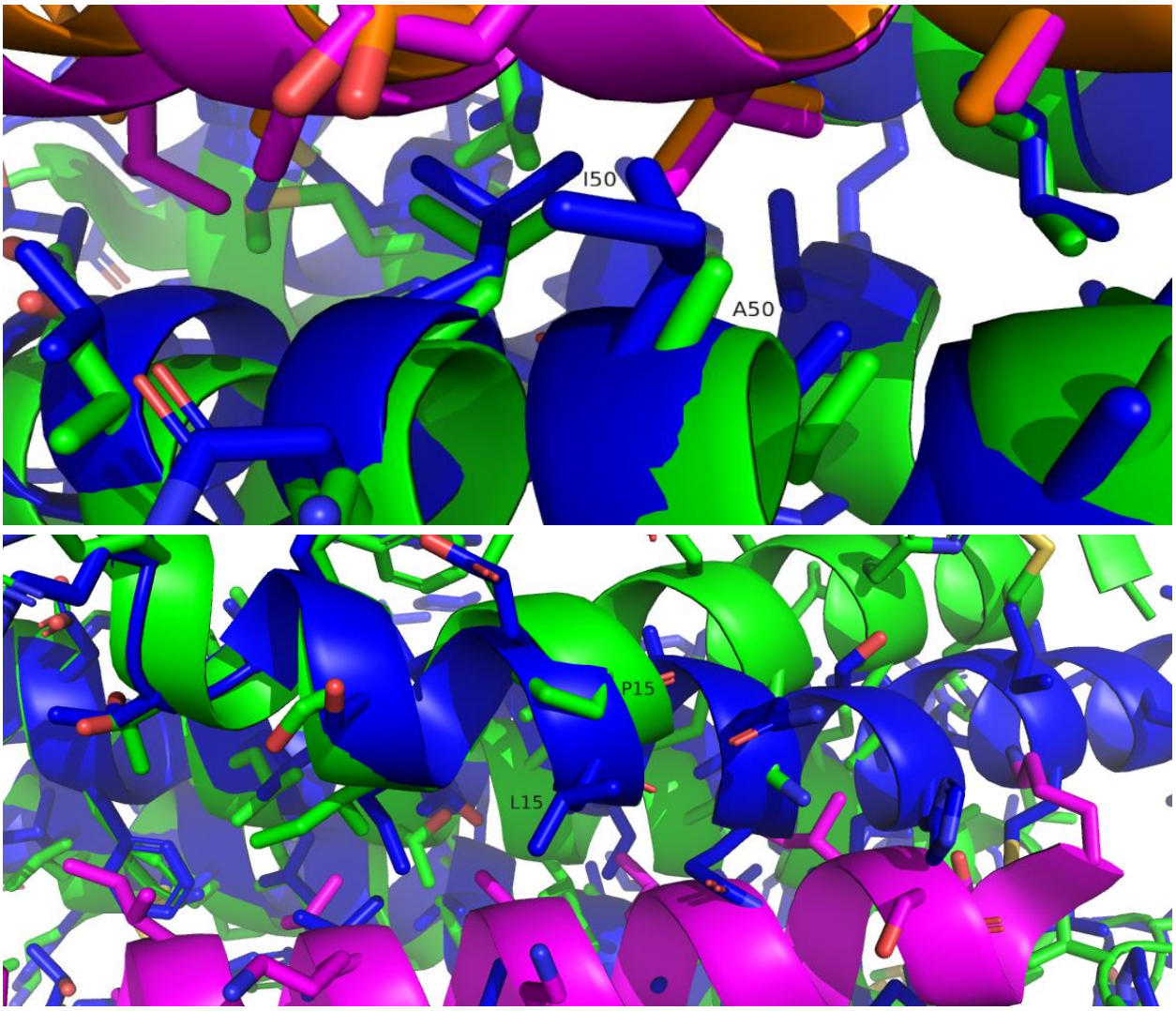

Figure 36-(Top) PyMOL model depicting the A50I VD1 mutation, the larger hydrophobic isoleucine causing possibly limiting a VBS interaction with the VD1 hydrophobic core.(Bottom) PyMOL model depicting the P15L mutation that would cause an alteration in the α1 helix of VD1 again possibly restricting a talin VBS from binding. PDB 4DJ9,Yogesha et al.,2012.PDB 3S90,Yogesha et al., 2011.

When the WT VD1-H50 structure is compared to WT VD1-H33 structure, some similarities and differences are seen. Both share the lysine interacting with the α1 helix

Histidine, however H33's K1544 seems not to be able to interact with Histidine 27 as is seen in the H50 structure. The H33 structure VD1 α1 helix is shifted away from the H33 peptide but not to the same degree as the H50 structure (figure 36). A sequence alignment shows that both H50 and H33 share residue conservation broadly especially

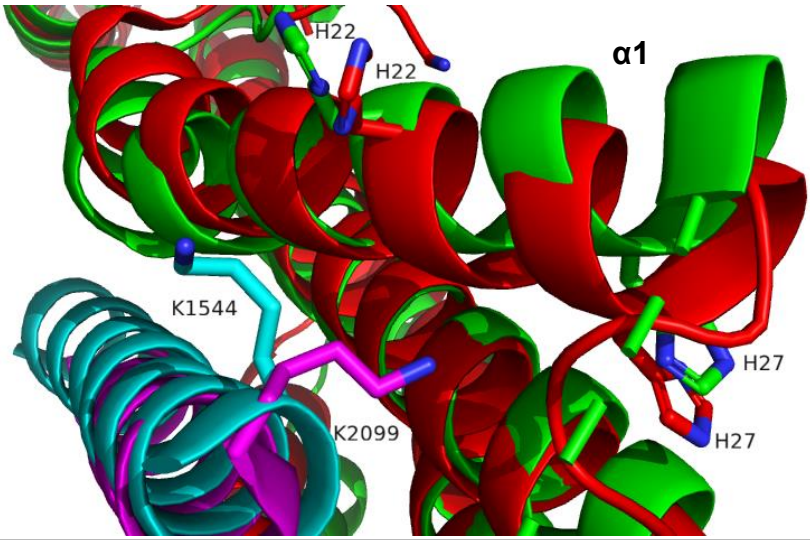

Figure 37-A structural comparison between the WT VD1-H50 (green, pink) structure and the WT VD1 - H33 (red, cyan) structure shows the conserved lysine is positioned differently, in the H50 structure K2099 appears to be orientated more towards both H22 and 27 in α1 helix of VD1 and as such the α1 helix is positioned further away from the H50 peptide. In the H33 structure K1544 appears to be orientated in a position where H27 has a weaker interaction and as such K1544 seems to orientate solely by the position of Histidine 22, this allows VD1 helix one to be able to associate more closely with H33 than in the H50 structure. PDB 3S90,(Yogesha et al., 2011)

with the hydrophobic residues, but some differences are seen between residues towards the C-terminus of the VBS (figure 37). The H50 VBS has three key residue differences in this region compared to H33, in H33 the residues A1537, K1541 and T1542 and in H50 these are all substituted with residues with smaller sidechains G2092, S2096 and A2097, respectively.

Additionally, the VD1-H50 and VD1-H33 complexes differ in the number of interactions between the VD1 and VBS, VD1-H50 has only one hydrogen bond whereas the VD1-H33 complex has five hydrogen bonds as well as a salt bridge. The difference in

residues size and the lack of constraint caused by polar/electrostatic interactions may mean that the H50 is able to accommodate the A50I and P15L mutants.

```
Talin_H4|607-636         ------------PLLQAAKGLAGAVSELLRSAQPASAEPRQN-30
Talin_H33|1512-1546      ASARTANPTAKRQFVQSAKEVANSTANLVKTIKA-------- 34
Talin_H36|1628-1652      --------PRWSVLAGHSRTVSDSIKKLITSMR--------- 25
Talin_H50|2078-2099      -----------VVLINAVKDVAKALGDLISATK--------- 22
                                    :    : :: :  .*: : :
```

Figure 38-MSA using Clustal Omega of talin helices containing VBSs, H50 appears to have residues with smaller sidechains (yellow) which may aid in its ability to accommodate the VD1 mutants such as A50I and P15L.

The ability of the P15LW253X (376 nM) double mutant to bind with a higher affinity when compared to the single P15L (1258 nM) mutant also shows how the α1 helix shift seen in the W253X-H50 complex may occur, with the W253X mutation creating another level of accommodation for mutations.

4.3 Project 3:α-catulin structural characterisation and comparison to Vinculin

The structural homology of α-catulin to vinculin and α-catenin indicated that possibly α-catulin could possibly engage in some of the same binding interactions seen in Vinculin but are also shared in α-catenin.

Through an FP assay an interaction between the ACT and paxillin's LD2 domain was seen although the K_d could not be determined as the interaction is weak, though GF an interaction between the ACT and VD1 was not seen so remains inconclusive.

4.3.1 The ACT binds weakly to Paxillin's LD2 motif much like the VT

The VT was shown to interact with paxillin (Turner et al., 1990) and specifically to paxillin's LD2 domain (Brown et al., 1996) by performing an FP assay the ACT appears to bind the LD2 motif with as well with the same weak binding curved observed for the VT (figure 28).While the binding curve can only indicate an inconclusive result, having very similar curves, both VT and the ACT sharing similar structure and the knowledge that the VT interacts with the LD2 domain raises the possibility that the ACT can interact with the LD2 domain.

Paxillin has been shown to bind both vinculin and talin (Zacharchenko et al., 2016) and is implicated in the recruitment of both to FACs (Pasapera et al., 2010). Paxillin alongside kindlin and FAK are thought to localise to the cell membrane and form pre-adhesion complexes and subsequently recruit talin and vinculin which then go on to form mature FACs (Atherton et al., 2020).

The interaction between the ACT and paxillin LD2 could indicate that α-catulin like vinculin may be recruited to FACs and once there it may regulate several signalling

pathways such as remodelling actin networks through its interaction with the Lbc Rho Guanine Nucleotide Exchange Factor (Park et al., 2002). This α-catulin: paxillin interaction also could suggest that paxillin may be recruited and present in the DAPC.

4.3.2 The ACT appears not to interact with VD1

The structural similarity between the α-catulin and vinculin suggested the possibility that α-catulin might undergo head to tail autoinhibitory interactions much like vinculin does (Khan and Goult, 2019). The ACH was not able to be expressed but its similarity in with VD1 meant that perhaps the ACT could interact with VD1, as such the ACT-VD1 interaction was solely investigated. Using GF, the ACT was shown not to interact with VD1 however the assay was only preliminary, and issues with varying protein concentrations mean that the result itself is still inconclusive.

A Phyre2 (Kelley et al., 2016) generated model of the ACT overlaid over the VT in the VD1-VT structure (PDB 1RKE,(Izard et al., 2004) does show similarities in the binding interface however although with reduced hydrogen bonds present between the ACT and VD1 in comparison to the VT. Also, in the ACT the α4 helix appears to be a disordered loop at the region that is in contact with the VD1, in the VT this is a fully structured α-helix and has some hydrophobic and polar bonds with VD1. These differences may indicate why the ACT does not associate with VD1 however, this is purely based of Phyre2 models in PyMOL, and would require repeating the GF and perhaps performing other binding assays such a using microscale thermophoresis (MST) to prove if any interaction is present.

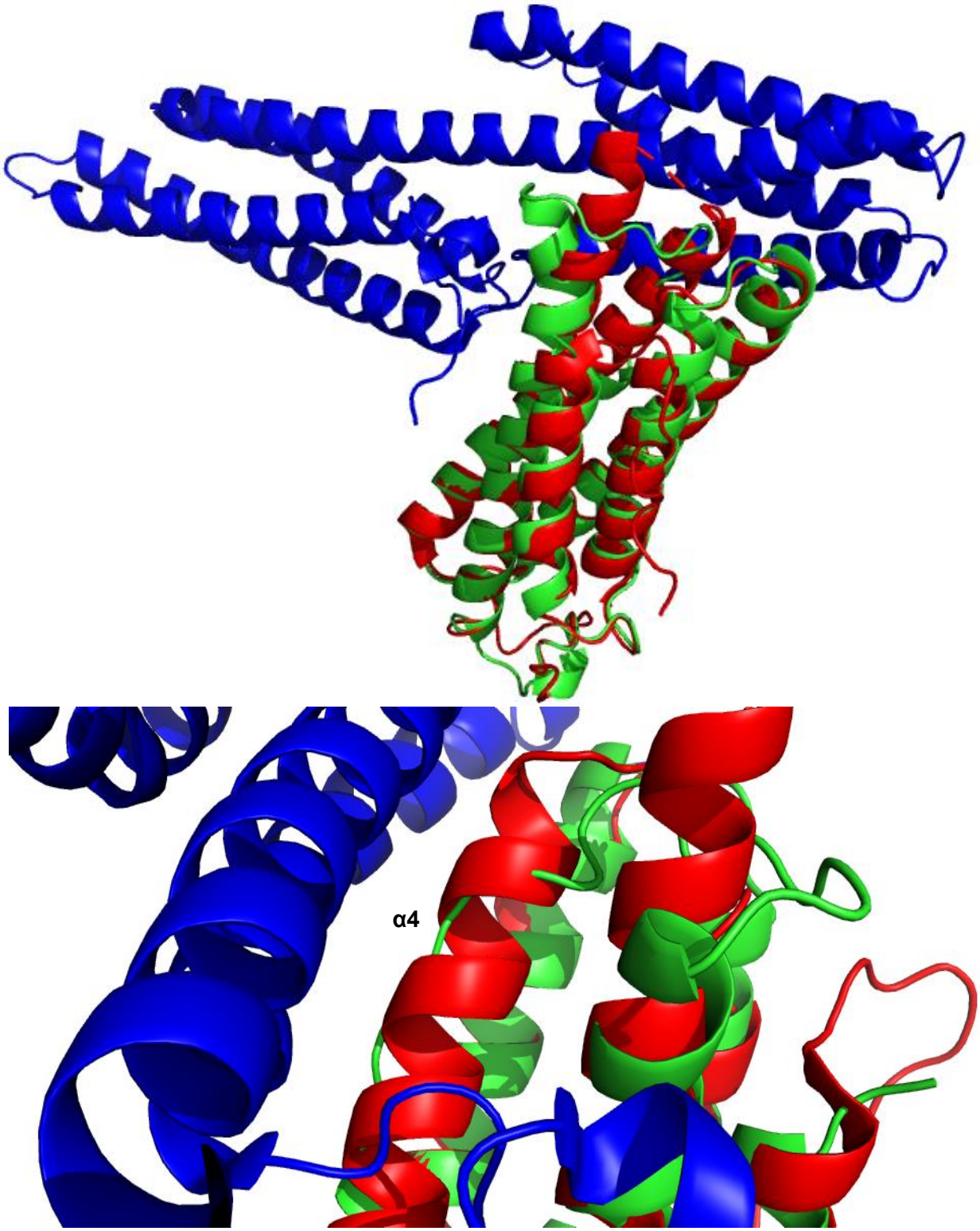

Figure 39-(Top) Overlay of the ACT (green) with VT (red) in an autoinhibited conformational with VD1 (blue). (Bottom) The α4 helix in the VT has a α-helical structure which enables it to interact with VD1 through polar and hydrophobic bonds. The ACT lacks α-helical structure in this region and could possibly result in less stable interactions between this region and VD1. PDB 1RKE, Izard et al., 2004.

4.2.3 Is it possible for the ACH bind to talin VBS in the same way as VD1?

The ACH's homology to VD1 suggested that the ACH could indeed bind to talin VBS in the same helical bundle method as VD1, however with the ACH not expressing and attempts to clone the ACH into more suitable vectors were unsuccessful this prediction was not able to be tested.

However by using Phyre2 a model of the ACH can be overlaid with the WT VD1-Helix4 (PDB1SYQ,(Izard and Vonrhein, 2004) structure to give some idea as if the ACH could indeed bind talin VBS (figure 39A). Overlaying the two structures conserved residues in VD1 are seen in the ACH, P15 which in VD1 allows the α1 helix to incorporate VBS is present at the same point in the ACH P42 as well as the semi conserved VD1 Q19 which hydrogen bonds with serine in many VBS and also is seen in the ACH Q46 (figure 39B).

Many of the hydrophobic residues found in the core of the VD1 interaction with VBSs are also seen in the ACH, one residue difference in the ACH however may inhibit a talin VBS binding to the ACH. In VD1 L54 is positioned between two hydrophobic residues in the VBS peptide and contributes to the VBS tight binding, in the ACH the leucine is replaced by F81, while phenylalanine is hydrophobic its large aromatic ring may disrupt the VBS peptide from properly aligning with the other hydrophobic residues that line the VD1 hydrophobic core (figure 39C). While the position of F81 could disrupt binding the homology of ACH to VD1 still suggests the possibility of the ACH binding to a talin VBS in the same way as VD1.

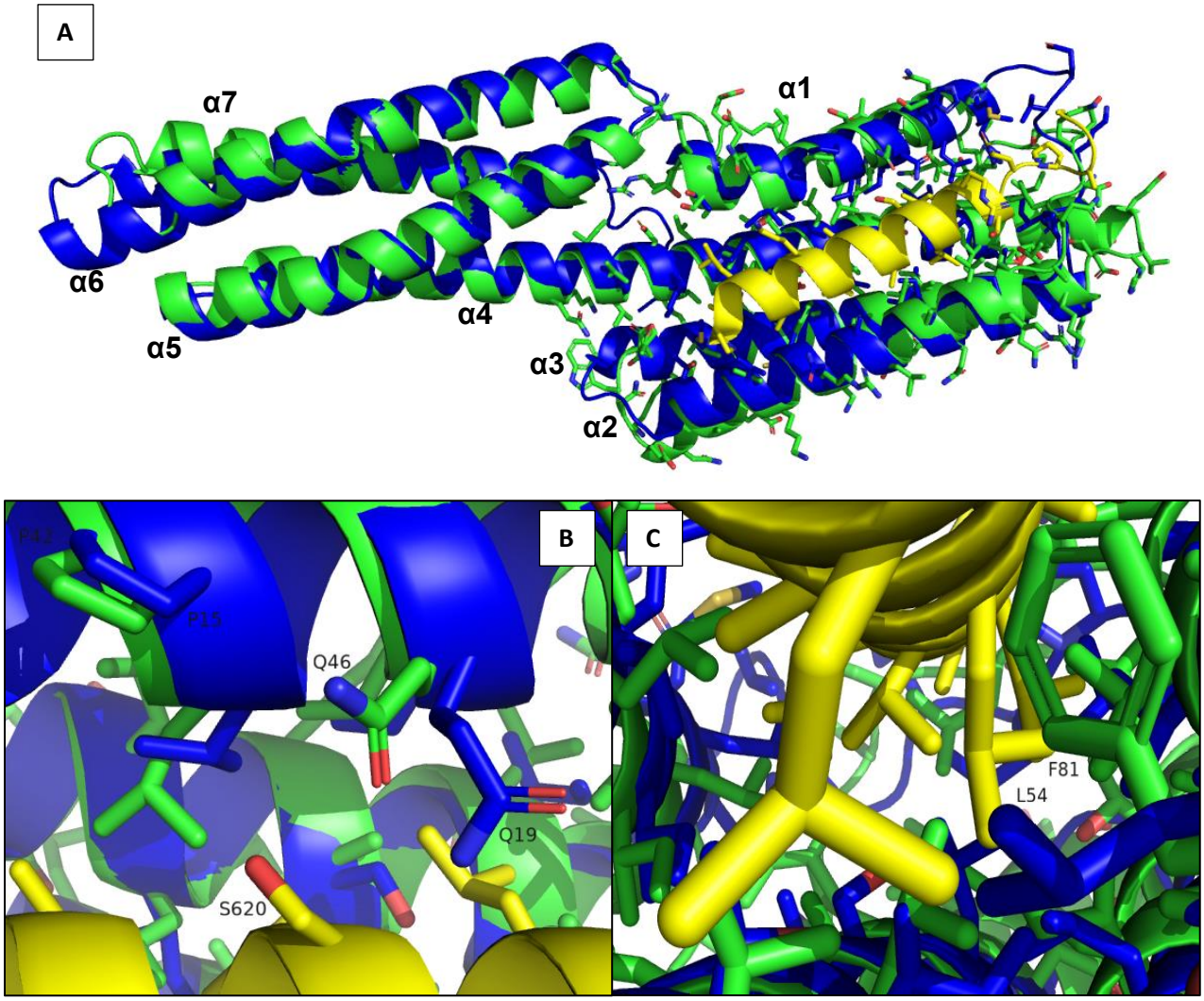

Figure 40-A) Overlay of the ACH (green) with WT VD1-H4 (blue, yellow) with interface residues side chains are modelled using the interfaceresidues.py script in PyMOL. B) Both P15 and Q19 are conserved in the ACH as P42 and Q46, the proline enables the curve seen in the α1 helix of VD1 and the glutamine enables a conserved hydrogen bond between serine. C) The hydrophobic core of VD1 and ACH are similar in hydrophobic residue placement and amino acid, apart from in the ACH the large F81 residue replaces L54 in VD1. F81 could interfere with talin VBS helixes bind to the ACH. PDB 1SYQ, Izard and Vonrhein, 2004.

α-catulin could bind to a talin though a ACH-VBS interaction after being transported to FACs through its interaction with paxillin's LD2 motif in a very similar manner to vinculin, α-catulin's further signalling roles could help regulate and remodel FACs much as it does in the DAPC.

5 Future work

5.1 Project 1:*C.caviae* TarP VBS study

The ability of TarP VBS3 to bind to VD1 and TarP VBS1-3 being shown to interact with VD1 in a 1:3 ratio has opened the idea that all three TarP VBS can bind tightly to VD1 at once and each TarP VBS may have specific roles in pathogenesis. To aid in corroborating the 1:3 ratio of VD1 binding to *C.caviae* TarP VBS1-3, the affinity of the *C.caviae* TarP VBS2 for VD1 will need to be quantified by FP much like TarP VBS1 and 3. *C.caviae* TarP also contains two actin binding regions either side of TarP VBS3, comparisons in actin's ability to bind to TarP in the presence of VD1 could prove if the binding of actin and VD1 are mutually exclusive or perhaps exist in varying stoichiometries of VD1 binding. A crystal structure of both the TarP VBS2 with VD1 would complete the trio of TarP VBS and allow analysis and comparison between the three TarP VBS. Also, a crystal structure of TarP VBS1-3 with VD1 could also aid in clarifying if the stoichiometry of 1:3 TarP VBS1-3 to VD1 binding is correct. Lastly the difference in affinity between TarP VBS1 and three was proposed to because of a pair of threonines in TarP VBS1 replacing a valine and leucine. By mutating the pair of threonines to a valine and leucine and then performing an FP assay could confirm if it is indeed these threonines causing the difference in affinity.

5.2 Project 2:VD1 lethality rescuing mutant study

While the W253X-H50 structure was obtained and some unique binding interactions are seen the W253X mutant itself does not interfere with the talin VBS binding, and while the W253X has shown to rescue lethality in *Drosophila* with hyperactive vinculin the

W253X-H50 does not reveal clear mechanism of how. A proteomic approach may help to identify if any additional interactions are seen with the W253X mutant, that may identify how it rescues the lethality phenotype. To acquire crystal structures of the A50I and P15L mutants as well as possibly some double mutants such P15LW253X in a complex with H50 would allow a better understanding of why H50 seems more able to incorporate VD1 mutations when binding.

5.3 Project 3:α-catulin-vinculin homology study

To better understand whether α-catulin shares binding interactions with many of the same proteins as vinculin, constructs such like the ACH could be cloned into a more suitable expression vector and binding assays such as FP, MST, NMR and crystal structures could be performed with talin VBSs to ascertain if the ACH can interact with talin in the same helical bundle method as VD1.

The interaction between the ACT and VD1 was inconclusive and would need repeating with proper controls and additionally if the ACH was able to be expressed GF/SEC-MALS assays could be performed to examine the interaction between the ACH and ACT, which could possibly mimic the VD1-VT autoinhibited structure seen in vinculin. Both the VT and α-catenin tail have been shown to bind and bundle actin, an actin co-sedimentation assay could be performed identify whether the ACT also binds and bundles actin.

α-catenin has been shown to contain a VBS which can bind to VD1 (Rangarajan and Izard, 2012; Yao et al., 2014b), this VBS is not conserved in vinculin, however it appears to be conserved in α-catulin (figure 40). By performing an FP assay with a α-

catulin VBS peptide with VD1 a possible interaction could be identified (Note a peptide of the α-catulin VBS was designed and ordered but production was unsuccessful).

```
BAD AVG GOOD
α-catulinVBS|335-369    AYTSHEHRERILELSSQARTELQQLLSVWMQTQSR
α-cateninVBS|323-357    SCTRDDRRERIVAECNAVRQALQDLLSEYMGNAGR
cons                    : * .::****:  .. .*  **:*** :* . .*
```

Figure 41-MSA of the α-catulin VBS and the α-catenin VBS indicating high conservation of residues between the two, indicating that α-catulin may possibly be able to bind Vinculin as α-catenin has been shown to. Alignment made using T-Coffee alignment server.

Additionally, a GF/SEC-MALS assay could be performed with the α-catulin VBS present in a larger 'α-catulin VBS' construct and run with VD1 could identify an interaction (Note attempts to clone the 'α-catulin VBS' from the α-catulin full length were attempted but unsuccessful). Additionally the α-catenin VBS is present in a force dependant domain that exposes the VBS only when force is applied across the domain (Yao et al., 2014b), α-catulin appears to share homology in this region and single molecule force stretching experiments could indicate if α-catulin's proposed VBS is also positioned in a force dependant domain.

Lastly α-catulin residues 1-377 has been shown to interact with α-dystrobrevin 1 residues 468-590 (Oh et al., 2012) and further analysis of the α-dystrobrevin 1 residues 468-590 reveals what could be a VBS, which could in theory then interact with the ACH.A MSA reveals some conservation between this α-dystrobrevin 1 VBS and talin helix 58 VBS (figure 41). If able to express the ACH a FP assay could be performed with a peptide of the α-dystrobrevin 1 VBS.(Note like the α-catulin VBS mentioned in above a peptide of the α-dystrobrevin 1 VBS was designed and ordered failed to be synthesised).

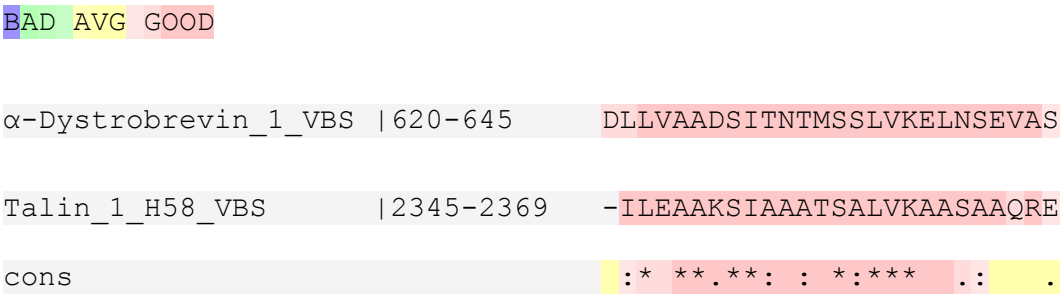

Figure 42-MSA of the proposed α-Dystrobrevin-1-VBS and the talin VBS helix 58 indicating good conservation of residues which may indicate that the ACH interacts with the α-Dystrobrevin-1's C-terminal through a VBS interaction much like is seen between talin VBS and VD1. Alignment made using T-Coffee alignment server.

6 Final conclusions

Throughout this study new data has been collected that help to answer some questions on the role of vinculin in the chlamydial pathogenesis cycle, also to visualise the W253X lethality mutant and its unique interaction with talin helix 50 VBS and lastly identify and explore some structural similarities between vinculin and one of its homologs α-catulin. Many of the experiments carried out in this study were in progress when the COVID-19 pandemic arose and the labs were closed, as such attempts to repeat some less complete results were hindered unfortunately.

6.1 Project 1 *C.caviae* TarP VBS study

The data shown in chapter one suggests that *C.caviae* TarP VBS3 does bind VD1 and with a higher affinity than TarP VBS1, and the TarP VBS3-VD1 crystal identifies residue differences that may indicate why the affinities for TarP VBS1 and 3 are different. The GST pulldown data also suggests that all three of *C.caviae* TarP VBS can be bound to VD1 at once. This data suggests that all three of *C.caviae* TarP VBSs can bind to VD1, but with TarP VBS1 and VBS3 showing different affinities this could indicate that each VBS is required only at certain steps in the chlamydial pathogenesis cycle.

6.2 Project 2 VD1 lethality rescuing mutant study

The W253X-H50 crystal structure identified some small but key differences from the lack of the last 6 residues in VD1, such as the α1 helix movement towards the H50 VBS as well as a change of orientation of a key K2099 residue when compared to the WT VD1-H50 structure. Sequence and structural comparison of the H50 VBS with other talin VBSs identified that smaller side chain residues, alongside K2099's potential to interact with the α1 helix may allow flexibility in H50 VBS binding to the VD1 lethality rescuing mutants such as A50I and P15L.

6.3 Project 3 α-catulin-vinculin homology study

The similarities between vinculin and α-catulin were seen in some Far UV CD secondary structure analysis confirming α-helical structure of the ACT. It was also shown that the ACT potentially interacts with paxillin's LD2 domain like the VT and opens the possibility that the α-catulin like vinculin could be recruited to FACs through an interaction with paxillin. Sequence analysis as well as models of the ACH overlaid on VD1 revealed the possibility that the ACH could bind talin VBS in the same helical bundle method as VD1. This indicates the potential for α-catulin binding to talin in FACs and potentially regulating actin networks, as well asking the question of whether all the talin VBS are specific to vinculin or perhaps could the two structurally homologous members of the vinculin superfamily α-catulin and α-catenin possibly also bind these 'VBS'.

7 Bibliography

Abdelrahman, Y.M., Belland, R.J., 2005. The chlamydial developmental cycle. FEMS Microbiol. Rev. 29, 949–59.

Abraham, L.S., Oh, H.J., Sancar, F., Richmond, J.E., Kim, H., 2010. An alpha-catulin homologue controls neuromuscular function through localization of the dystrophin complex and BK channels in Caenorhabditis elegans. PLoS Genet. 6.

Adams, M.E., Tesch, Y., Percival, J.M., Albrecht, D.E., Conhaim, J.I., Anderson, K., Froehner, S.C., 2008. Differential targeting of nNOS and AQP4 to dystrophin-deficient sarcolemma by membrane-directed α-dystrobrevin. J. Cell Sci. 121, 48–54.

Alatortsev, V.E., Kramerova, I.A., Frolov, M. V., Lavrov, S.A., Westphal, E.D., 1997. Vinculin gene is non-essential in Drosophila melanogaster. FEBS Lett. 413, 197–201.

Amann, K.J., Renley, B.A., Ervasti, J.M., 1998. A cluster of basic repeats in the dystrophin rod domain binds F-actin through an electrostatic interaction. J. Biol. Chem. 273, 28419–23.

Anthis, N.J., Wegener, K.L., Ye, F., Kim, C., Goult, B.T., Lowe, E.D., Vakonakis, I., Bate, N., Critchley, D.R., Ginsberg, M.H., Campbell, I.D., 2009. The structure of an integrin/talin complex reveals the basis of inside-out signal transduction. EMBO J. 28, 3623–3632.

Atherton, P., Lausecker, F., Carisey, A., Gilmore, A., Critchley, D., Barsukov, I., Ballestrem, C., 2020. Relief of talin autoinhibition triggers a force-independent association with vinculin. J. Cell Biol. 219, 1–16.

Atherton, P., Stutchbury, B., Wang, D.Y., Jethwa, D., Tsang, R., Meiler-Rodriguez, E., Wang, P., Bate, N., Zent, R., Barsukov, I.L., Goult, B.T., Critchley, D.R., Ballestrem, C., 2015. Vinculin controls talin engagement with the actomyosin machinery. Nat. Commun. 6.

Auernheimer, V., Goldmann, W.H., 2014. Serine phosphorylation on position 1033 of vinculin impacts cellular mechanics. Biochem. Biophys. Res. Commun. 450, 1095–1098.

Bakolitsa, C., Cohen, D.M., Bankston, L.A., Bobkov, A.A., Dadwell, G.W., Jennings, L., Crithcley, D.R., Craig, S.W., Liddington, R.C., 2004. Structural basis for vinculin activation at sites of cell adhesion. Nature 430, 583–586.

Bakolitsa, C., De Pereda, J.M., Bagshaw, C.R., Critchley, D.R., Liddington, R.C., 1999. Crystal structure of the vinculin tail suggests a pathway for activation. Cell 99, 603–613.

Barstead, R.J., Waterston, R.H., 1991. Vinculin is essential for muscle function in the nematode. J. Cell Biol. 114, 715–724.

Beeckman, D.S.A., Vanrompay, D.C.G., 2010. Bacterial secretion systems with an emphasis on the chlamydial Type III secretion system. Curr. Issues Mol. Biol. 12, 17–41.

Belhasan, D.C., Akaaboune, M., 2020. The role of the dystrophin glycoprotein complex on the neuromuscular system. Neurosci. Lett. 722, 134833.

Böhme, L., Albrecht, M., Riede, O., Rudel, T., 2010. Chlamydia trachomatis-infected host cells resist dsRNA-induced apoptosis. Cell. Microbiol. 12, 1340–1351.

Bois, P.R.J., O'Hara, B.P., Nietlispach, D., Kirkpatrick, J., Izard, T., 2006. The vinculin binding sites of talin and α-actinin are sufficient to activate vinculin. J. Biol. Chem. 281, 7228–7236.

Bouchet, B.P., Gough, R.E., Ammon, Y.C., van de Willige, D., Post, H., Jacquemet, G., Maarten Altelaar, A.F., Heck, A.J.R., Goult, B.T., Akhmanova, A., 2016. Talin-KANK1 interaction controls the recruitment of cortical microtubule stabilizing complexes to focal adhesions. Elife 5, 1–23.

Bowe, M.A., Mendis, D.B., Fallon, J.R., 2000. The small leucine-rich repeat proteoglycan biglycan binds to α-dystroglycan and is upregulated in dystrophic muscle. J. Cell Biol. 148, 801–810.

Brown, M.C., Perrotta, J.A., Turner, C.E., 1996. Identification of LIM3 as the principal determinant of paxillin focal adhesion localization and characterization of a novel motif on paxillin directing vinculin and focal adhesion kinase binding. J. Cell Biol. 135, 1109–1123.

Burridge, K., Connell, L., 1983. Talin: a cytoskeletal component concentrated in adhesion plaques and other sites of actin-membrane interaction. Cell Motil. 3, 405–417.

Burridge, K., Wennerberg, K., 2004. Rho and Rac Take Center Stage. Cell 116, 167–179.

Calderwood, D.A., Zent, R., Grant, R., Rees, D.J.G., Hynes, R.O., Ginsberg, M.H., 1999. The talin head domain binds to integrin β subunit cytoplasmic tails and regulates integrin activation. J. Biol. Chem. 274, 28071–28074.

Cao, C., Chen, Y., Masood, R., Sinha, U.K., Kobielak, A., 2012. A-Catulin Marks the Invasion Front of Squamous Cell Carcinoma and Is Important for Tumor Cell Metastasis. Mol. Cancer Res. 10, 892–903.

Carabeo, R.A., Grieshaber, S.S., Fischer, E., Hackstadt, T., 2002. Chlamydia trachomatis induces remodeling of the actin cytoskeleton during attachment and entry into HeLa cells. Infect. Immun. 70, 3793–3803.

Chandrasekar, I., Stradal, T.E.B., Holt, M.R., Entschladen, F., Jockusch, B.M., Ziegler, W.H., 2005. Vinculin acts as a sensor in lipid regulation of adhesion-site turnover. J. Cell Sci. 118, 1461–1472.

Chang, W.J., Iannaccone, S.T., Lau, K.S., Masters, B.S.S., Mccabe, T.J., Mcmillan, K., Padre, R.C., Spencer, M.J., Tidball, J.G., Stull, J.T., 1996. Neuronal nitric oxide synthase and dystrophin-deficient muscular dystrophy. Proc. Natl. Acad. Sci. U. S. A. 93, 9142–9147.

Changede, R., Xu, X., Margadant, F., Sheetz, M.P., 2015. Nascent Integrin Adhesions Form on All Matrix Rigidities after Integrin Activation. Dev. Cell 35, 614–621.

Chen, H., Choudhury, D.M., Craig, S.W., 2006. Coincidence of actin filaments and talin is required to activate vinculin. J. Biol. Chem. 281, 40389–40398.

Chinthalapudi, K., Patil, D.N., Rangarajan, E.S., Rader, C., Izard, T., 2015. Lipid-directed vinculin dimerization. Biochemistry 54, 2758–2768.

Chishti, A., Kim, A., Hoover, K.B., 1998. The FERM domain: a unique module involved in the linkage of cytoplasmic proteins to the membrane. Tibs 0004, 281–282.

Choi, C.K., Vicente-Manzanares, M., Zareno, J., Whitmore, L.A., Mogilner, A., Horwitz, A.R., 2008. Actin and alpha-actinin orchestrate the assembly and maturation of nascent adhesions in a myosin II

motor-independent manner. Nat. Cell Biol. 10, 1039–1050.

Chorev, D.S., Moscovitz, O., Geiger, B., Sharon, M., 2014. Regulation of focal adhesion formation by a vinculin-Arp2/3 hybrid complex. Nat. Commun. 5.

Ciobanasu, C., Faivre, B., Le Clainche, C., 2014. Actomyosin-dependent formation of the mechanosensitive talin-vinculin complex reinforces actin anchoring. Nat. Commun. 5, 3095.

Clifton, D.R., Dooley, C.A., Grieshaber, S.S., Carabeo, R.A., Fields, K.A., Hackstadt, T., 2005. Tyrosine phosphorylation of the chlamydial effector protein Tarp is species specific and not required for recruitment of actin. Infect. Immun. 73, 3860–3868.

Clifton, D.R., Fields, K.A., Grieshaber, S.S., Dooley, C.A., Fischer, E.R., Mead, D.J., Carabeo, R.A., Hackstadt, T., 2004. A chlamydial type III translocated protein is tyrosine-phosphorylated at the site of entry and associated with recruitment of actin. Proc. Natl. Acad. Sci. U. S. A.

Cohen, D.M., Chen, H., Johnson, R.P., Choudhury, B., Craig, S.W., 2005. Two distinct head-tail interfaces cooperate to suppress activation of vinculin by talin. J. Biol. Chem. 280, 17109–17117.

Conant, C.G., Stephens, R.S., 2007. Chlamydia attachment to mammalian cells requires protein disulfide isomerase. Cell. Microbiol. 9, 222–232.

Conti, F.J., Monkley, S.J., Wood, M.R., Critchley, D.R., Müller, U., 2009. Talin 1 and 2 are required for myoblast fusion, sarcomere assembly and the maintenance of myotendinous junctions. Development 136, 3597–3606.

Deconinck, A.E., Rafael, J.A., Skinner, J.A., Brown, S.C., Potter, A.C., Metzinger, L., Watt, D.J., Dickson, J.G., Tinsley, J.M., Davies, K.E., 1997. Utrophin-dystrophin-deficient mice as a model for Duchenne muscular dystrophy. Cell 90, 717–727.

Dedden, D., Schumacher, S., Kelley, C.F., Zacharias, M., Biertümpfel, C., Fässler, R., Mizuno, N., 2019. The Architecture of Talin1 Reveals an Autoinhibition Mechanism. Cell 179, 120-131.e13.

DeMali, K.A., Barlow, C.A., Burridge, K., 2002. Recruitment of the Arp2/3 complex to vinculin: Coupling membrane protrusion to matrix adhesion. J. Cell Biol. 159, 881–891.

Dereeper, A., Guignon, V., Blanc, G., Audic, S., Buffet, S., Chevenet, F., Dufayard, J.-F., Guindon, S., Lefort, V., Lescot, M., Claverie, J.-M., Gascuel, O., 2008. Phylogeny.fr: robust phylogenetic analysis for the non-specialist. Nucleic Acids Res. 36, W465–W469.

Di Paolo, G., Pellegrini, L., Letinic, K., Cestra, G., Zoncu, R., Voronov, S., Chang, S., Guo, J., Wenk, M.R., De Camilli, P., 2002. Recruitment and regulation of phosphatidylinositol phosphate kinase type 1γ by the FERM domain of talin. Nature 420, 85–89.

Di Tommaso, P., Moretti, S., Xenarios, I., Orobitg, M., Montanyola, A., Chang, J.M., Taly, J.F., Notredame, C., 2011. T-Coffee: A web server for the multiple sequence alignment of protein and RNA sequences using structural information and homology extension. Nucleic Acids Res. 39, 13–17.

Eko, F.O., Talin, B.A., Lubitz, W., 2008. Development of a Chlamydia trachomatis bacterial ghost vaccine to fight human blindness. Hum. Vaccin. 4, 176–183.

Elwell, C., Mirrashidi, K., Engel, J., 2016. Chlamydia cell biology and pathogenesis. Nat. Rev. Microbiol. 14, 385–400.

Engler, A.J., Sen, S., Sweeney, H.L., Discher, D.E., 2006. Matrix Elasticity Directs Stem Cell Lineage Specification. Cell 126, 677–689.

Ervasti, J.M., Ohlendieck, K., Kahl, S.D., Gaver, M.G., Campbell, K.P., 1990. Deficiency of a glycoprotein component of the dystrophin complex in dystrophic muscle. Nature 345, 315–319.

Fan, L.C., Chiang, W.F., Liang, C.H., Tsai, Y.T., Wong, T.Y., Chen, K.C., Hong, T.M., Chen, Y.L., 2011. α-Catulin knockdown induces senescence in cancer cells. Oncogene 30, 2610–2621.

Fässler, R., Georges-Labouesse, E., Hirsch, E., 1996. Genetic analyses of integrin function in mice. Curr. Opin. Cell Biol. 8, 641–646.

Franco, S.J., Rodgers, M.A., Perrin, B.J., Han, J., Bennin, D.A., Critchley, D.R., Huttenlocher, A., 2004. Calpain-mediated proteolysis of talin regulates adhesion dynamics. Nat. Cell Biol. 6, 977–983.

Frisch, S.M., Francis, H., 1994. Disruption of epithelial cell-matrix interactions induces apoptosis. J. Cell

Biol. 124, 619–626.

Gawor, M., Prószyński, T.J., 2018. The molecular cross talk of the dystrophin–glycoprotein complex. Ann. N. Y. Acad. Sci. 1412, 62–72.

Gilmore, A.P., Jackson, P., Waites, G.T., Critchley, D.R., 1992. Further characterisation of the talin-binding site in the cytoskeletal protein vinculin. J. Cell Sci. 103, 719–731.

Gingras, A.R., Bate, N., Goult, B.T., Hazelwood, L., Canestrelli, I., Grossmann, J.G., Liu, H., Putz, N.S.M., Roberts, G.C.K., Volkmann, N., Hanein, D., Barsukov, I.L., Critchley, D.R., 2008. The structure of the C-terminal actin-binding domain of talin. EMBO J. 27, 458–469.

Gingras, A.R., Ziegler, W.H., Frank, R., Barsukov, I.L., Roberts, G.C.K., Critchley, D.R., Emsley, J., 2005. Mapping and consensus sequence identification for multiple vinculin binding sites within the talin rod. J. Biol. Chem. 280, 37217–37224.

Gingras, J., Gawor, M., Bernadzki, K.M., Mark Grady, R., Hallock, P., Glass, D.J., Sanes, J.R., Proszynski, T.J., 2016. α-Dystrobrevin-1 recruits Grb2 and α-catulin to organize neurotransmitter receptors at the neuromuscular junction. J. Cell Sci. 129, 898–911.

Giubellino, A., Burke Jr, T.R., Bottaro, D.P., 2008. Grb2 signaling in cell motility and cancer. Expert Opin. Ther. Targets 12, 1021–1033.

Goksoy, E., Ma, Y.Q., Wang, X., Kong, X., Perera, D., Plow, E.F., Qin, J., 2008. Structural Basis for the Autoinhibition of Talin in Regulating Integrin Activation. Mol. Cell 31, 124–133.

Golji, J., Mofrad, M.R.K., 2013. The Interaction of Vinculin with Actin. PLoS Comput. Biol. 9, e1002995.

Golji, J., Mofrad, M.R.K., 2010. A molecular dynamics investigation of vinculin activation. Biophys. J. 99, 1073–1081.

Golji, J., Wendorff, T., Mofrad, M.R.K., 2012. Phosphorylation primes vinculin for activation. Biophys. J. 102, 2022–2030.

Gough, R.E., Goult, B.T., 2018. The tale of two talins – two isoforms to fine-tune integrin signalling. FEBS

Lett. 592, 2108–2125.

Goult, B.T., Bate, N., Anthis, N.J., Wegener, K.L., Gingras, A.R., Patel, B., Barsukov, I.L., Campbell, I.D., Roberts, G.C.K., Critchley, D.R., 2009. The structure of an interdomain complex that regulates Talin activity. J. Biol. Chem. 284, 15097–15106.

Goult, B.T., Bouaouina, M., Elliott, P.R., Bate, N., Patel, B., Gingras, A.R., Grossmann, J.G., Roberts, G.C.K., Calderwood, D.A., Critchley, D.R., Barsukov, I.L., 2010. Structure of a double ubiquitin-like domain in the talin head: A role in integrin activation. EMBO J. 29, 1069–1080.

Goult, B.T., Xu, X.P., Gingras, A.R., Swift, M., Patel, B., Bate, N., Kopp, P.M., Barsukov, I.L., Critchley, D.R., Volkmann, N., Hanein, D., 2013a. Structural studies on full-length talin1 reveal a compact auto-inhibited dimer: Implications for talin activation. J. Struct. Biol. 184, 21–32.

Goult, B.T., Yan, J., Schwartz, M.A., 2018. Talin as a mechanosensitive signaling hub. J. Cell Biol. 217, 3776–3784.

Goult, B.T., Zacharchenko, T., Bate, N., Tsang, R., Hey, F., Gingras, A.R., Elliott, P.R., Roberts, G.C.K., Ballestrem, C., Critchley, D.R., Barsukov, I.L., 2013b. RIAM and vinculin binding to talin are mutually exclusive and regulate adhesion assembly and turnover. J. Biol. Chem. 288, 8238–8249.

Grashoff, C., Bd, H., Zhou, R., Parsons, M., Mt, Y., Sg, S., Cs, C., Ha, T., Ma, S., 2010. Measuring mechanical tension across vinculin reveals regulation of focal adhesion dynamics . Nature 466, 9198.

Gudipaty, S.A., Conner, C.M., Rosenblatt, J., Montell, D.J., 2018. Unconventional Ways to Live and Die: Cell Death and Survival in Development, Homeostasis, and Disease. Annu. Rev. Cell Dev. Biol. 34, 311–332.

Hamiaux, C., van Eerde, A., Parsot, C., Broos, J., Dijkstra, B.W., 2006. Structural mimicry for vinculin activation by IpaA, a virulence factor of Shigella flexneri. EMBO Rep. 7, 794–799.

Han, J., Lim, C.J., Watanabe, N., Soriani, A., Ratnikov, B., Calderwood, D.A., Puzon-McLaughlin, W., Lafuente, E.M., Boussiotis, V.A., Shattil, S.J., Ginsberg, M.H.H., 2006. Reconstructing and

Deconstructing Agonist-Induced Activation of Integrin αIIbβ3. Curr. Biol. 16, 1796–1806.

Han, M.K.L., Van Der Krogt, G.N.M., De Rooij, J., 2017. Zygotic vinculin is not essential for embryonic development in zebrafish. PLoS One 12, 1–22.

Harburger, D.S., Bouaouina, M., Calderwood, D.A., 2009. Kindlin-1 and -2 directly bind the C-terminal region of β integrin cytoplasmic tails and exert integrin-specific activation effects. J. Biol. Chem. 284, 11485–11497.

Hazan, R.B., Kang, L., Roe, S., Borgen, P.I., Rimm, D.L., 1997. Vinculin is associated with the E-cadherin adhesion complex. J. Biol. Chem. 272, 32448–32453.

Hemmings, L., Rees, D.J.G., Ohanian, V., Bolton, S.J., Gilmore, A.P., Patel, B., Priddle, H., Trevithick, J.E., Hynes, R.O., Critchley, D.R., 1996. Talin contains three actin-binding sites each of which is adjacent to a vinculin-binding site. J. Cell Sci. 109, 2715–2726.

Hernandez-Varas, P., Berge, U., Lock, J.G., Strömblad, S., 2015. A plastic relationship between vinculin-mediated tension and adhesion complex area defines adhesion size and lifetime. Nat. Commun. 6.

Hillier, B.J., Christopherson, K.S., Prehoda, K.E., Bredt, D.S., Lim, W.A., 1999. Unexpected modes of PDZ domain scaffolding revealed by structure of nNOS-syntrophin complex. Science (80-.). 284, 812–815.

Howie, S.E., Horner, P.J., Horne, A.W., Entrican, G., 2011. Immunity and vaccines against sexually transmitted Chlamydia trachomatis infection. Curr. Opin. Infect. Dis. 24, 56–61.

Hu, Y.L., Lu, S., Szeto, K.W., Sun, J., Wang, Y., Lasheras, J.C., Chien, S., 2014. FAK and paxillin dynamics at focal adhesions in the protrusions of migrating cells. Sci. Rep. 4, 1–7.

Hughes, P.E., Diaz-Gonzalez, F., Leong, L., Wu, C., McDonald, J.A., Shattil, S.J., Ginsberg, M.H., 1996. Breaking the Integrin Hinge. J. Biol. Chem. 271, 6571–6574.

Hüttelmaier, S., Bubeck, P., Rüdiger, M., Jockusch, B.M., 1997. Characterization of two F-actin-binding and oligomerization sites in the cell-contact protein vinculin. Eur. J. Biochem. 247, 1136–1142.

Hüttelmaier, S., Mayboroda, O., Harbeck, B., Jarchau, T., Jockusch, B.M., Rüdiger, M., 1998. The interaction of the cell-contact proteins VASP and vinculin is regulated by phosphatidylinositol-4,5-bisphosphate. Curr. Biol. 8, 479–488.

Hybiske, K., Stephens, R.S., 2007. Mechanisms of host cell exit by the intracellular bacterium Chlamydia. Proc. Natl. Acad. Sci. U. S. A. 104, 11430–11435.

Hynes, R.O., 2002. Integrins: Bidirectional, Allosteric Signaling Machines. Cell 110, 673–687.

Irmler, M., Thome, M., Hahne, M., Schneider, P., Hofmann, K., Steiner, V., Bodmer, J.L., Schröter, M., Burns, K., Mattmann, C., Rimoldi, D., French, L.E., Tschopp, J., 1997. Inhibition of death receptor signals by cellular FLIP. Nature 388, 190–195.

Isaac, C., Wright, A., Usas, A., Li, H., Tang, Y., Mu, X., Greco, N., Dong, Q., Vo, N., Kang, J., Wang, B., Huard, J., 2013. Dystrophin and utrophin “double knockout” dystrophic mice exhibit a spectrum of degenerative musculoskeletal abnormalities. J. Orthop. Res. 31, 343–349.

Izard, T., Evans, G., Borgon, R.A., Rush, C.L., Bricogne, G., Bois, P.R.J., 2004. Vinculin activation by talin through helical bundle conversion. Nature 427, 171–175.

Izard, T., Vonrhein, C., 2004. Structural basis for amplifying vinculin activation by talin. J. Biol. Chem. 279, 27667–27678.

Jacquemet, G., Hamidi, H., Ivaska, J., 2015. Filopodia in cell adhesion, 3D migration and cancer cell invasion. Curr. Opin. Cell Biol. 36, 23–31.

Janssens, B., Staes, K., van Roy, F., 1999. Human α-catulin, a novel α-catenin-like molecule with conserved genomic structure, but deviating alternative splicing. Biochim. Biophys. Acta - Gene Struct. Expr. 1447, 341–347.

Jewett, T.J., Fischer, E.R., Mead, D.J., Hackstadt, T., 2006. Chlamydial TARP is a bacterial nucleator of actin. Pnas 103, 15599–604.

Jiwani, S., Ohr, R.J., Fischer, E.R., Hackstadt, T., Alvarado, S., Romero, A., Jewett, T.J., 2012. Chlamydia trachomatis Tarp cooperates with the Arp2/3 complex to increase the rate of actin

polymerization. Biochem. Biophys. Res. Commun. 420, 816–821.

Johnson, R.P., Craig, S.W., 2000. Actin activates a cryptic dimerization potential of the vinculin tail domain. J. Biol. Chem. 275, 95–105.

Johnson, R.P., Craig, S.W., 1994. An intramolecular association between the head and tail domains of vinculin modulates talin binding. J. Biol. Chem. 269, 12611–12619.

Johnson, R.P., Niggli, V., Durrer, P., Craig, S.W., 1998. A conserved motif in the tail domain of vinculin mediates association with and insertion into acidic phospholipid bilayers. Biochemistry 37, 10211–10222.

Jones, D.T., 1999. Protein secondary structure prediction based on position-specific scoring matrices. J. Mol. Biol. 292, 195–202.

Jung, D., Yang, B., Meyer, J., Chamberlain, J.S., Campbell, K.P., 1995. Identification and characterization of the dystrophin anchoring site on β-dystroglycan. J. Biol. Chem. 270, 27305–27310.

Kalli, A.C., Wegener, K.L., Goult, B.T., Anthis, N.J., Campbell, I.D., Sansom, M.S.P., 2010. The Structure of the Talin/Integrin Complex at a Lipid Bilayer: An NMR and MD Simulation Study. Structure 18, 1280–1288.

Karpińska, K., Cao, C., Yamamoto, V., Gielata, M., Kobielak, A., 2020. Alpha-Catulin, a New Player in a Rho Dependent Apical Constriction That Contributes to the Mouse Neural Tube Closure. Front. Cell Dev. Biol. 8, 1–18.

Kelley, C.F., Litschel, T., Schumacher, S., Dedden, D., Schwille, P., Mizuno, N., 2020. Phosphoinositides regulate force-independent interactions between talin, vinculin, and actin. Elife 9, 1–30.

Kelley, L.A., Mezulis, S., Yates, C.M., Wass, M.N., Sternberg, M.J., 2016. The Phyre2 web portal for protein modeling, prediction and analysis. Nat. Protoc. 10, 845–858.

Khan, R.B., Goult, B.T., 2019. Adhesions Assemble!—Autoinhibition as a Major Regulatory Mechanism of Integrin-Mediated Adhesion. Front. Mol. Biosci. 6, 1–16.

Kim, H., Pierce-Shimomura, J.T., Oh, H.J., Johnson, B.E., Goodman, M.B., McIntire, S.L., 2009. The dystrophin complex controls BK channel localization and muscle activity in Caenorhabditis elegans. PLoS Genet. 5.

Kim, J.H., Jiang, S., Elwell, C.A., Engel, J.N., 2011. Chlamydia trachomatis co-opts the FGF2 signaling pathway to enhance infection. PLoS Pathog. 7.

Kioka, N., Sakata, S., Kawauchi, T., Amachi, T., Akiyama, S.K., Okazaki, K., Yaen, C., Yamada, K.M., Aota, S.I., 1999. Vinexin: A novel vinculin-binding protein with multiple SH3 domains enhances actin cytoskeletal organization. J. Cell Biol. 144, 58–69.

Koenig, M., Kunkel, L.M., 1990. Detailed analysis of the repeat domain of dystrophin reveals four potential hinge segments that may confer flexibility. J. Biol. Chem. 265, 4560–4566.

Kreiseder, B., Holper-SchichlM, Y., Muellauer, B., Jacobi, N., Pretsch, A., Schmid, J.A., De Martin, R., Hundsberger, H., Eger, A., Wiesner, C., 2015. Alpha-Catulin contributes to drug-resistance of melanoma by activating NF-?B and AP-1. PLoS One 10, 1–18.

Lai, M.T., Hua, C.H., Tsai, M.H., Wan, L., Lin, Y.J., Chen, C.M., Chiu, I.W., Chan, C., Tsai, F.J., Sheu, J.C.J., 2011. Talin-1 overexpression defines high risk for aggressive oral squamous cell carcinoma and promotes cancer metastasis. J. Pathol. 224, 367–376.

Lau, T.-L., Kim, C., Ginsberg, M.H., Ulmer, T.S., 2009. The structure of the integrin αIIbβ3 transmembrane complex explains integrin transmembrane signalling. EMBO J. 28, 1351–1361.

Lee, H.S., Lim, C.J., Puzon-McLaughlin, W., Shattil, S.J., Ginsberg, M.H., 2009. RIAM activates integrins by linking talin to Ras GTPase membrane-targeting sequences. J. Biol. Chem. 284, 5119–5122.

Lee, J.H., Vonrhein, C., Bricogne, G., Izard, T., 2013. Crystal structure of the N-terminal domains of the surface cell antigen 4 of Rickettsia. Protein Sci. 22, 1425–1431.

Leerberg, J.M., Yap, A.S., 2013. Vinculin, cadherin mechanotransduction and homeostasis of cell-cell junctions. Protoplasma 250, 817–829.

Li, W., Metcalf, D.G., Gorelik, R., Li, R., Mitra, N., Nanda, V., Law, P.B., Lear, J.D., DeGrado, W.F.,

Bennett, J.S., 2005. A push-pull mechanism for regulating integrin function. Proc. Natl. Acad. Sci. U. S. A. 102, 1424–1429.

Ling, K., Doughman, R.L., Firestone, A.J., Bunce, M.W., Anderson, R.A., 2002. Type Iγ phosphatidylinositol phosphate kinase targets and regulates focal adhesions. Nature 420, 89–93.

Litvinov, R.I., Mravic, M., Zhu, H., Weisel, J.W., DeGrado, W.F., Bennett, J.S., 2019. Unique transmembrane domain interactions differentially modulate integrin αvβ3 and αIIbβ3 function. Proc. Natl. Acad. Sci. U. S. A. 116, 12295–12300.

Lucas, A.L., Ouellette, S.P., Kabeiseman, E.J., Cichos, K.H., Rucks, E.A., 2015. The trans-Golgi SNARE syntaxin 10 is required for optimal development of Chlamydia trachomatis. Front. Cell. Infect. Microbiol. 5, 1–11.

Luo, B.H., Carman, C. V., Takagi, J., Springer, T.A., 2005. Disrupting integrin transmembrane domain heterodimerization increases ligand binding affinity, not valency or clustering. Proc. Natl. Acad. Sci. U. S. A. 102, 3679–3684.

Luo, B.H., Springer, T.A., Takagi, J., 2004. A specific interface between integrin transmembrane helices and affinity for ligand. PLoS Biol. 2.

Lyssand, J.S., Whiting, J.L., Lee, K.S., Kastl, R., Wacker, J.L., Bruchas, M.R., Miyatake, M., Langeberg, L.K., Chavkin, C., Scott, J.D., Gardner, R.G., Adams, M.E., Hague, C., 2010. α-Dystrobrevin-1 recruits α-catulin to the α 1D-adrenergic receptor/dystrophin-associated protein complex signalosome. Proc. Natl. Acad. Sci. U. S. A. 107, 21854–21859.

Maartens, A.P., Wellmann, J., Wictome, E., Klapholz, B., Green, H., Brown, N.H., 2016. Drosophila vinculin is more harmful when hyperactive than absent, and can circumvent integrin to form adhesion complexes. J. Cell Sci. 129, 4354–4365.

Madeira, F., Park, Y.M., Lee, J., Buso, N., Gur, T., Madhusoodanan, N., Basutkar, P., Tivey, A.R.N., Potter, S.C., Finn, R.D., Lopez, R., 2019. The EMBL-EBI search and sequence analysis tools APIs in 2019. Nucleic Acids Res. 47, W636–W641.

Mandai, K., Nakanishi, H., Satoh, A., Takahashi, K., Satoh, K., Nishioka, H., Mizoguchi, A., Takai, Y., 1999. Ponsin/SH3P12: An 1-afadin- and vinculin-binding protein localized at cell-cell and cell-matrix adherens junctions. J. Cell Biol. 144, 1001–1017.

Matsumura, K., Ervasti, J.M., Ohlendieck, K., Kahl, S.D., Campbell, K.P., 1992. Association of dystrophin-related protein with dystrophin-associated proteins in mdx mouse muscle. Nature 360, 588–591.

McGregor, A., Blanchard, A.D., Rowe, A.J., Critchley, D.R., 1994. Identification of the vinculin-binding site in the cytoskeletal protein α-actinin. Biochem. J. 301, 225–233.

Michael, M., Parsons, M., 2020. New perspectives on integrin-dependent adhesions. Curr. Opin. Cell Biol. 63, 31–37.

Monkley, S.J., Zhou, X.H., Kinston, S.J., Giblett, S.M., Hemmings, L., Priddle, H., Brown, J.E., Pritchard, C.A., Critchley, D.R., Fässler, R., 2000. Disruption of the talin gene arrests mouse development at the gastrulation stage. Dev. Dyn. 219, 560–574.

Mungrue, I.N., Bredt, D.S., 2004. nNOS at a glance: Implications for brain and brawn. J. Cell Sci. 117, 2627–2629.

Oak, S.A., Russo, K., Petrucci, T.C., Jarrett, H.W., 2001. Mouse α1-syntrophin binding to Grb2: Further evidence of a role for syntrophin in cell signaling. Biochemistry 40, 11270–11278.

Oh, H.J., Abraham, L.S., Van Hengel, J., Stove, C., Proszynski, T.J., Gevaert, K., DiMario, J.X., Sanes, J.R., Van Roy, F., Kim, H., 2012. Interaction of α-catulin with dystrobrevin contributes to integrity of dystrophin complex in muscle. J. Biol. Chem. 287, 21717–21728.

Ohlendieck, K., Campbell, K.P., 1991. Dystrophin-associated proteins are greatly reduced in skeletal muscle from mdx mice. J. Cell Biol. 115, 1685–1694.

Omachi, T., Ichikawa, T., Kimura, Y., Ueda, K., Kioka, N., 2017. Vinculin association with actin cytoskeleton is necessary for stiffness-dependent regulation of vinculin behavior. PLoS One 12, 1–14.

Park, B., Nguyen, N.T., Dutt, P., Merdek, K.D., Bashar, M., Sterpetti, P., Tosolini, A., Testa, J.R., Toksoz,

D., 2002. Association of Lbc Rho guanine nucleotide exchange factor with α-catenin-related protein, α-catulin/CTNNAL1, supports serum response factor activation. J. Biol. Chem. 277, 45361–45370.

Park, H.J., Lee, J.H., Gouin, E., Cossart, P., Izard, T., 2011a. The Rickettsia surface cell antigen 4 applies mimicry to bind to and activate vinculin. J. Biol. Chem. 286, 35096–35103.

Park, H.J., Valencia-Gallardo, C., Sharff, A., Van Nhieu, G.T., Izard, T., 2011b. Novel vinculin binding site of the IpaA invasin of Shigella. J. Biol. Chem.

Pasapera, A.M., Schneider, I.C., Rericha, E., Schlaepfer, D.D., Waterman, C.M., 2010. Myosin II activity regulates vinculin recruitment to focal adhesions through FAK-mediated paxillin phosphorylation. J. Cell Biol. 188, 877–890.

Pearson, M.A., Reczek, D., Bretscher, A., Karplus, P.A., 2000. Structure of the ERM protein moesin reveals the FERM domain fold masked by an extended actin binding tail domain. Cell 101, 259–270.

Pedrosa, A.T., Murphy, K.N., Nogueira, A.T., Brinkworth, A.J., Thwaites, T.R., Aaron, J., Chew, T.-L., Carabeo, R.A., 2020. A post-invasion role for Chlamydia type III effector TarP in modulating the dynamics and organization of host cell focal adhesions . J. Biol. Chem. jbc.RA120.015219.

Peng, X., Cuff, L.E., Lawton, C.D., DeMali, K.A., 2010. Vinculin regulates cell-surface E-cadherin expression by binding to β-catenin. J. Cell Sci. 123, 567–577.

Petrof, B.J., Shrager, J.B., Stedman, H.H., Kelly, A.M., Sweeney, H.L., 1993. Dystrophin protects the sarcolemma from stresses developed during muscle contraction. Proc. Natl. Acad. Sci. U. S. A. 90, 3710–3714.

Puolakkainen, M., Kuo, C.C., Campbell, L.A., 2005. Chlamydia pneumoniae uses the mannose 6-phosphate/insulin-like growth factor 2 receptor for infection of endothelial cells. Infect. Immun. 73, 4620–4625.

Rafii, M.S., Hagiwara, H., Mercado, M.L., Seo, N.S., Xu, T., Dugan, T., Owens, R.T., Hook, M., McQuillan, D.J., Young, M.F., Fallon, J.R., 2006. Biglycan binds to α- and γ-sarcoglycan and regulates their expression during development. J. Cell. Physiol. 209, 439–447.

Rangarajan, E.S., Izard, T., 2012. The cytoskeletal protein α-catenin unfurls upon binding to vinculin. J. Biol. Chem. 287, 18492–18499.

Repository, Z.O., Glen, B., Marvin, E., Stanley, C., 2002. University of Zurich The postsynaptic submembrane machinery at the neuromuscular junction : requirement for rapsyn and the utrophin / dystrophin-associated complex The postsynaptic submembrane machinery at the neuromuscular junction : requirement for raps 32.

Rimm, D.L., Koslov, E.R., Kebriaei, P., Cianci, C.D., Morrow, J.S., 1995. α1(E)-catenin is an actin-binding and -bundling protein mediating the attachment of F-actin to the membrane adhesion complex. Proc. Natl. Acad. Sci. U. S. A. 92, 8813–8817.

Russ, W.P., Engelman, D.M., 2000. The GxxxG motif: A framework for transmembrane helix-helix association. J. Mol. Biol. 296, 911–919.

Rybakova, I.N., Amann, K.J., Ervasti, J.M., 1996. A new model for the interaction of dystrophin with F-actin. J. Cell Biol. 135, 661–672.

Sadoulet-Puccio, H.M., Rajala, M., Kunkel, L.M., 1997. Dystrobrevin and dystrophin: An interaction through coiled-coil motifs. Proc. Natl. Acad. Sci. U. S. A. 94, 12413–12418.

Saunders, R.M., Holt, M.R., Jennings, L., Sutton, D.H., Barsukov, I.L., Bobkov, A., Liddington, R.C., Adamson, E.A., Dunn, G.A., Critchley, D.R., 2006. Role of vinculin in regulating focal adhesion turnover. Eur. J. Cell Biol. 85, 487–500.

Senetar, M.A., Foster, S.J., McCann, R.O., 2004. Intrasteric inhibition mediates the interaction of the I/LWEQ module proteins Talin1, Talin2, Hip1, and Hip12 with actin. Biochemistry 43, 15418–15428.

Shattil, S.J., Kim, C., Ginsberg, M.H., 2010. The final steps of integrin activation: the end game. Nat. Rev. Mol. Cell Biol. 11, 288–300.

Slepenkin, A., Motin, V., De la Maza, L.M., Peterson, E.M., 2003. Temporal expression of type III secretion genes of Chlamydia pneumoniae. Infect. Immun. 71, 2555–2562.

Snavely, E.A., Kokes, M., Dunn, J.D., Saka, H.A., Nguyen, B.D., Bastidas, R.J., Mccafferty, D.G.,

Valdivia, R.H., 2014. Reassessing the role of the secreted protease CPAF in Chlamydia trachomatis infection through genetic approaches. Pathog. Dis. 71, 336–351.

Song, X., Yang, J., Hirbawi, J., Ye, S., Perera, H.D., Goksoy, E., Dwivedi, P., Plow, E.F., Zhang, R., Qin, J., 2012. A novel membrane-dependent on/off switch mechanism of talin FERM domain at sites of cell adhesion. Cell Res. 22, 1533–1545.

Stallmann, S., Hegemann, J.H., 2016. The Chlamydia trachomatis Ctad1 invasin exploits the human integrin β1 receptor for host cell entry. Cell. Microbiol. 18, 761–775.

Subbarayal, P., Karunakaran, K., Winkler, A.-C., Rother, M., Gonzalez, E., Meyer, T.F., Rudel, T., 2015. EphrinA2 Receptor (EphA2) Is an Invasion and Intracellular Signaling Receptor for Chlamydia trachomatis. PLOS Pathog. 11, e1004846.

Taraktchoglou, M., Pacey, A.A., Turnbull, J.E., Eley, A., 2001. Infectivity of Chlamydia trachomatis serovar LGV but not E is dependent on host cell heparan sulfate. Infect. Immun. 69, 968–976.

Thievessen, I., Thompson, P.M., Berlemont, S., Plevock, K.M., Plotnikov, S. V., Zemljic-Harpf, A., Ross, R.S., Davidson, M.W., Danuser, G., Campbell, S.L., Waterman, C.M., 2013. Vinculin-actin interaction couples actin retrograde flow to focal adhesions, but is dispensable for focal adhesion growth. J. Cell Biol. 202, 163–177.

Thwaites, T.R., Pedrosa, A.T., Peacock, T.P., Carabeo, R.A., 2015. Vinculin Interacts with the Chlamydia Effector TarP Via a Tripartite Vinculin Binding Domain to Mediate Actin Recruitment and Assembly at the Plasma Membrane. Front. Cell. Infect. Microbiol. 5, 88.

Tolchard, J., Walpole, S.J., Miles, A.J., Maytum, R., Eaglen, L.A., Hackstadt, T., Wallace, B.A., Blumenschein, T.M.A., 2018. The intrinsically disordered Tarp protein from chlamydia binds actin with a partially preformed helix. Sci. Rep. 8, 1960.

Tran Van Nhieu, G., Izard, T., 2007. Vinculin binding in its closed conformation by a helix addition mechanism. EMBO J. 26, 4588–4596.

Turner, C.E., Glenney, J.R., Burridge, K., 1990. Paxillin: A new vinculin-binding protein present in focal

adhesions. J. Cell Biol. 111, 1059–1068.

Van Reeuwijk, J., Janssen, M., Van Den Elzen, C., Beltran-Valero De Bernabé, D., Sabatelli, P., Merlini, L., Boon, M., Scheffer, H., Brockington, M., Muntoni, F., Huynen, M.A., Verrips, A., Walsh, C.A., Barth, P.G., Brunner, H.G., Van Bokhoven, H., 2005. POMT2 mutations cause α-dystroglycan hypoglycosylation and Walker-Warburg syndrome. J. Med. Genet. 42, 907–912.

Watabe-Uchida, M., Uchida, N., Imamura, Y., Nagafuchi, A., Fujimoto, K., Uemura, T., Vermeulen, S., Van Roy, F., Adamson, E.D., Takeichi, M., 1998. α-Catenin-vinculin interaction functions to organize the apical junctional complex in epithelial cells. J. Cell Biol. 142, 847–857.

Wen, K.K., Rubenstein, P.A., DeMali, K.A., 2009. Vinculin nucleates actin polymerization and modifies actin filament structure. J. Biol. Chem. 284, 30463–30473.

Whitewood, A.J., Singh, A.K., Brown, D.G., Goult, B.T., 2018. Chlamydial virulence factor TarP mimics talin to disrupt the talin-vinculin complex. FEBS Lett. 592, 1751–1760.

Wiesner, C., Winsauer, G., Resch, U., Hoeth, M., Schmid, J.A., Van Hengel, J., Van Roy, F., Binder, B.R., De Martin, R., 2008. α-Catulin, a Rho signalling component, can regulate NF-κB through binding to IKK-β, and confers resistance to apoptosis. Oncogene 27, 2159–2169.

Wilkins, M.R., Gasteiger, E., Bairoch, A., Sanchez, J.C., Williams, K.L., Appel, R.D., Hochstrasser, D.F., 1999. Protein identification and analysis tools in the ExPASy server. Methods Mol. Biol. 112, 531–552.

Winder, S.J., Gibson, T.J., Kendrick-Jones, J., 1995. Dystrophin and utrophin: the missing links! FEBS Lett. 369, 27–33.

Winograd-Katz, S.E., Fässler, R., Geiger, B., Legate, K.R., 2014. The integrin adhesome: from genes and proteins to human disease. Nat. Rev. Mol. Cell Biol. 15, 273–88.

Wood, C.K., Turner, C.E., Jackson, P., Critchley, D.R., 1994. Characterisation of the paxillin-binding site and the C-terminal focal adhesion targeting sequence in vinculin. J. Cell Sci. 107, 709–717.

Xiong, J., Stehle, T., Diefenbach, B., Zhang, R., Scott, D.L., Joachimiak, A., Goodman, S.L., Amin, M.,

2010. Crystal Structure of the Extracellular Segment of Integrin αVβ3 294, 339–345.

Xu, W., Baribault, H., Adamson, E.D., 1998. Vinculin knockout results in heart and brain defects during embryonic development. Development 125, 327–337.

Yang, B., Jung, D., Motto, D., Meyer, J., Koretzky, G., Campbell, K.P., 1995a. SH3 domain-mediated interaction of dystroglycan and Grb2. J. Biol. Chem.

Yang, B., Jung, D., Rafael, J.A., Chamberlain, J.S., Campbell, K.P., 1995b. Identification of α-syntrophin binding to syntrophin triplet, dystrophin, and utrophin. J. Biol. Chem.

Yao, M., Goult, B.T., Chen, H., Cong, P., Sheetz, M.P., Yan, J., 2014a. Mechanical activation of vinculin binding to talin locks talin in an unfolded conformation. Sci. Rep. 4.

Yao, M., Goult, B.T., Klapholz, B., Hu, X., Toseland, C.P., Guo, Y., Cong, P., Sheetz, M.P., Yan, J., 2016. The mechanical response of talin. Nat. Commun. 7.

Yao, M., Qiu, W., Liu, R., Efremov, A.K., Cong, P., Seddiki, R., Payre, M., Lim, C.T., Ladoux, B., Mège, R.-M., Yan, J., 2014b. Force-dependent conformational switch of α-catenin controls vinculin binding. Nat. Commun. 5, 4525.

Yogesha, S.D., Rangarajan, E.S., Vonrhein, C., Bricogne, G., Izard, T., 2012. Crystal structure of vinculin in complex with vinculin binding site 50 (VBS50), the integrin binding site 2 (IBS2) of talin. Protein Sci. 21, 583–588.

Yogesha, S.D., Sharff, A., Bricogne, G., Izard, T., 2011. Intermolecular versus intramolecular interactions of the vinculin binding site 33 of talin. Protein Sci. 20, 1471–1476.

Yoshida, M., Hama, H., Ishikawa-Sakurai, M., Imamura, M., Mizuno, Y., Araishi, K., Wakabayashi-Takai, E., Noguchi, S., Sasaoka, T., Ozawa, E., 2000. Biochemical evidence for association of dystrobrevin with the sarcoglycan-sarcospan complex as a basis for understanding sarcoglycanopathy. Hum. Mol. Genet. 9, 1033–1040.

Zacharchenko, T., Qian, X., Goult, B.T.T., Jethwa, D., Almeida, T.B.B., Ballestrem, C., Critchley, D.R.R., Lowy, D.R.R., Barsukov, I.L.L., 2016. LD Motif Recognition by Talin: Structure of the Talin-DLC1

Complex. Structure 24, 1130–1141.

Zemljic-harpf, A.E., Ponrartana, S., Avalos, R.T., Jordan, M.C., Roos, K.P., Dalton, N.D., Phan, V.Q., Adamson, E.D., Ross, R.S., 2004. Heterozygous Inactivation of the Vinculin Gene. Microscopy 165, 1033–1044.

Zhang, W., Mao, Y.Q., Wang, H., Yin, W.J., Zhu, S.X., Wang, W.C., 2015. MiR-124 suppresses cell motility and adhesion by targeting talin 1 in prostate cancer cells. Cancer Cell Int. 15, 1–9.

Zhang, Z., Izaguirre, G., Lin, S.-Y., Lee, H.Y., Schaefer, E., Haimovich, B., 2004. The Phosphorylation of Vinculin on Tyrosine Residues 100 and 1065, Mediated by Src Kinases, Affects Cell Spreading. Mol. Biol. Cell 15, 4234–4247.

Zhang, Z., Yang, X. feng, Huang, K. qiang, Ren, L., Zhao, S., Gou, W. feng, Shen, D. fu, Sun, H. zhi, Takano, Y., Zheng, H. chuan, 2016. The upregulated α-catulin expression was involved in head-neck squamous cell carcinogenesis by promoting proliferation, migration, invasion, and epithelial to mesenchymal transition. Tumor Biol. 37, 1671–1681.